NASA Contractor Report 189702

Advanced Aeroservoelastic Stabilization Techniques for Hypersonic Flight Vehicles

Samuel Y. Chan and Peter Y. Cheng
McDonnell Aircraft Company
McDonnell Douglas Corporation
St. Louis, Missouri

Thomas T. Myers, David H. Klyde,
Raymond E. Magdaleno, and Duane T. McRuer
Systems Technology, Inc.
Hawthorne, California

Contract NAS1-18763
November 1992

National Aeronautics and
Space Administration

Langley Research Center
Hampton, Virginia 23665-5225

TABLE OF CONTENTS

TABLE OF CONTENTS (Continued)

List of Figures

List of Figures (Continued)

List of Figures (Continued)

List of Figures (Continued)

List of Tables

Nomenclature and Symbols

dB	Decibel
c.g.	Center of gravity
f_s	Stick force
g	Gravity
G_c	Superaugmented pitch loop forward path controller
G_{f_a}	Aft sensor signal blending filter
G_{f_f}	Forward sensor signal blending filter
G_{s1}	Structural filter 1
G_{s2}	Structural filter 2
Hz	Hertz
K_a	Aft sensor signal blending filter gain
K_f	Forward sensor signal blending filter gain
ksi	Kilopounds per square inch
q	Pitch rate
q_c	Pitch rate command
n_z	Normal acceleration or load factor
n_{zp}	Normal acceleration at the pilot's station
s	Laplace operator
ss	Steady state
$1/T_{\theta 2}$	Zero of pitch rate to control surface deflection transfer function
α	Angle of attack
δ	Pitch control surface deflection
Δ_ζ	Normalized uncertainty level for structural mode damping ratio
Δ_ϕ	Normalized uncertainty level for structural mode shape
Δ_ω	Normalized uncertainty level for structural mode frequency
ζ_s	Structural mode damping ratio
ϕ_s	Structural mode shape
ω_s	Structural mode frequency
(ξ)	Shorthand notation for " $s + \xi$ "
$[\zeta,\omega]$	Shorthand notation for " $s^2 + 2\zeta\omega s + \omega^2$ "

Acronyms and Abbreviations

AMRL	Aero Medical Research Laboratory
FAMUSS	Flexible Aircraft Modeling Using State Space
FCS	Flight control system
FS	Fuselage station
HSV	Hypersonic vehicle
HPS	Hybrid phase stabilization
LaRC	Langley Research Center
MAVRIC	Modern Aerospace Vehicle Robust H-Infinity Control
MCAIR	McDonnell Aircraft Company
NASA	National Aeronautics and Space Administration
NASP	National Aerospace Plane
SCAS	Stability and control augmentation system
STI	Systems Technology, Incorporated
VMS	Visual/Motion Simulator

Section I

INTRODUCTION

A. Contract Objectives and Scope

The objectives of this contract (i.e., Task Assignment 17) are to advance the hybrid phase stabilization (HPS) design procedures which were developed under Task Assignment 10 entitled, "Aeroservoelastic Stabilization Techniques for Hypersonic Flight Vehicles" for NAS1-18763 (Ref. 1); to further develop residual response metrics as a basis for alternative structural stability specifications; and to develop strategies for validating HPS design and specification concepts in manned simulation studies.

In this report, Task 10 and Task 17 are referred to as Phase I and Phase II, respectively. This report presents the results, conclusions and recommendations of the second phase of the contract. The Phase II work is a logical continuation of the Phase I work, both in development of improved flight control system designs and in refinements to the methods for assessing these designs.

B. Technical Approach

The motivation for the overall project began with a recognition that hypersonic vehicle (HSV), such as the National Aerospace Plane (NASP), can be expected to be particularly challenging with respect to the interaction of structural dynamics and flight control. Basically, this stems from the relatively low frequency structural modes inherent in the long, slender HSV configurations. The HSV model used to date has its first structural mode at about 2 Hertz (Hz). The low frequency modes create problems for flight control system (FCS) design which are compounded by the increased bandwidth requirements for relaxed static stability configurations such as the project model.

Conventional treatment of these problems, i.e., gain stabilization in the FCS design using notch filters applied to selected structural modes, can, of course, be applied to meet existing gain and phase margin requirements of MIL-F-87242 (Ref. 2). However, as confirmed in the Phase I analysis, such notch filters applied to the low frequency structural modes of HSV inevitably create very high levels of effective time delay. This creates a significant problem in connection with manual flight control. The Phase I work indicated

the inherent difficulty in meeting the MIL-STD-1797 (Ref. 3) Level 1 effective time delay requirements using conventional gain stabilized FCS architectures.

Reduction in the effective time delay to aid manual control motivated the primary flight control concept being pursued in this project - hybrid phase stabilization (HPS). HPS is simply the combination of conventional gain stabilization with phase stabilization. For this application, the essence of phase stabilization is manipulation of open loop zeros with respect to their companion poles so that there is a favorable increase in phase near each structural dipole. This creates a situation where closed loop stability will be desensitized with respect to feedback loop gain variations. As illustrated in Figure 1, this basically requires placing the zero below the pole. In the pitch rate-based FCS designs used in this work, zero placement is mechanized by appropriate mixing of signals from a forward mounted and an aft mounted pitch rate gyro. The first task of the Phase II work was devoted to improving the Phase I HPS design. Significant improvements were achieved and these are discussed in Section II-B.

Application of an unconventional FCS concept such as HPS requires careful consideration of the existing design requirements - not only to determine if they are adequate to insure safe designs, but also to insure that they do not unreasonably restrict application of new concepts. The second point is critical for HSV where unprecedented design challenges do not allow designers the luxury of overly conservative design requirements. The requirements must be as good and as well-founded as the FCS designs themselves! Thus, regardless of whether or not the HPS concept is ultimately the best design approach for HSV FCS, the intrinsic difficulty of this design problem requires careful examination of the design requirements. Such an examination has been part of this project from Phase I.

Among the most fundamental design requirements are the gain and phase margin requirements of MIL-F-87242 (which have been carried forward from its predecessors MIL-F-9490D and earlier specs). These specifications are essentially traditional robustness requirements that have not been re-validated for the new HSV class. Furthermore, robustness specifications such as these are not explicitly linked to physical phenomena which can be re-examined in the context of a new aircraft type. Thus, as part of the Phase-II study, two phenomena of particular significance to the requirements for applying HPS to HSV have been examined. One, the impact of HPS on structural fatigue, is "aircraft-centered"; that is, it is independent of human pilots and passengers. The other, biodynamic interaction between the pilot, the FCS and the structural dynamics, is human-

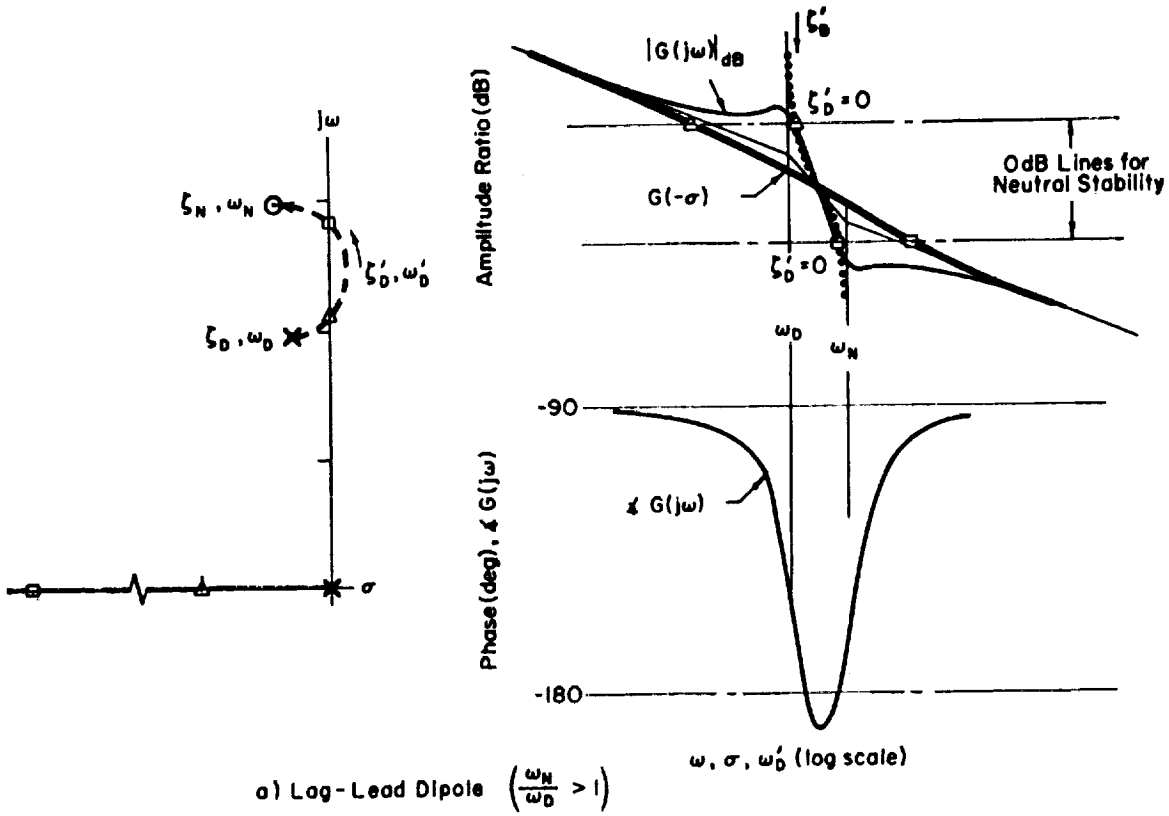

a) Log-Lead Dipole $\left(\frac{\omega_N}{\omega_D} > 1\right)$

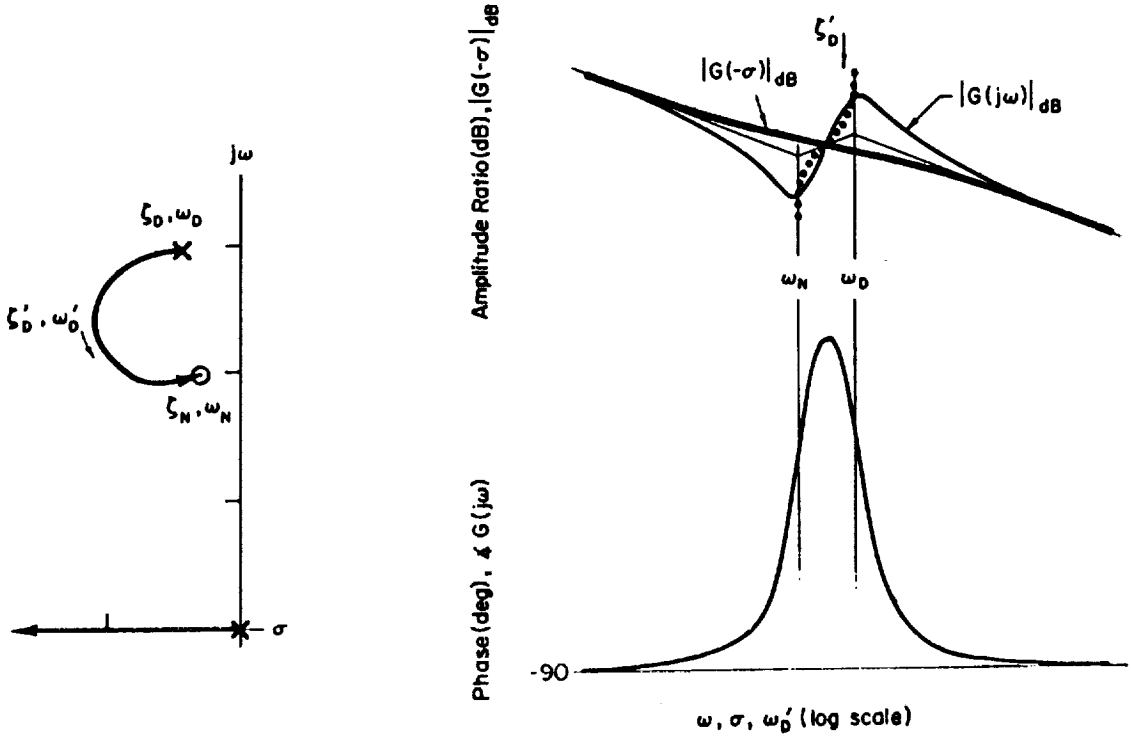

b) Lead-Lag Dipole $\left(\frac{\omega_N}{\omega_D} < 1\right)$

Figure 1. Phase Stable Flight Control Systems Through Structural Zero Placement

centered (i.e., it would not occur in an automatic FCS mode). These analyses are discussed in Section IV.

As noted above, the existing relevant design specifications, the gain and phase margin specs of MIL-F-87242, address robustness. However, application of HPS raises some new robustness questions, specifically the impact of uncertainty in structural mode zeros which are not explicitly addressed by the MIL-F-87242 specs. Thus in Phase II, the relative sensitivity of conventional and HPS designs to uncertainties in the structural model was examined. The results are discussed in Section III.

The linearized dynamic model developed in Phase I for a power-on Mach 6 flight condition was used in Phase II with some extensions. Specifically, the original structural dynamic model was extended to generate a consistent representation of the normal acceleration (n_z). This was done to replace the rough estimate of n_z used in Phase I which was not derived directly from the structural model. The improved n_z model was used to revise the Phase I residual response metric (Section IV-A) and the analyses of aircraft-centered and pilot-centered phenomena impacted by HPS (Section IV).

In Section II, the refinement of the n_z model is discussed first, followed by the refinement of the Phase I HPS design. The remainder of the report is devoted to assessment of the final Phase II HPS design (referred to here as the "Phase IIa HPS" design). It will be seen that significant improvements were achieved in developing the Phase IIa HPS design, however, the assessments have given a clearer understanding of issues which should be further examined as well ideas for new approaches. These are discussed in Section V. Finally, the conclusions and recommendations for future research are presented in Section VI.

Section II

REFINEMENTS OF FLEXIBLE HSV MODEL AND HPS DESIGNS

A. Refinement of Flexible HSV Model

The flexible HSV model has been extended to provide normal acceleration per wing rotation at the pilot's station, fuselage station (FS) 84. The frequency response is shown in Figure 2. The development of the normal acceleration model is similar to that of the pitch rate model (Ref. 1).

As shown previously in Phase I work, the HSV is modeled with uncoupled rigid body and flexible dynamics. These dynamics are combined as depicted in Figure 3. The derivation of the accelerometer output equation is presented in detail in Appendix C.

B. Refinement of HPS Designs

1. Overview of Phase I and Phase II Designs

At the conclusion of the Phase II work, four basic flight control system designs have been developed. These are designated as:

- Gain Stabilized Reference Design
- Phase I HPS Design
- Initial Phase II HPS Design
- Final Phase IIa HPS Design

The final Phase IIa design is considered the best HPS design to date. The gain stabilized reference design was developed in Phase I and has been used through Phase II as the basic comparison with standard FCS design practice. A variant (referred to as "gain stabilized II") was considered in connection with the robustness analysis and is discussed only in Section III. Finally, reference is occasionally made to the "baseline" system. This system is not considered an actual flight control design because it consists of only the superaugmented pitch loop designed in Phase I based on the rigid body dynamics without treatment of the structural dynamic modes.

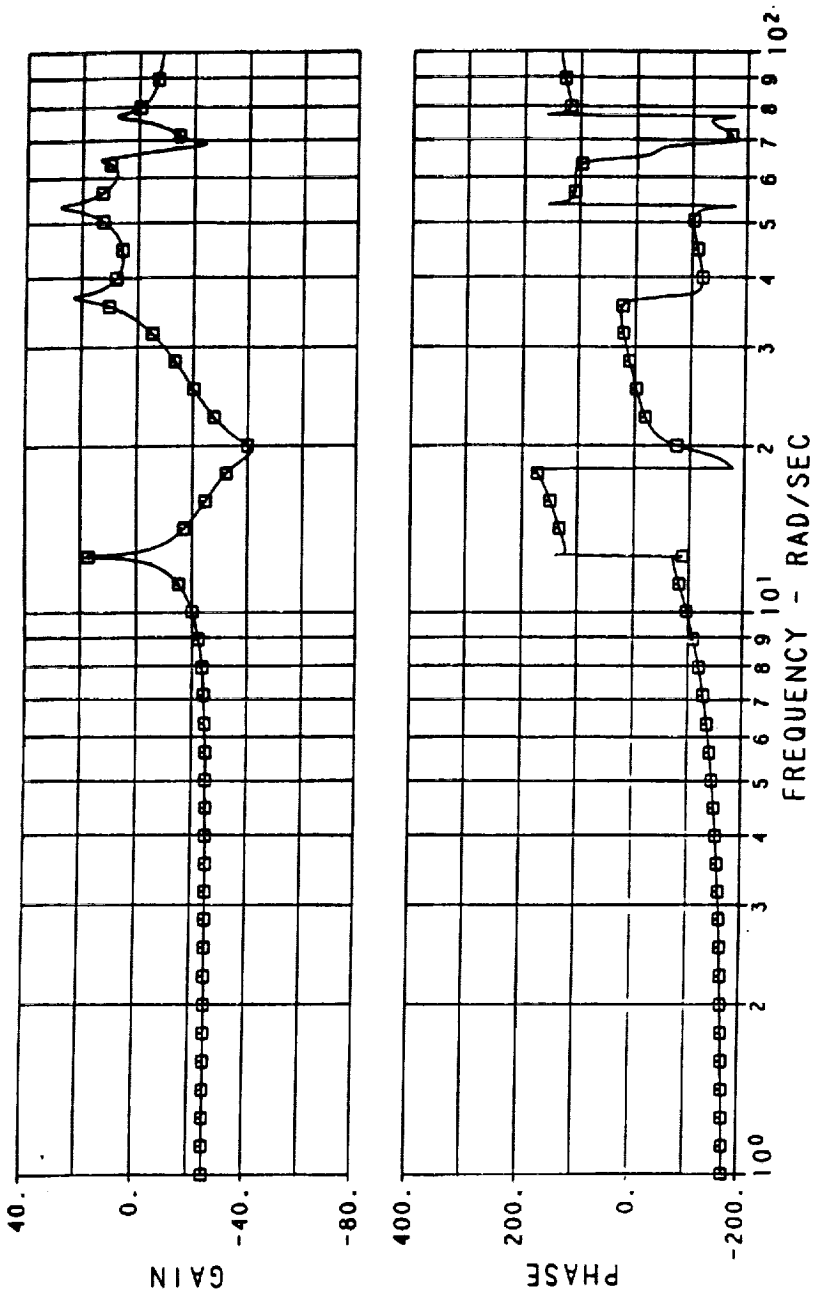

Figure 2. Flexible Normal Acceleration Response at the Pilot's Station

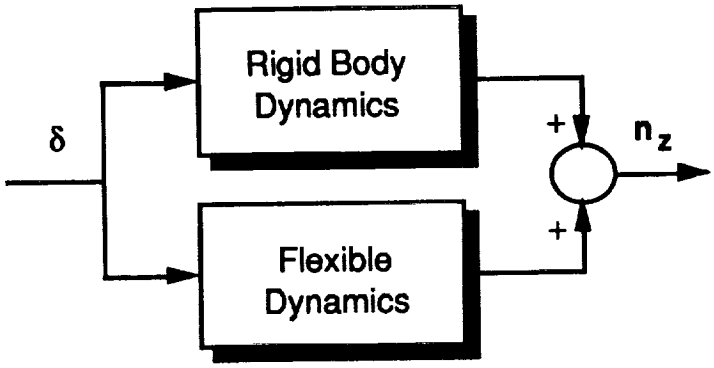

Figure 3. Aircraft Dynamics Modeling

All four designs, along with the baseline system, can be represented by one generic block diagram as shown in Figure 4. The G_c element is the basic "rigid body" control law which is the same in all designs and would constitute the final design if there were no structural modes. The gain stabilized reference design uses only the signal from the forward pitch rate gyro (FS 84) passed through a notch filter (G_{s1}, placed near the first structural mode) and a higher frequency lag (G_{s2}). The frequency response of the gain stabilized design is shown for reference in Figure 5. All three HPS designs are based on the blending of signals from forward and aft pitch rate gyros suitably filtered to position the zeros associated with the lower frequency structural dipoles. The differences in the three HPS designs are in the G_{s1} and G_{s2} elements. The evolution of these elements are discussed in the following subsections. The block containing the gain function $1/(K_a + K_f)$ was included to insure that the gyro signal blending would not change the rigid body crossover frequency and distort the closed loop short period mode.

2. Review of the Phase I HPS Design

As noted previously, the HPS concept is to combine conventional gain stabilization with phase stabilization in a way that exploits the advantages of both schemes and accommodates their disadvantages to produce a superior design. However, a wide variety of design requirements must be considered in the design tradeoffs. In reality, and of particular concern for HSV designs, these requirements must include much more than the gain and phase requirements of MIL-F-87242. These additional "implied requirements" have been an integral part of this study from the beginning and are discussed in more detail in Section IV.

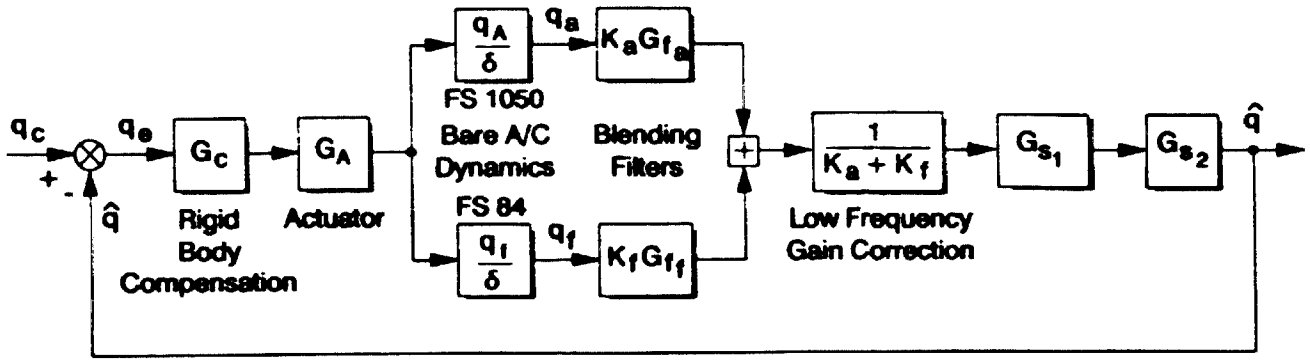

$$G_C = \frac{1.647(s + 1.4)}{s} \frac{(s + 2.31)}{(s + 0.133)} \qquad G_A = \frac{30.6}{(s + 30.6)\left[\left(\frac{s}{272.9}\right)^2 + 2\left(\frac{0.5075}{272.9}\right)s + 1\right]}$$

SYSTEM	ELEMENT					
	K_p	K_a	G_{f_f}	G_{f_a}	G_{s_1}	G_{s_2}
Baseline (no treatment)	1	0	1	0	1	1
Gain Stabilized Reference	1	0	1	0	$\frac{[s^2 + 2(0.01)12.5s + 12.5^2]}{[s^2 + 2(0.30)12.5s + 12.5^2]}$	$\frac{40.0^2}{[s^2 + 2(0.5)40.0s + 40.0^2]}$
Phase I HPS	1.0	0.8	$\frac{0.025(s + 1000)}{(s + 25)}$	$\frac{2.083(s + 12)}{(s + 25)}$	$\frac{25}{(s + 25)}$	1.0
Initial Phase II HPS	1.0	0.8	$\frac{0.025(s + 1000)}{(s + 25)}$	$\frac{2.083(s + 12)}{(s + 25)}$	$\frac{(s + 40)}{40}$	1.0
Final Phase IIa HPS	1.0	0.8	$\frac{0.025(s + 1000)}{(s + 25)}$	$\frac{2.083(s + 12)}{(s + 25)}$	$\frac{(s + 40)}{40}$	$\frac{2.5(s + 10)}{(s + 25)}$

Figure 4. Flight Control System Block Diagram

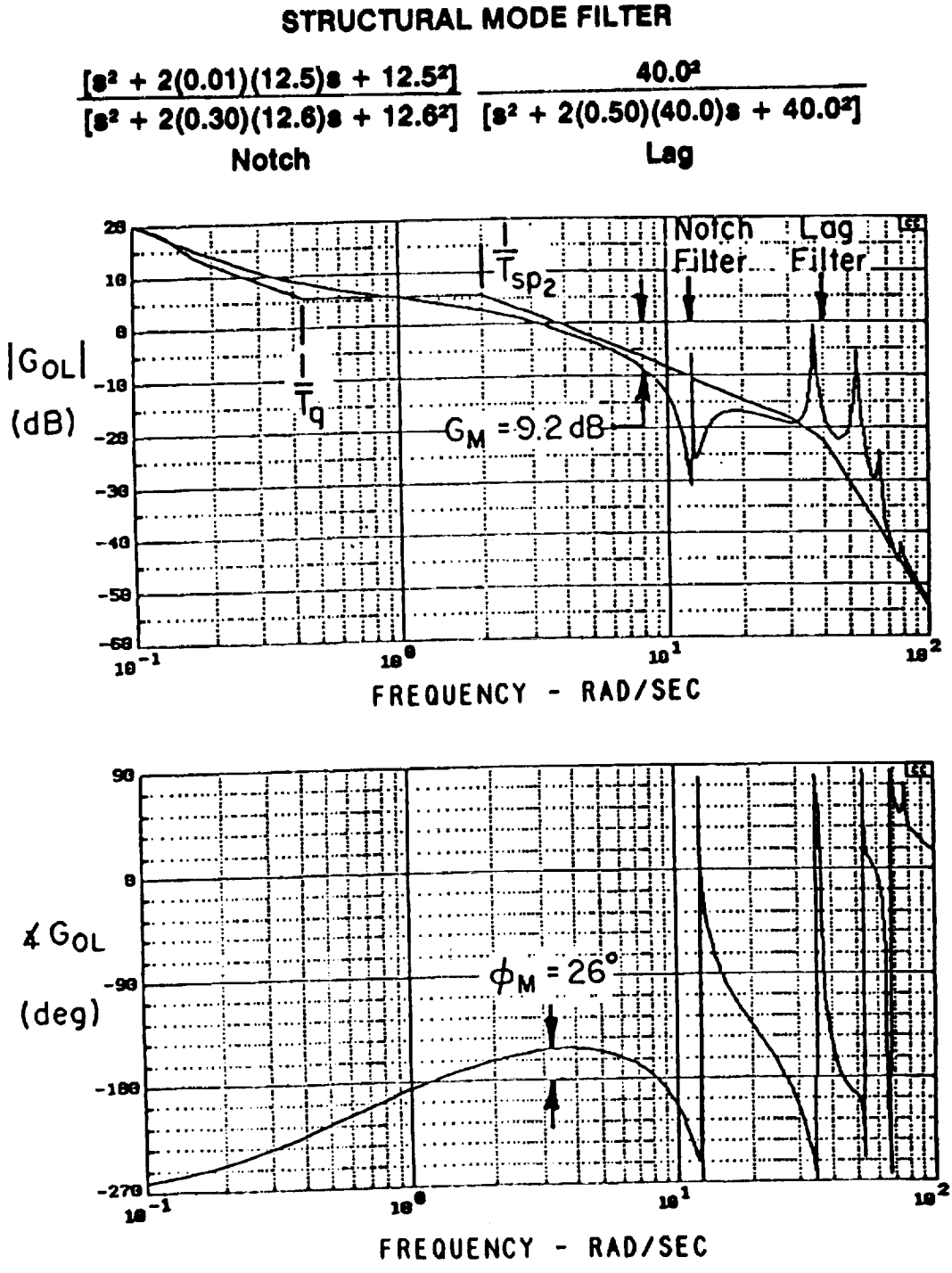

Figure 5. Frequency Response of the Conventional Gain Stabilized Reference Design

The requirement motivating HPS is the need to reduce effective time delay associated with the notch and lag filters used in conventional gain stabilized designs. As will be seen, HPS provides significant time delay reductions as well as improvements in stability. The disadvantages of HPS are associated with increased "residual (uncommanded) response" arising from the structural modes. In addition, because phase stabilization depends on the proper placement of open loop structural zeros, there is concern about the robustness of phase stabilized designs with respect to uncertainty in these zeros. However, conventional designs have their own robustness problems if notch filters are not placed and scheduled properly. The robustness issue is discussed in Section III.

The initial investigations of Phase I led to the approach of phase stabilizing only the first structural mode and using a lag filter (but no notch filter) to gain stabilize the higher frequency mode. This was truly a hybrid architecture where application of phase stabilization only to the first structural mode maximized the reduction of effective time delay (by eliminating the low frequency notch). It also minimized robustness problems on the assumption that at least the first structural mode zero could be defined with reasonable certainty.

The potential of this strategy can be seen in Figure 6, a special root locus plot in the region of the first structural mode. Here, the basic (rigid body) pitch loop is closed (with only the G_c equalization) using the pitch rate signal from one of four different gyro locations for each closure. The range of zero locations seen in Figure 6 suggests that, by blending signals from several gyros, an effective zero could be located to insure phase stability of the first structural mode. This was done in the Phase I HPS design as documented in Ref. 1. The G_{f_a} and G_{f_f} filters in the forward and aft pitch rate signal paths, as shown in Figure 4, allow the effective zero to be placed at will. Figure 7 shows a system survey of the pitch loop closure for the Phase I HPS design.

The first level of assessments for all of the designs are related to stability. These are summarized in Table 1 in terms of gain, phase and time delay margins. The last column is effective time delay which is not strictly a stability issue for the flight control system loop closure, but is of primary concern for the human pilot's closed loop manual control. The cells in Table 1 are hatched where the corresponding stability metrics do not meet the MIL-F-87242 requirements. (Note there is no MIL-spec requirement on delay margin). It can be seen that all of the designs fail to meet the low frequency gain margin specification. This occurred because no specific effort was made to meet this specification

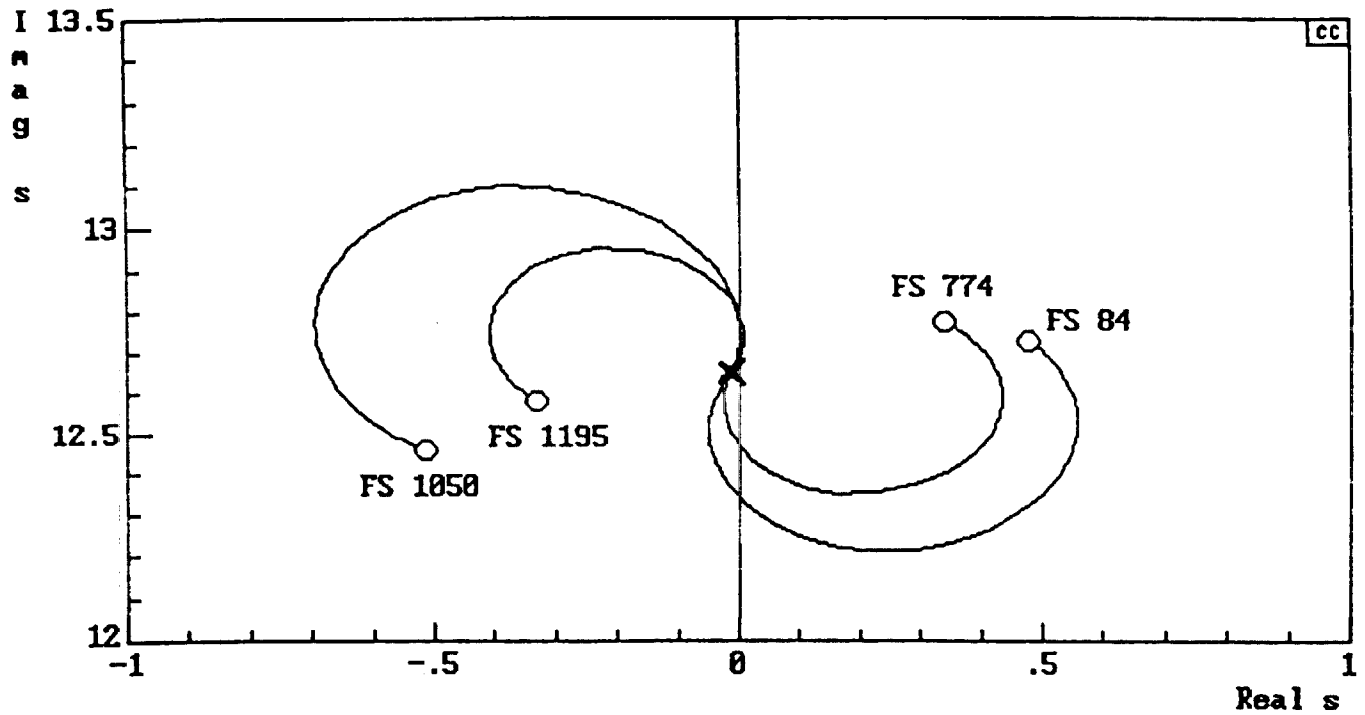

Figure 6. Pitch Loop Closures at the FIrst Bending Mode for Four Sensor Positions

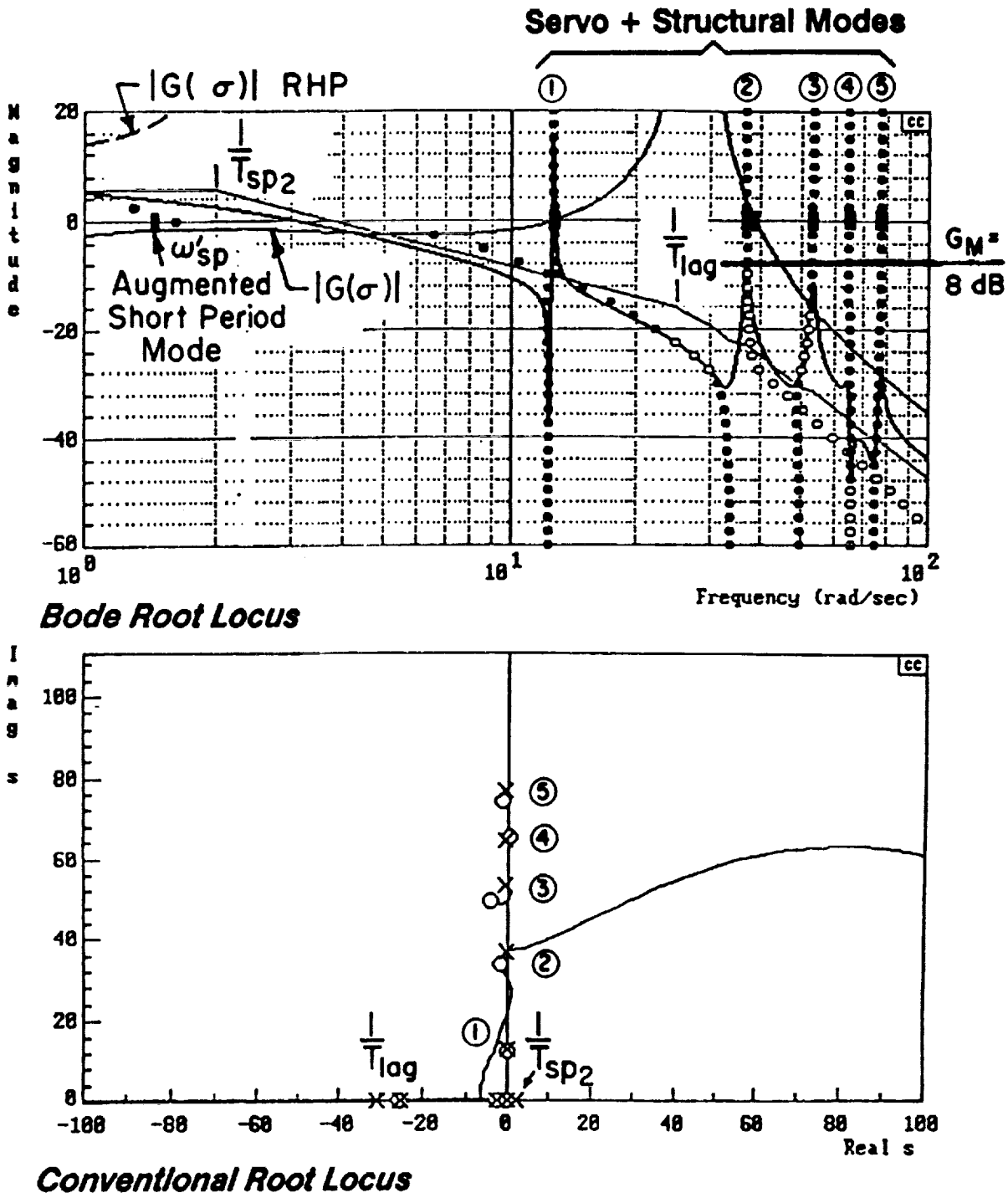

Figure 7. Phase I HPS Pitch Loop Closure

Table 1. Comparison of Stability Metrics

GAIN MARGIN			PHASE MARGIN				Delay Margin	Time Delay
Design Case	GM(dB) @ Low Freq. -180° Crossover	GM(dB) @ High Freq. -180° Crossover	ϕ_M (deg) Low Freq.	ϕ_M (deg) 1st Flexible Mode	ϕ_M (deg) 2nd Flexible Mode	ϕ_M (deg) 3rd Flexible Mode	τ_M (sec) (higher better)	τ_e (sec) (lower better) ($\omega > 9$ r/s)
Requirement MIL-F-87242	6.0	8.0	45	60	60	60	N/A	0.10
Baseline (no treatment)	5.13	< 0	41.8	N/A	N/A	N/A	0.223	0.051
Gain Stabilized Ref. Design	5.0	9.20	26.2	N/A	N/A	N/A	0.142	0.218
HPS Phase I	5.20	20.26	35.3	31.6	N/A	N/A	0.192	0.077
Initial HPS Phase II	5.48	16.53	47.6	74.75	124	52.02*	0.256	0.048
Final HPS Phase IIa	5.75	8.51	60.6	97	79.8	27.2*	0.306	0.036

* Phase Stable

which is not of particular concern in this study. This issue is discussed briefly in Appendix A.

The major problem of the gain stabilized reference design is the expected large effective time delay which greatly exceeds the MIL-F-87242 maximum. The initial Phase I design resulted in a significant reduction in the effective time delay below the MIL-spec limit. Both the gain stabilized design and the Phase I HPS design also fail to meet the low frequency phase margin requirements, although the Phase I HPS design comes significantly closer. The stability assessment of the Phase II HPS designs will be discussed in the following subsections.

Stability can also be viewed by comparing the closed loop damping ratios of the structural modes. This only provides some insight into the relative effect of the different designs on structural damping. Phase stabilization should generally increase closed loop damping and this is seen, for the first structural mode, when the Phase I HPS design is compared to the gain stabilized reference design. However, as shown in Table 2, the damping ratios for the second and third structural modes are actually reduced by the Phase I HPS design. This is consistent with the fact that no attempt was made to extend phase stabilization to higher modes to enhance the damping. Assessing the overall significance of these various damping ratios requires measures of residual response which will be addressed in Section IV. In terms of residual response, however, the Phase I HPS design was judged significantly deficient (Ref. 1) and this largely motivated the Phase II HPS refinements discussed next.

Table 2. Comparison of Flexible Mode Damping Ratio

Design Case	Flexible Mode Closed Loop Damping Ratios				
	1st Mode	2nd Mode	3rd Mode	4th Mode	5th Mode
Gain Stabilized Ref.	0.00097	0.01940	0.01070	0.00942	0.00998
Phase I HPS	0.00471	0.00629	0.00815	0.01020	0.09700
Initial Phase II HPS	0.00781	0.01640	0.00808	0.01080	0.01040
Final Phase IIa HPS	0.00842	0.02870	0.01490	0.01040	0.01310

3. The Initial Phase II HPS Design

The essence of the Phase I HPS design process was to position the zero more or less directly below its companion pole in the first flexible mode dipole. The separation of the pole and zero is set by adjusting the lead in the filter G_{f_a} in the aft gyro signal path. In the Phase I design this lead was set at 12 rad/sec. Among the first refinements considered in Phase II was adjustment of the first flexible dipole separation using the G_{f_a} filter. A survey of the sensitivity to the zero of this flexible dipole, beyond what was done in Phase I, revealed that there was very little potential for design improvement at this level (Ref. 4).

Thus, the Phase I HPS design was examined at a more fundamental level in a search for improvements. The Bode root locus of Figure 7 indicates that the second structural mode is critical in the Phase I HPS design. (The dots in the Bode root locus are open where the closed loop roots are unstable indicating a gain margin of about 8 dB at the second mode). However, examination of the overall Figure 7 system survey reveals some basic topological anomalies in the root loci of this design. These are seen most readily in the conventional root locus of Figure 7 where the locus departs directly to the right half plane from the second flexible mode. The companion zero is serviced by a locus emerging from the real axis. Thus, in a sense, this design causes the rigid body dynamics to couple to the structural dynamics in a way that is not particularly desirable. Furthermore, examination of the third structural dipole shows that, while it is phase stable in configuration (i.e., the zero is below the pole), the local root locus does not reflect this. It is not concave into the left half plane based on the Figure 1 ideal.

This insight focused development on the potential for phase stabilizing the next several structural modes as well as the first. Figure 8 displays the root loci near the second and third flexible modes. As in Figure 6, the basic (rigid body) pitch loop is closed (with only the G_c equalization) using the pitch rate signal from just one of four different gyro locations for each of four closures. It can be seen that, as with the first flexible mode, blending the FS 84 and FS 1050 pitch rate signals has some apparent potential for phase stabilizing the second and third flexible mode.

Thus, the basic pitch blending used in the Phase I HPS design was examined at the second and third flexible modes as was done for the first mode in the Phase I HPS design (Ref. 1). As shown in Figure 9, the blending of the FS 84 and FS 1050 sensor signals, using the established blending filters but with no lag in G_{s1}, was treated as a root locus

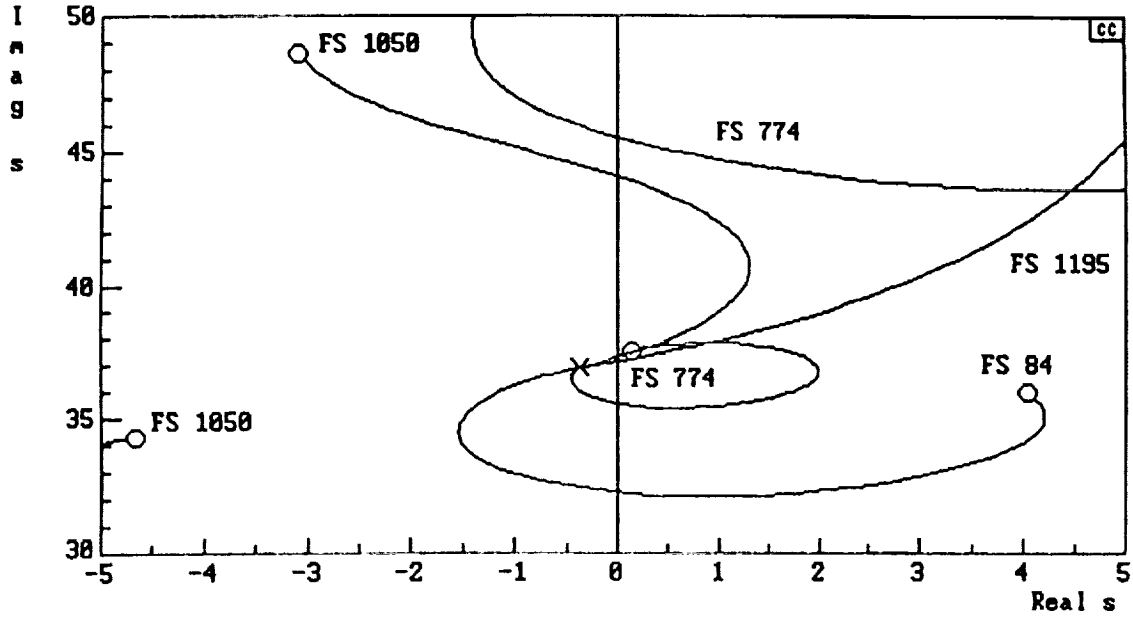

a) Second Structural Mode

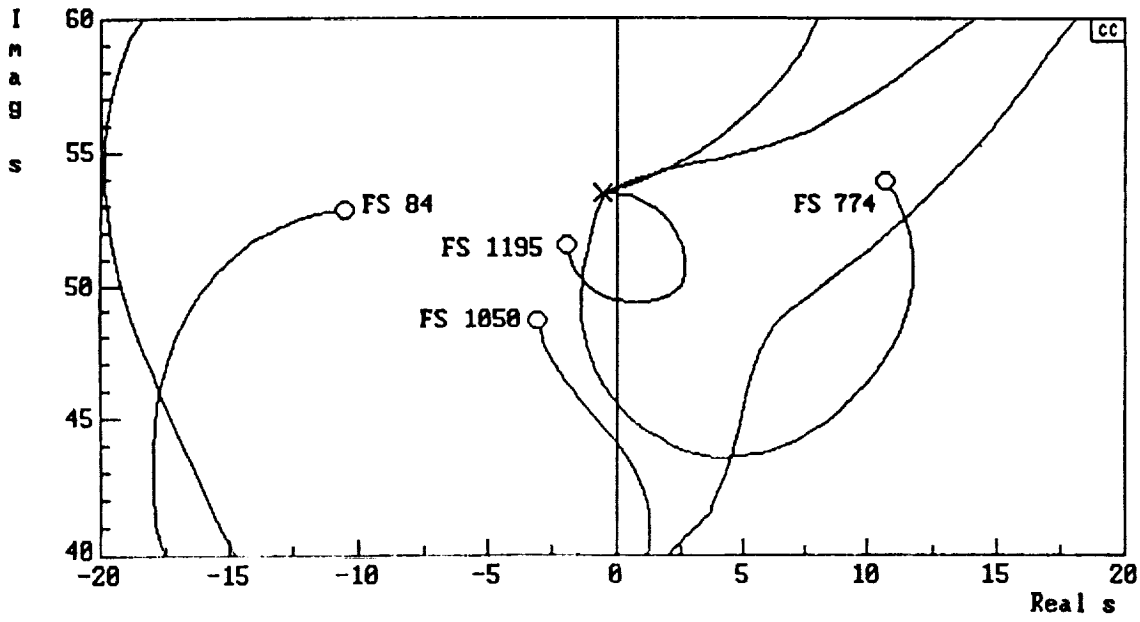

b) Third Structural Mode

Figure 8. Root Locus of 2nd and 3rd Bending Modes for Each of Four Sensor Positions

problem. It can be seen that phase stable dipoles can be created using the same K_a and K_f gain of the original Phase I HPS design. This established the fact that the topological anomaly seen in the Figure 7 root locus was created by the lag in G_{s1}.

Having established that the next several flexible modes could also be phase stabilized, the lag filter in the element G_{s1} was replaced with a lead filter to achieve extended phase stabilization. To set the frequency of the lead, a survey was made in which the lead frequency was varied from 20 to 40 rad/sec. A lead frequency of 40 rad/sec was selected for two reasons. First, it provided the maximum potential damping of the four phase stabilized modes. Second, for the phase unstable fourth flexible mode, the selected lead filter provided the maximum gain margin.

Figures 10 and 11 show the system survey plots. From the Bode root locus plot in Figure 10, it can be seen that the 8 dB gain margin requirements have been exceeded by at least a factor of two. Note that all modes, except the fourth flexible mode, are phase stable. The Bode plots of Figure 11 show the gain and phase margins tabulated in Table 1.

This design constitutes the initial Phase II HPS design which is compared to the two Phase I designs in terms of the stability metrics in Table 1. The initial Phase II HPS design shows significant reduction in the effective time delay, an important result since this motivates the HPS concept. This design does not have the low frequency phase margin problem that the earlier designs exhibited. However, it does fail to meet the MIL-spec phase margin at the third flexible mode. This mode is phase stable so gain uncertainty is not a problem, but phase uncertainty (such as from unmodeled higher frequency modes) remains a concern.

The closed loop damping ratios of the structural modes with the initial Phase II HPS design are compared to those in the two earlier designs in Table 2. It can be seen that the damping ratios of the initial Phase II design are generally somewhat higher (first and second modes) or about the same as the HPS Phase I. However as noted above in connection with Table 2, the overall impact of these damping changes cannot be assessed without addressing residual response metrics as will be done in Section IV-A-3. But as shown in Figure 12, the closed loop pitch rate response (at the pilot's station, FS 84) to a unit step input does give some indication of the residual response. Comparisons of Figures 12 and 13 indicate that the residual response of this HPS design is similar to that of the HPS Phase I design, but both of these designs have more residual response than the gain stabilized reference. The dominant 2 Hz residual oscillation seen in the HPS designs

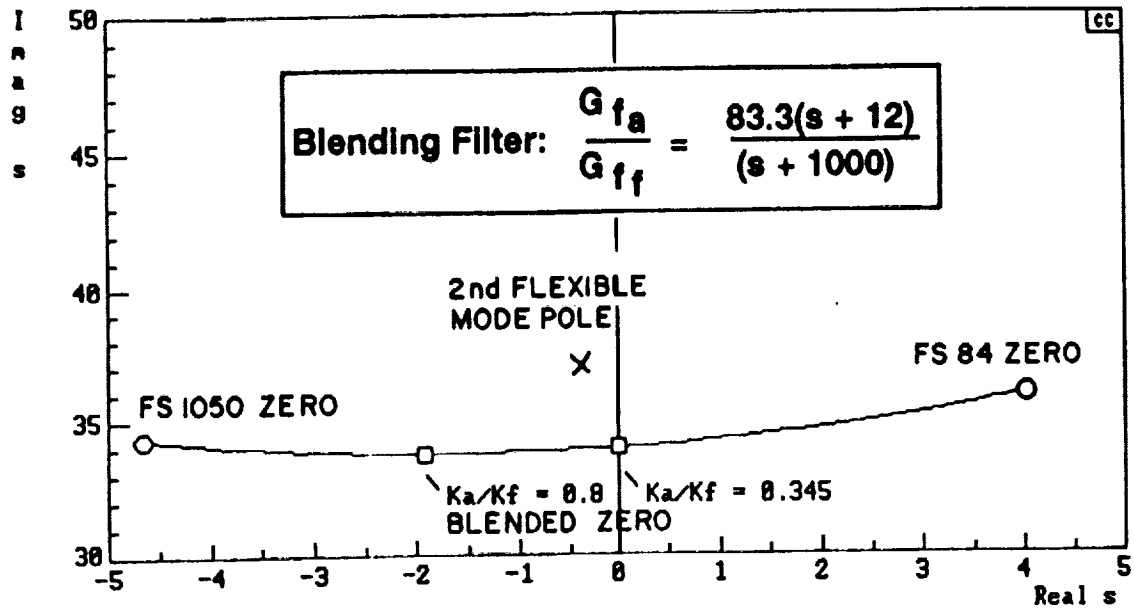

2nd FLEXIBLE MODE

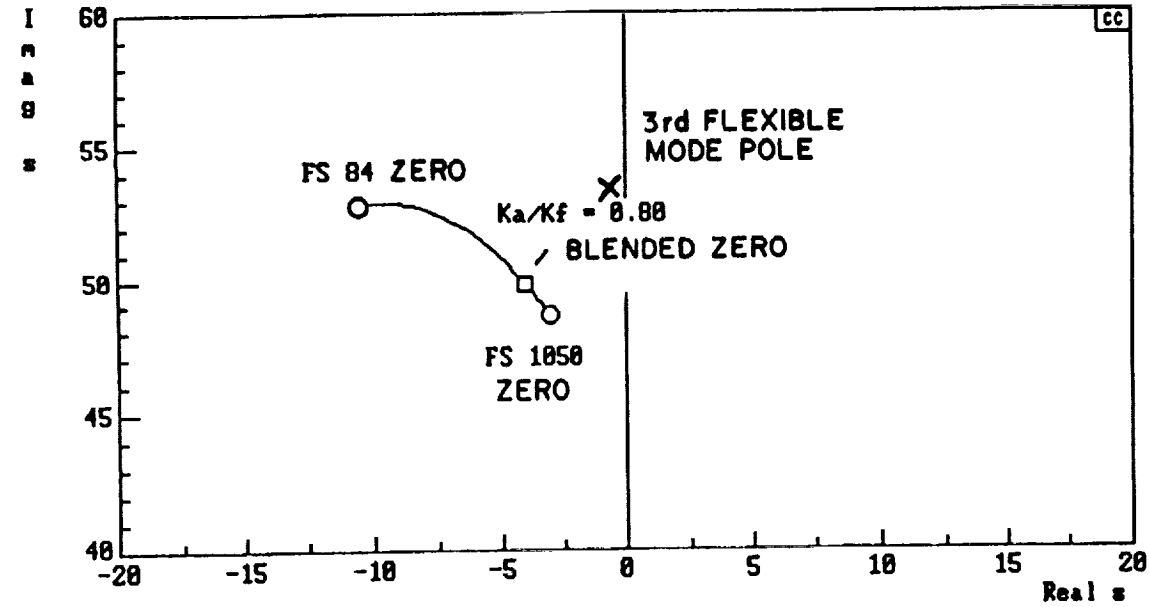

3rd FLEXIBLE MODE

Figure 9. HPS Blending of 2nd and 3rd Flexible Mode Numerator Zeros

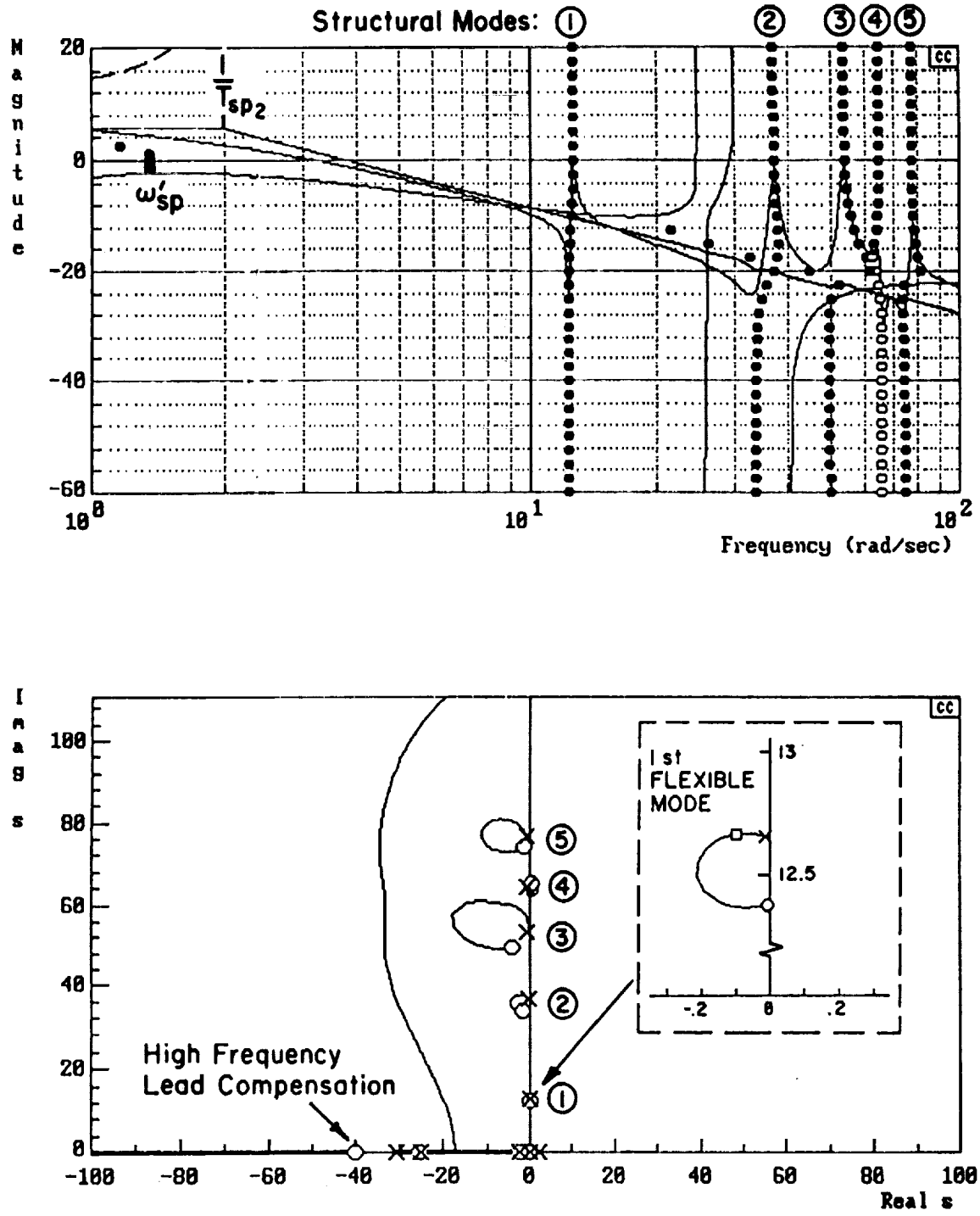

Figure 10. System Survey of the Initial Phase II Design with Phase Stable Higher Frequency Structural Modes

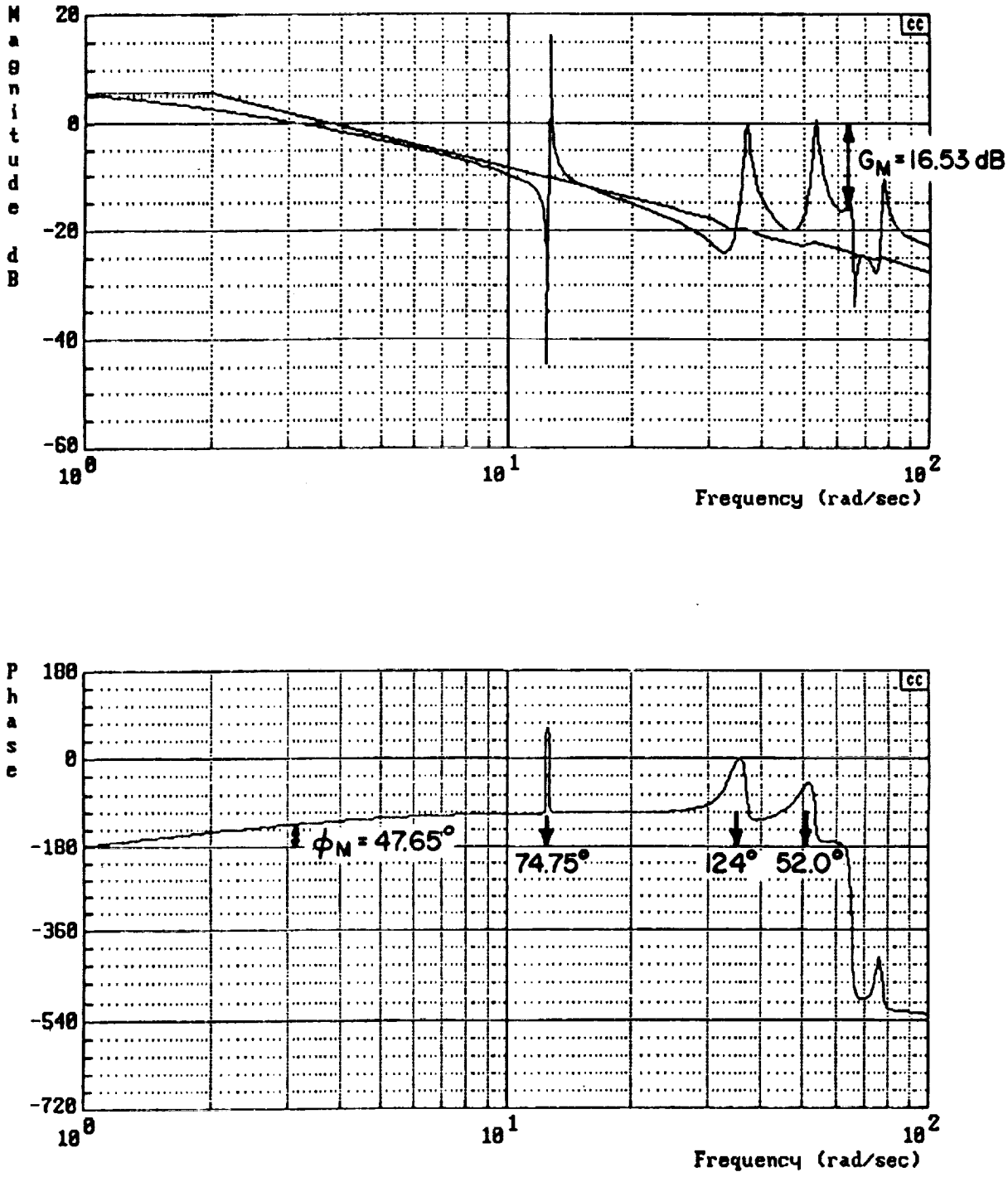

Figure 11. Open Loop Frequency Response for Initial Phase II HPS Design

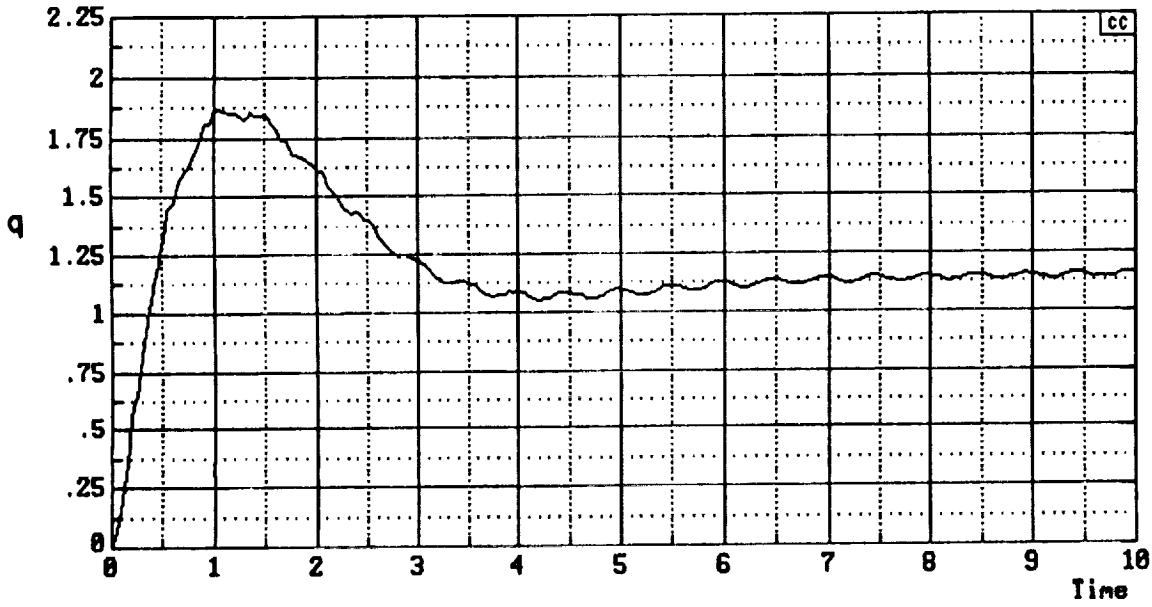

$$\left.\frac{q}{q_c}\right|_{C.L.} = \frac{\begin{array}{c}-6868.3\ (.169)(.44)(2.31)[-3.75E\text{-}02,\ 12.7](25)[-.1110,\ 36.3][.196,\ 53.9] \\ [-3.66E\text{-}02,\ 65.5][9.61E\text{-}03,\ 76.6](-1257.3)\end{array}}{\begin{array}{c}(.140)[.701,\ 1.347][(2.31)[7.81E\text{-}03,\ 12.66](24.8)(29.3)[1.64E\text{-}02,\ 37.2] \\ [8.08E\text{-}03,\ 54.0][1.08E\text{-}02,\ 64.6][1.04E\text{-}02,\ 77.2][.516,\ 265.7]\end{array}}$$

Figure 12. Closed Loop Pitch Rate Response at the Pilot's Station to a Unit Step Input for the Initial Phase II HPS Design

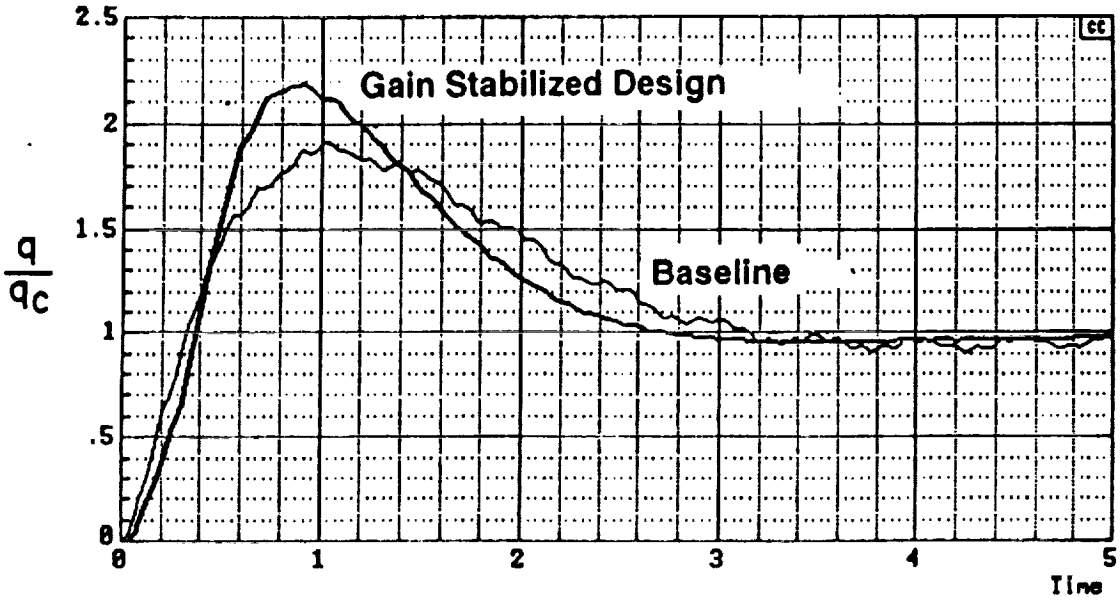

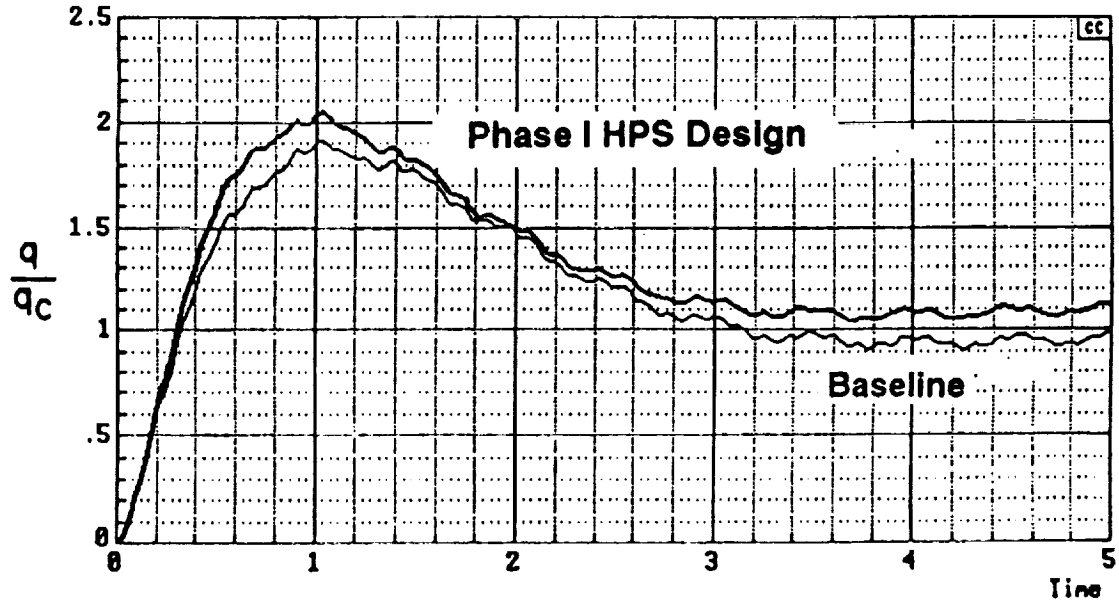

Figure 13. Response Comparison of Pitch Rate to Unit Pitch Rate Command

arises from the first structural mode which is, of course, notch filtered in the gain stabilized design.

In general, phase stabilization does have the potential to significantly reduce residual response by increasing the damping (as distinct from reducing magnitude of the response with a notch filter). However, this potential is not realized in the first two HPS designs. Insight into this can be obtained from examination of the root loci in Figures 10 and 14 for the initial Phase II HPS design. It can be seen that, for each of the structural modes, the actual damping ratio achieved is considerably less than what could be achieved if the loop gain was increased. It is important to note that a simple increase in the loop gain cannot be made to improve the flexible mode damping without seriously degrading the closed loop short period (rigid body) dynamics. Design alternatives to resolve this conflict lead to the final Phase IIa HPS design discussed in the next section.

4. The Final Phase IIa HPS Design

The basis of the final Phase IIa HPS design was to boost the loop gain in the flexible mode frequency range in order to increase the flexible mode damping without changing the loop gain in the region of the rigid body crossover which sets the closed loop short period dynamics. This suggested inserting a filter into the pitch loop, with unity gain at low frequencies and higher gain in the structural mode region. The first order lead-lag filter shown in Figure 4 was used in the G_{S2} element to accomplish this. An alternative of using a second order lead-lag filter was also examined (Ref. 4) but the first order filter selection proved superior and this Phase IIa HPS design is the only configuration that will be discussed here.

The system survey for the Phase IIa HPS design is shown in Figure 15. The zero of the lead-lag filter was placed at 10 rad/sec just below the first flexible mode frequency. This flattens the Bode asymptote which provides increased gain and thus increased damping to the phase stabilized flexible modes. The pole was placed at 25 rad/sec to gain stabilize the higher modes consistent with the HPS concept. This lag break frequency was selected to provide the required 8 dB gain margin at the fourth flexible mode - the only mode that is not phase stable.

From Table 1, it can be seen that the final Phase IIa HPS design results in the lowest effective time delay (36 msec) of the four designs. This is notably lower than the baseline system which has no added structural filters. This, of course, results from the

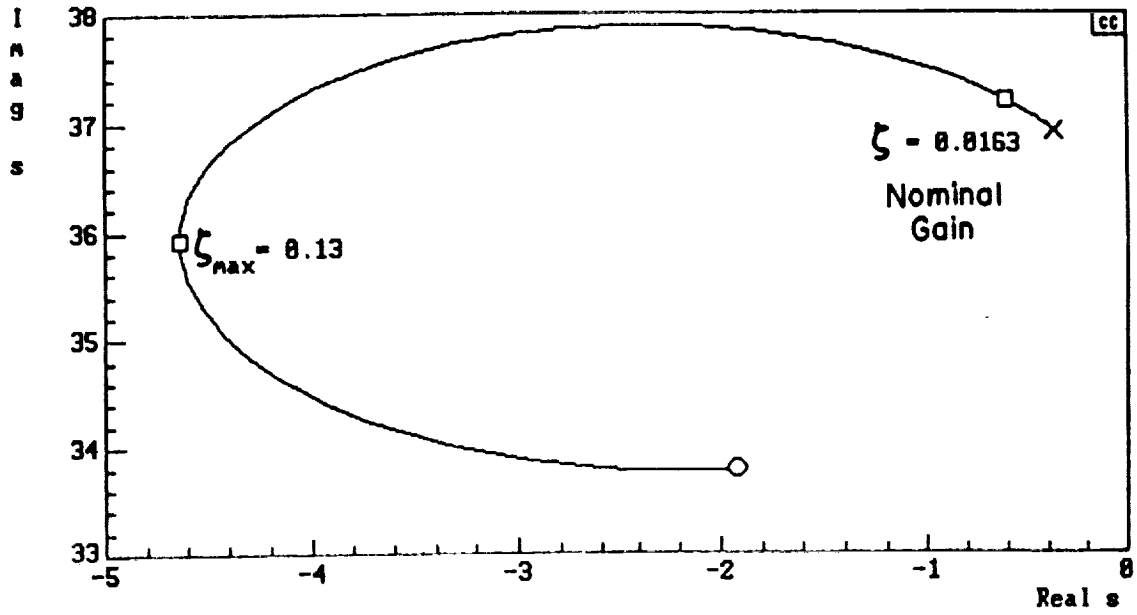

2nd FLEXIBLE MODE

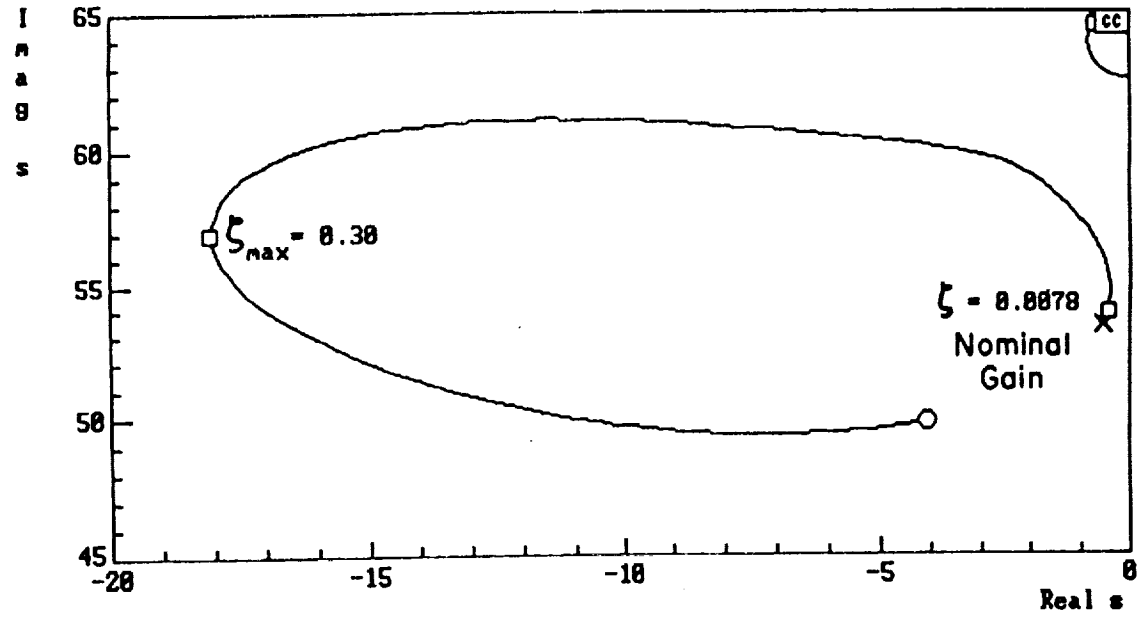

3rd FLEXIBLE MODE

Figure 14. Modal Damping Potential of Initial Phase II HPS Design

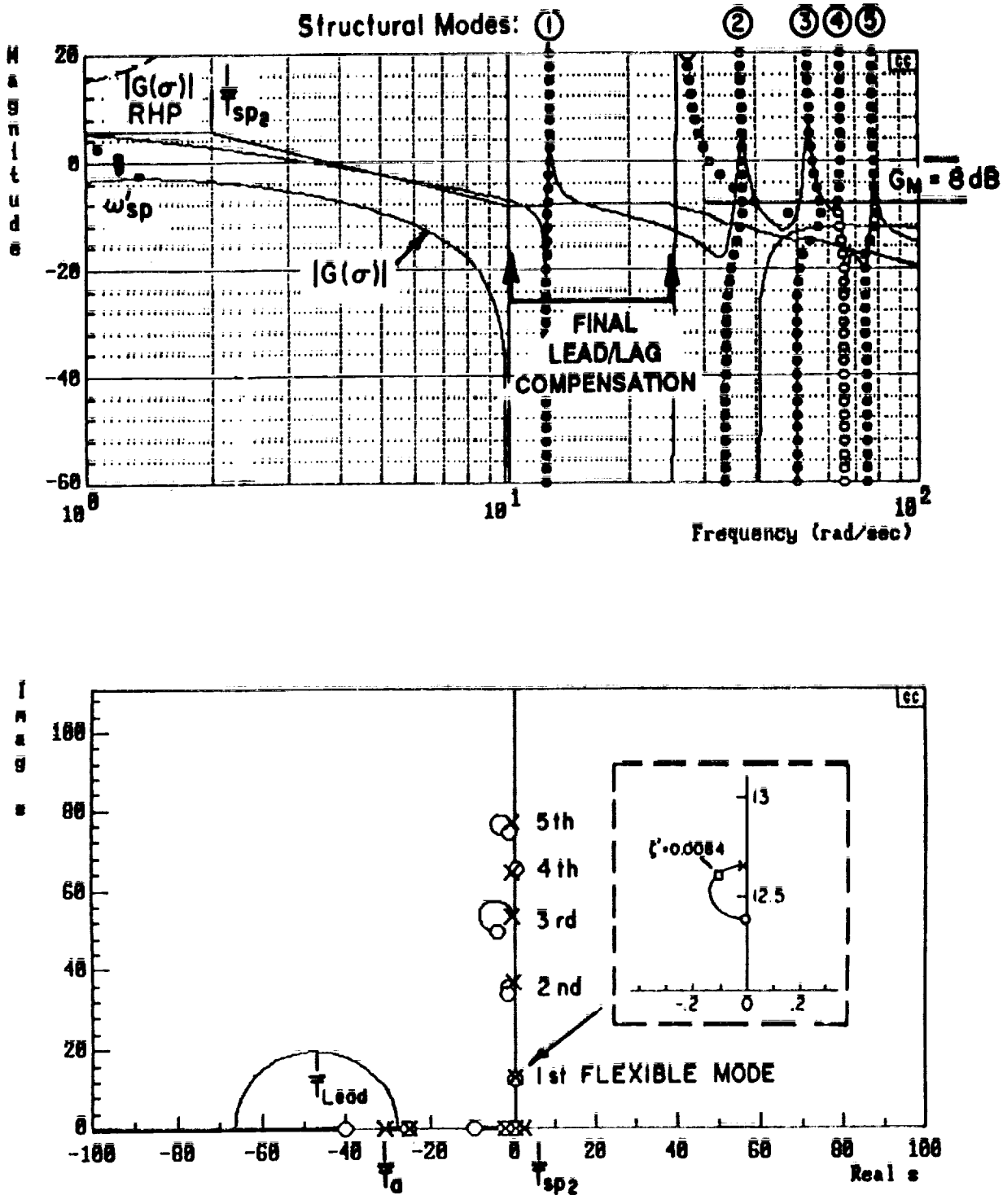

Figure 15. System Survey of Phase IIa HPS Pitch Loop Closure

lead introduced to increase the structural mode damping. It is worth noting that there are alternatives to phase stabilization which would also effectively introduce lead. For example, various pitch acceleration estimation schemes exist that are based on pitch rate measured at a single fuselage station. This suggests a more complete investigation of the relationship between these two concepts as part of future design refinements.

The gain and phase margins of the final Phase IIa HPS design are shown in Figure 16. There is a phase margin subtlety which applies to other designs and certainly should be noted for the final Phase IIa HPS design. Near structural modes, for example the second mode, the magnitude peaks cross the 0 dB line - an unconventional situation. Thus, there are phase margins defined at each of the zero crossings near the second flexible mode peak (-166.7° at 36.3 rad/sec and 79.8° at 37.8 rad/sec). The negative phase margin deserves some comment. The negative phase margin can be converted to a positive value by adding 360°. Hence, the phase margin -166.7° is equivalently 199.3°. By conventional reasoning, the smaller positive margin (i.e., 79.8°) is the more critical. In constructing Table 1, only the smallest positive phase margin of a modal pair is listed. However, for HPS designs, the customary thinking needs to be examined. This is done in Appendix B where it is noted that large positive phase margins do not necessarily imply robustness.

Table 1 indicates that the final Phase IIa HPS design meets all applicable MIL-spec requirements except, as with the initial Phase II HPS design, the phase margin at the third flexible mode. This phase margin is actually lower for the final Phase IIa HPS design than the initial Phase II design. As noted above, this mode is phase stable which reduces concern for gain uncertainty but not phase uncertainty.

The conventional root locus of Figure 15 shows that the damping of the first flexible mode has been slightly increased compared to the initial Phase II design (cf. Figure 10). Table 2 shows similar increases for the other phase stabilized flexible modes and, in fact, the final Phase IIa HPS design exhibits the highest structural damping ratios except for the fourth flexible mode where the initial Phase II HPS design produces higher damping. As noted previously, in connection with Table 2, no overall conclusions can be drawn from these damping ratios. The closed loop pitch rate response to a unit step pitch rate command shown in Figure 17 suggests some residual response improvement with respect to the initial Phase II HPS design, but the gain stabilized design still appears to have the advantage in residual response over all HPS designs. The significance of these differences will be addressed in Section IV.

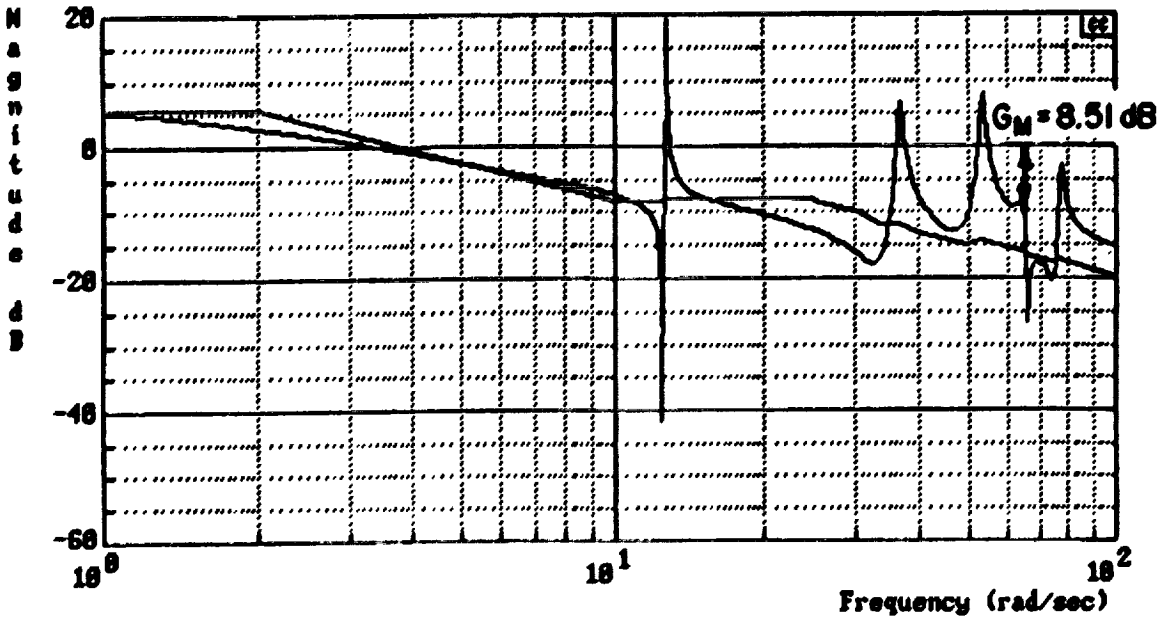

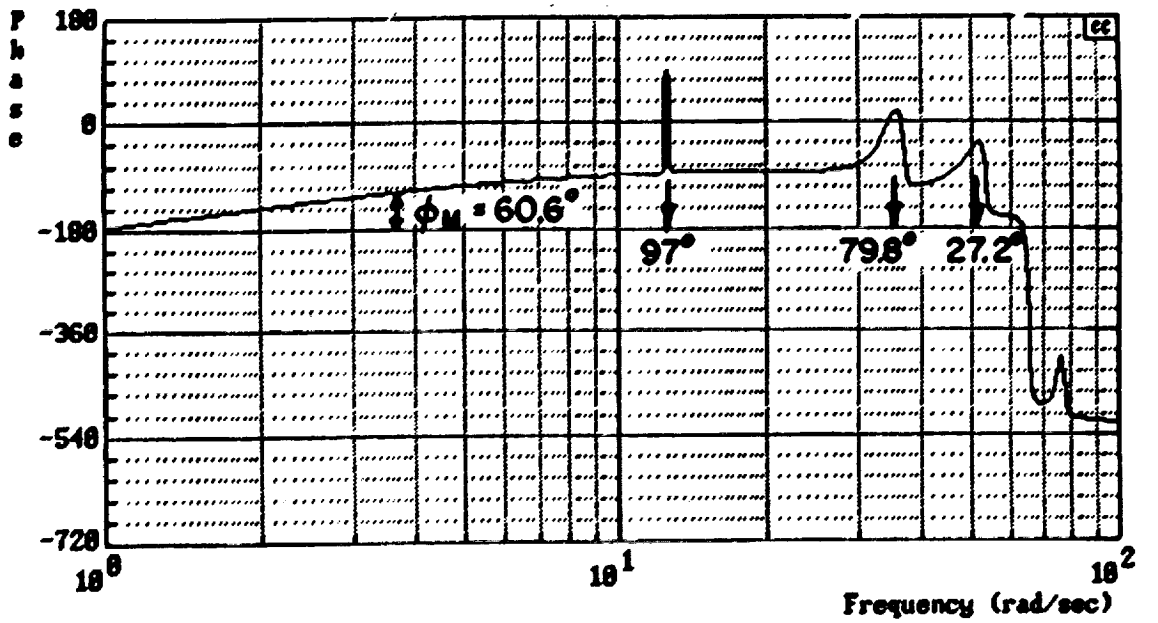

Figure 16. Open Loop Frequency Response of Final Phase IIa HPS Design

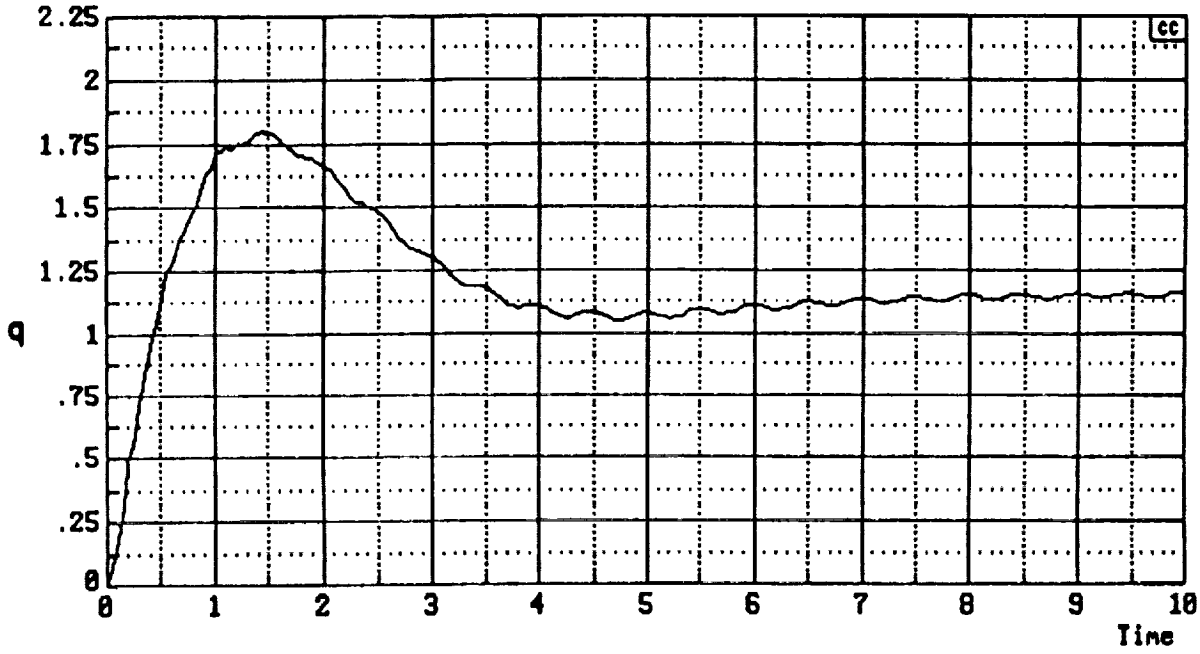

$$\left.\frac{q}{q_c}\right|_{C.L.} = \frac{-6870(\ .169)(\ .44)(\ 2.31)[-.0375,\ 12.7](\ 25)^2\ [-.111,\ 36.3]\ [\ .196,\ 53.9][-.0366,\ 65.5][\ .00961,\ 76.6](-1260)}{(\ .14)[\ .667,\ 1.2](\ 2.31)[\ .00842,\ 12.6](\ 25.3)[\ .958,\ 31.2]\ [\ .0287,\ 37.3][\ .0149,\ 54.8][\ .0104,\ 64.3][\ .0131,\ 77.6]\ [\ .526,\ 253]}$$

Figure 17. Closed Loop Pitch Rate Response at the Pilot's Station to a Unit Step Input for the Phase IIa HPS Design

Finally, it should be noted that the evolution of the HPS design has led to a final Phase IIa HPS design which is clearly unconventional. Specifically, the lead-lag filter in G_{s2} produces an effect directly opposite to the notch and lag filters used in conventional gain stabilization (which can be viewed as an "inverse notch" filter). The premise here is that the improved flexible mode damping will reduce the residual response to acceptable levels. This is certainly consistent with the original idea that HPS design is a matter of finding the best mix of gain and phase stabilization. This in turn suggests a formal optimal control approach. However, as will be further supported by the developments in Section IV, the complex and specialized design requirements of this problem require more attention at this point than the mechanics of optimization.

The very low value of effective time delay achieved in the final Phase IIa HPS design (36 msec) implies a potential for further design optimization. Because there is no benefit for grossly exceeding the MIL-spec requirement, the effective time delay could be relaxed to tune the design for other requirements. Again, it is the specialized requirements for HSV design that are most critical at this stage.

This page is intentionally left blank.

Section III

SENSITIVITY OF HPS DESIGNS TO STRUCTURAL UNCERTAINTIES

Variations in structural mode parameters can have a significant destabilizing effect on a control system that would otherwise be considered a good design with proper and adequate compensation of structural mode interaction. This section examines the sensitivity of HPS designs to structural uncertainties. Results of two gain stabilized designs are also included for reference and comparison.

A. Modeling

The flexible vehicle model was developed using FAMUSS, an aeroservoelastic modeling tool widely used at MCAIR (Ref. 5). The FAMUSS model can either be represented by a transfer function (pole-zero) form or the standard state space form. For a single-input single-output system, the generic state and output equations, respectively, are

$$\begin{aligned} \dot{\underline{x}} &= \mathbf{A}\underline{x} + \mathbf{B}u \\ y &= \mathbf{C}\underline{x} + \mathbf{D}u \end{aligned} \tag{1}$$

where

$$\mathbf{A} = \begin{bmatrix} \mathbf{A}_1 & & & \\ & \mathbf{A}_2 & & \mathbf{0} \\ & & \cdot & \\ & \mathbf{0} & & \cdot \\ & & & \mathbf{A}_j \end{bmatrix}$$

$$\mathbf{B} = [\,0 \;\; 1 \;\; \cdot \;\; \cdot\,]^T$$

$$\mathbf{C} = [\,\mathbf{C}_1 \;\; \mathbf{C}_2 \;\; \cdot \;\; \cdot \;\; \mathbf{C}_j\,]$$

$$\mathbf{D} = d \;.$$

For the analysis that follows, three structural mode parameters are of primary concern: natural frequency (ω_s), damping ratio (ζ_s), and mode shape (ϕ_s). The FAMUSS

model lends itself nicely to incorporation of structural uncertainties. This becomes apparent by observing FAMUSS realization of **A** and **C**. Specifically, natural frequency and damping ratio are uniquely defined in **A** while mode shape is contained in **C**. Using the subscript "i" to indicate the ith structural mode,

$$\mathbf{A}_i = \begin{bmatrix} 0 & 1 \\ -\omega_{s,i}^2 & -2\,\zeta_{s,i}\,\omega_{s,i} \end{bmatrix}$$

$$\mathbf{C}_i = \phi_{s,i} \quad . \tag{2}$$

This realization allows direct substitution of the nominal values of natural frequency, damping ratio and mode shape with some new values that represent variations of these structural parameters. The new or corrupted values can be expressed as follow:

$$\begin{aligned} \omega'_{s,i} &= \left(1 \pm \Delta_\omega\right)\omega_{s,i} \\ \zeta'_{s,i} &= \left(1 \pm \Delta_\zeta\right)\zeta_{s,i} \\ \phi'_{s,i} &= \left(1 \pm \Delta_\phi\right)\phi_{s,i} \end{aligned} \tag{3}$$

where Δ_ω, Δ_ζ, and Δ_ϕ are the normalized uncertainty levels for natural frequency, damping ratio, and mode shape, respectively. Note that these parameters can be varied independently.

Figure 18 shows the frequency response characteristics of the flexible vehicle model alone. The mode shape uncertainty changes the slope while natural frequency uncertainty primarily shifts the structural mode up and down. Although not obvious from the figure, damping ratio uncertainty changes the peaks and valleys of the frequency response.

The pole-zero characteristics of the flexible vehicle model can be seen by expressing the input-output relationship in terms of the system matrices, i.e.,

$$\frac{\underline{y}}{u} = \frac{\mathbf{C}\,\mathrm{Adj}(s\mathbf{I}-\mathbf{A})\mathbf{B} + \det(s\mathbf{I}-\mathbf{A})\mathbf{D}}{\det(s\mathbf{I}-\mathbf{A})} \quad . \tag{4}$$

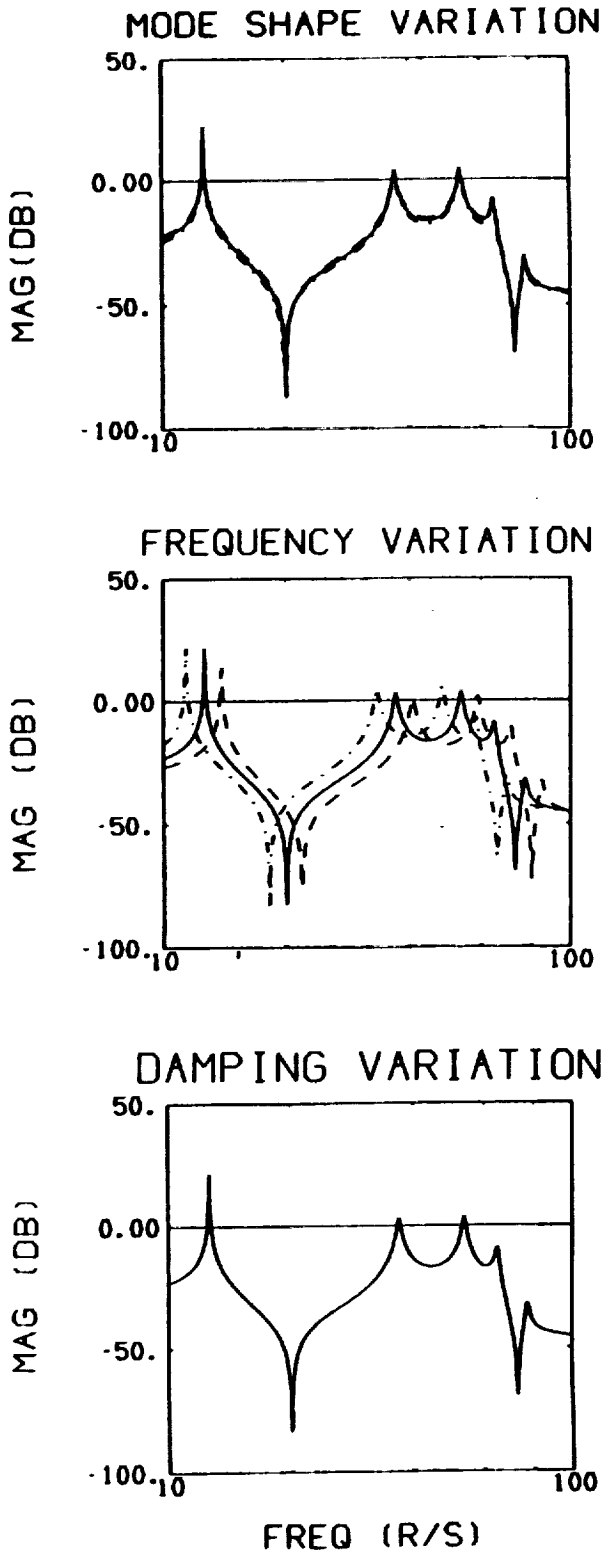

Figure 18. Frequency Responses of a Flexible Vehicle Subject to Structural Uncertainties

Equation 4 suggests that while mode shape uncertainty affects only the zero location of a structural mode, natural frequency and damping ratio uncertainties alter both pole and zero locations of a structural mode.

The uncertainty levels associated with the structural dynamics of the Space Shuttle Orbiter (Ref. 6) are listed in Table 3. These uncertainty levels were chosen for this contract since the Space Shuttle Orbiter is the only operational hypersonic vehicle to date. The same set of data was also used in the Modern Aerospace Vehicle Robust H-Infinity Control (MAVRIC) program, published in Ref. 7.

B. Analysis

The design evaluation space includes two gain stabilized and two HPS designs. The first gain stabilized design, labeled GS-I, is the gain stabilized reference design shown in Figure 4. The second gain stabilized design, labeled GS-II, employs a more conservative approach to gain stabilization than GS-I. The two HPS designs are Phase I and final Phase IIa HPS designs. Specific characteristics identifying each design are summarized in Table 4. It must be emphasized that each design will be evaluated against its own reference case, i.e., one that has no variation in any of the three structural mode parameters of interest.

Since the damping ratio uncertainty level was rather small, the uncertainty level was arbitrarily increased from ±2% to ±15%. The effect of this damping ratio uncertainty alone was determined. It was found that both HPS and gain stabilization were insensitive to variations in damping ratio. Thus, damping ratio was held at nominal value (i.e., $\Delta\zeta = 0$) in subsequent analyses.

Table 3. Structural Mode Uncertainty Levels

PARAMETER	UNCERTAINTY LEVEL (%)
Frequency	±10
Mode shape	±15
Damping ratio	±2

Table 4. Design Evaluation Space

GS-I	GS-II	PHASE I HPS	PHASE IIA HPS
Use of fwd sensor signal only	Use of fwd sensor signal only	Blending of fwd and aft sensor signals to phase stabilize first mode	Blending of fwd and aft sensor signals to phase stabilize first mode
Notch and low pass filters to gain stabilize structural modes	Notch and low pass filters to gain stabilize structural modes	First order lag to gain stabilize higher frequency structural modes	First order lead to enhance loci of higher structural modes
Aimed to achieve 8 dB gain margin (standard definition)	Aimed to achieve 8 dB peak clearance	--	First order lead-lag to increase structural damping

The stability margin results of the two gain stabilized designs are shown in Tables 5 and 6. As expected, the low frequency gain and phase margins as well as the high frequency gain margin (at ω_{HF1}) compare well with the reference case in the control bandwidth region (with frequency < 10 r/s).

In the structural mode region (with frequency > 10 r/s), as the structural modes move up and down due to variation in frequency, the notch filter frequency no longer coincides with the structural mode frequency, causing insufficient gain attenuation at the first mode. This in turn causes the magnitude of the first mode to cross over the zero dB line resulting in an additional phase margin. See Figures 19 and 20. Note from Table 5 or Figure 19 that another phase margin exists at the second mode for GS-I. This can be explained by recognizing that instead of meeting the more conservative 8 dB peak clearance, the GS-I design goal is to meet only the 8 dB gain margin definition. Table 5 indicates that several gain margins at ω_{HF3} (in the vicinity of the first mode) are well below the 8 dB spec. In addition, negative phase margins exist at the first mode for the cases with +10% frequency variation. Unlike Phase IIa HPS design (cf. Section II-B-4), the negative phase margin here implies instability. A detailed discussion of interpreting negative phase margin is provided in Appendix B.

The sensitivity results of GS-II is shown in Table 6. When compared with GS-I, GS-II appears to be more robust in meeting the gain margin requirement. This happens at the expense of a reduced low frequency phase margin, however. The phase margins at the first mode for GS-II do not quite meet the 60° spec. As expected, the results suggest that

Table 5. Sensitivity of Gain Stabilized Reference (GS-I) Design to Structural Uncertainties

Variations (%)		Phase Margins (Deg)			Gain Margins (dB)						
Mode Shape	Freq	Low Freq	1st Mode	2nd Mode	Low Freq	ω_{HF1}	ω_{HF2}	ω_{HF3}	ω_{HF4}	ω_{HF5}	ω_{HF6}
		~3.2 r/s	~11.3 r/s	~33 r/s	~1.2 r/s	~ 8.3 r/s	~12.5 r/s	~13.8 r/s	~26 r/s	~44 r/s	~65 r/s
0	0	26.15	--	--	-4.88	9.17	--	--	18.45	21.71	26.96
0	-10	25.65	81.94	131.97	-4.84	8.66	--	--	17.77	15.07	24.41
0	+10	26.51	-77.81	--	-4.90	9.49	40.04	5.32	18.88	22.86	30.20
-15	0	26.44	--	--	-4.90	9.35	--	--	18.56	22.31	28.39
-15	-10	26.02	84.80	154.13	-4.87	8.89	30.29	31.89	17.93	17.89	25.63
-15	+10	26.75	-98.94	--	-4.92	9.64	40.01	6.61	18.95	23.29	31.72
+15	0	25.85	--	143.43	-4.85	8.99	--	--	18.34	21.00	25.78
+15	-10	25.28	79.63	117.78	-4.81	8.44	--	--	17.62	13.08	23.36
+15	+10	26.26	-60.31	--	-4.88	9.35	40.06	4.19	18.81	22.41	28.92
Mil-spec.		*45*	*±60*	*±60*	*-6*	*6*	*8*	*8*	*8*	*8*	*8*

Table 6. Sensitivity of Gain Stabilized II (GS-II) Design to Structural Uncertainties

Variations (%)		PM (Deg)		Gain Margins (dB)						
Mode Shape	Freq	Low Freq	1st Mode	Low Freq	ω_{HF1}	ω_{HF2}	ω_{HF3}	ω_{HF4}	ω_{HF5}	ω_{HF6}
		~3.2 r/s	~11.3 r/s	~1.2 r/s	~7.7 r/s	~11.8 r/s	~12.5 r/s	~19.8 r/s	~38.4 r/s	~64.9 r/s
0	0	23.92	--	-4.81	7.27	--	--	16.61	21.32	36.54
0	-10	23.42	*58.89*	-4.77	6.94	20.09	39.09	16.43	20.00	32.73
0	+10	24.29	188.96	-4.84	7.48	40.27	8.58	16.75	23.03	39.78
-15	0	24.22	--	-4.83	7.40	--	--	16.60	22.21	38.13
-15	-10	23.79	61.50	-4.80	7.11	19.61	39.70	16.45	20.70	34.24
-15	+10	24.53	192.52	-4.86	7.58	40.50	9.05	16.72	24.08	41.41
+15	0	23.62	--	-4.79	7.14	--	--	16.62	20.55	35.20
+15	-10	23.04	*56.76*	-4.74	6.78	20.61	38.45	16.42	19.38	31.44
+15	+10	24.04	186.13	-4.82	7.38	40.03	8.19	16.78	22.12	38.40
Mil-spec.		***45***	***±60***	***-6***	***6***	***8***	***8***	***8***	***8***	***8***

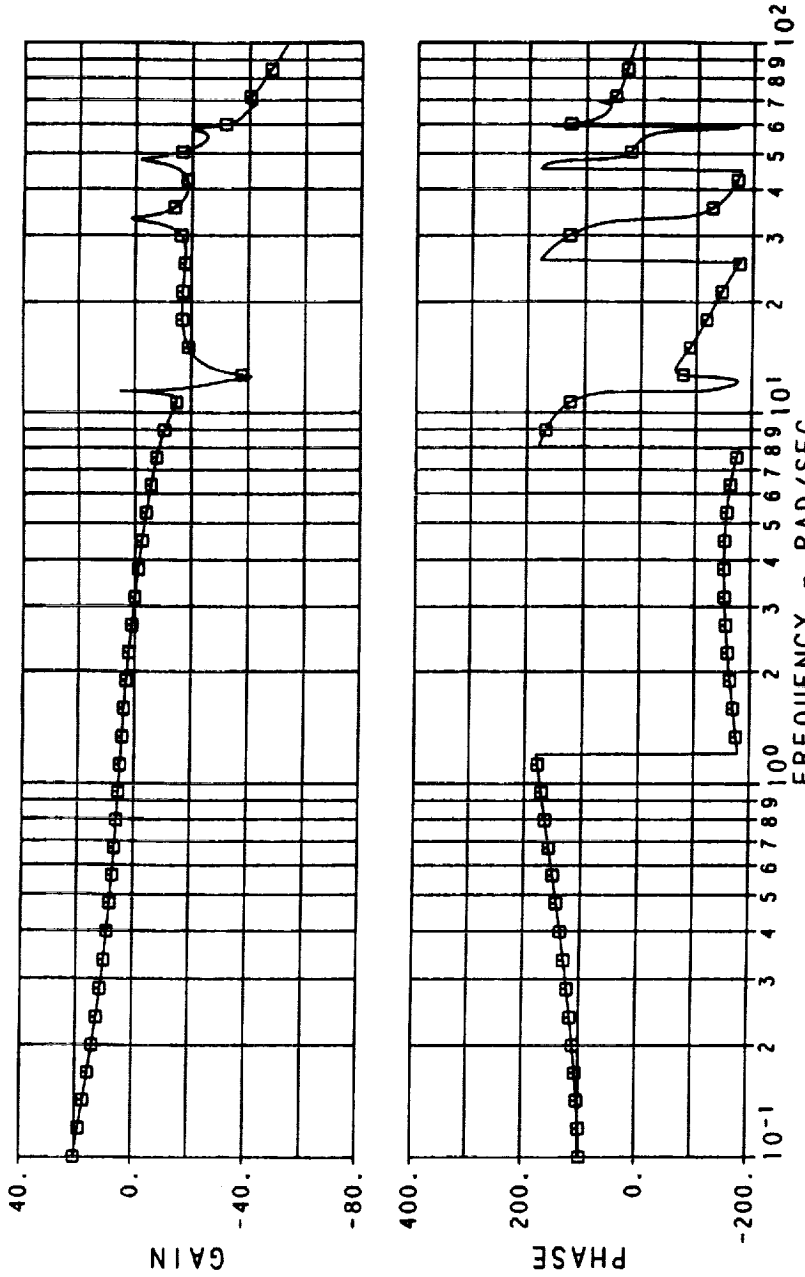

Figure 19. Frequency Response of GS-I Design with -10% Frequency Variation

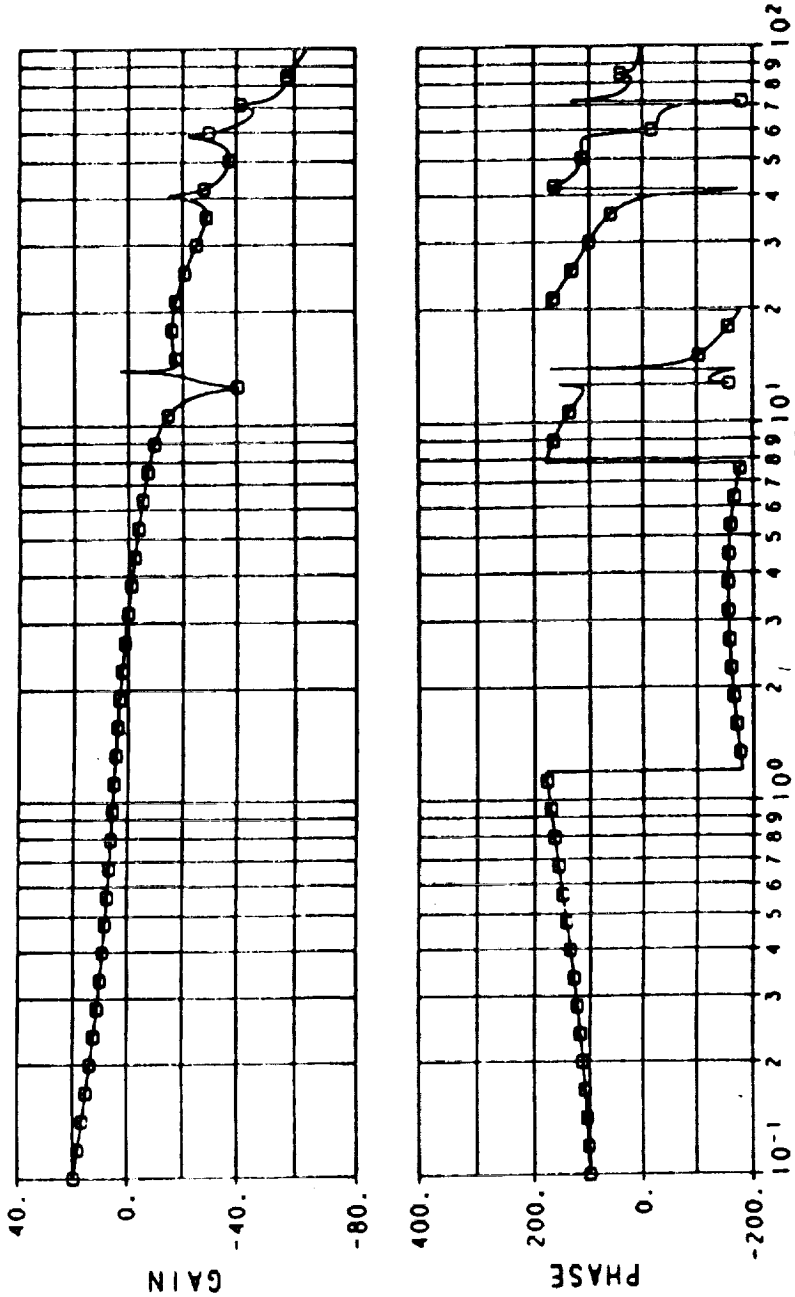

Figure 20. Frequency Response of GS-II Design with +10% Frequency Variation

gain stabilization, in general, is sensitive to variations in frequency, particularly at the first mode.

Tables 7 and 8 show the stability results of Phase I HPS and Phase IIa HPS, respectively. With the exception of a few cases where the gain margins actually fall below the desired value of 8 dB, the results do not show any significant cause for concern. Generally, HPS exhibits robust characteristics at the first elastic mode. This is illustrated in Figure 21. Conceptually, the objective of phase stabilization is to position the zero of a structural pole-zero pair below the pole. As shown in the figure, even in the presence of structural uncertainties, the right half plane zero can generally be placed somewhere below the pole. For higher frequency, the uncertainty regions of the pole and zero can potentially overlap. This obviously is a concern and thus a primary reason of the use of HPS instead of phase stabilization alone. Finally, like conventional gain stabilization, HPS is sensitive to variations in frequency, but it generally occurs at a much higher frequency.

Next, the root loci of the four designs are compared to its own reference case. It was observed that, when the frequency was varied, the root loci of GS-I and Phase I HPS were not maintained. See Figures 22 and 23. This would probably affect the loop gain sensitivity and ultimately the stability margins.

At this point, it would be unfair to claim that HPS is more robust than gain stabilization or vice versa. The point to make here is that each stabilization technique, whether it is gain stabilization or HPS, has its own unique problems and robustness characteristics. Tradeoff exists even within each individual class of stabilization techniques. The bottom line is that robustness or lack of it would likely not be the primary reason for prohibiting the use of hybrid phase stabilization.

Table 7. Sensitivity of Phase I HPS Design to Structural Uncertainties

Variations (%)		PM (Deg)		Gain Margins (dB)						
Mode Shape	Freq	Low Freq	1st Mode	Low Freq	ω_{HF1}	ω_{HF2}	ω_{HF3}	ω_{HF4}	ω_{HF5}	ω_{HF6}
		~3.2 r/s	~12.6 r/s	~1.06 r/s	~22.3 r/s	~30.3 r/s	~37.1 r/s	~49.7 r/s	~52.7 r/s	~65.7 r/s
0	0	35.47	31.54	-5.26	20.19	28.03	8.48	28.74	15.53	47.53
0	-10	35.74	35.13	-5.28	--	6.50	26.72	11.25	42.17	--
0	+10	35.27	30.91	-5.25	18.73	31.88	10.33	30.14	19.51	50.94
-15	0	35.28	--	-5.25	19.27	28.91	18.51	--	--	--
-15	-10	35.51	--	-5.27	--	16.66	25.42	20.91	--	--
-15	+10	35.12	--	-5.24	18.26	31.70	18.03	16.65	25.50	--
+15	0	35.63	--	-5.28	21.76	25.89	15.41	27.92	25.70	--
+15	-10	35.93	34.73	-5.30	--	14.72	26.25	18.33	--	--
+15	+10	35.40	--	-5.26	19.30	30.37	16.12	26.16	22.92	--
Mil-spec.		*45*	*±60*	*-6*	*8*	*8*	*8*	*8*	*8*	*8*

Table 8. Sensitivity of Phase IIa HPS Design to Structural Uncertainties

Variations (%)		Phase Margins (Deg)				Gain Margins (dB)	
Mode Shape	Freq	Low Freq	1st Mode	2nd Mode	3rd Mode	Low Freq	ω_{HF}
		~3.4 r/s	~12.5 r/s	~36.3 r/s	~52.3 r/s	~0.9 r/s	~63.4 r/s
0	0	61.08	96.97	79.71	27.01	-5.82	8.45
0	-10	61.27	97.01	81.20	24.79	-5.83	*7.24*
0	+10	60.94	96.71	79.54	29.94	-5.81	9.45
-15	0	60.95	97.00	82.49	30.38	-5.81	9.29
-15	-10	61.11	98.88	83.02	27.28	-5.82	8.13
-15	+10	60.83	96.91	82.62	34.32	-5.80	10.26
+15	0	61.21	97.05	77.88	24.75	-5.83	*7.70*
+15	-10	61.43	97.19	80.13	22.93	-5.84	*6.47*
+15	+10	61.04	96.62	76.77	27.16	-5.81	8.76
Mil-spec.		***45***	***±60***	***±60***	***±60***	***-6***	***8***

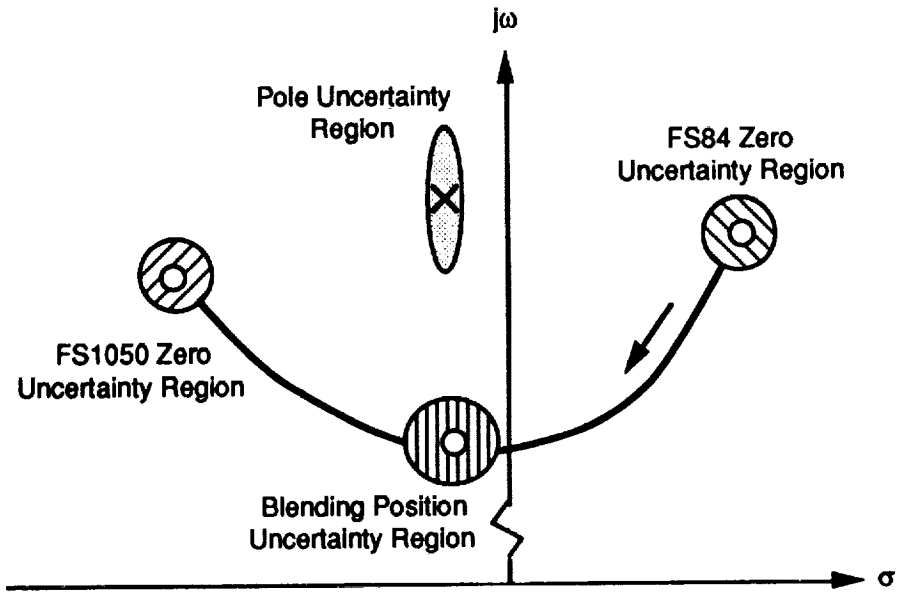

Figure 21. Conceptualization of Phase Stabilization in the Presence of Uncertainties

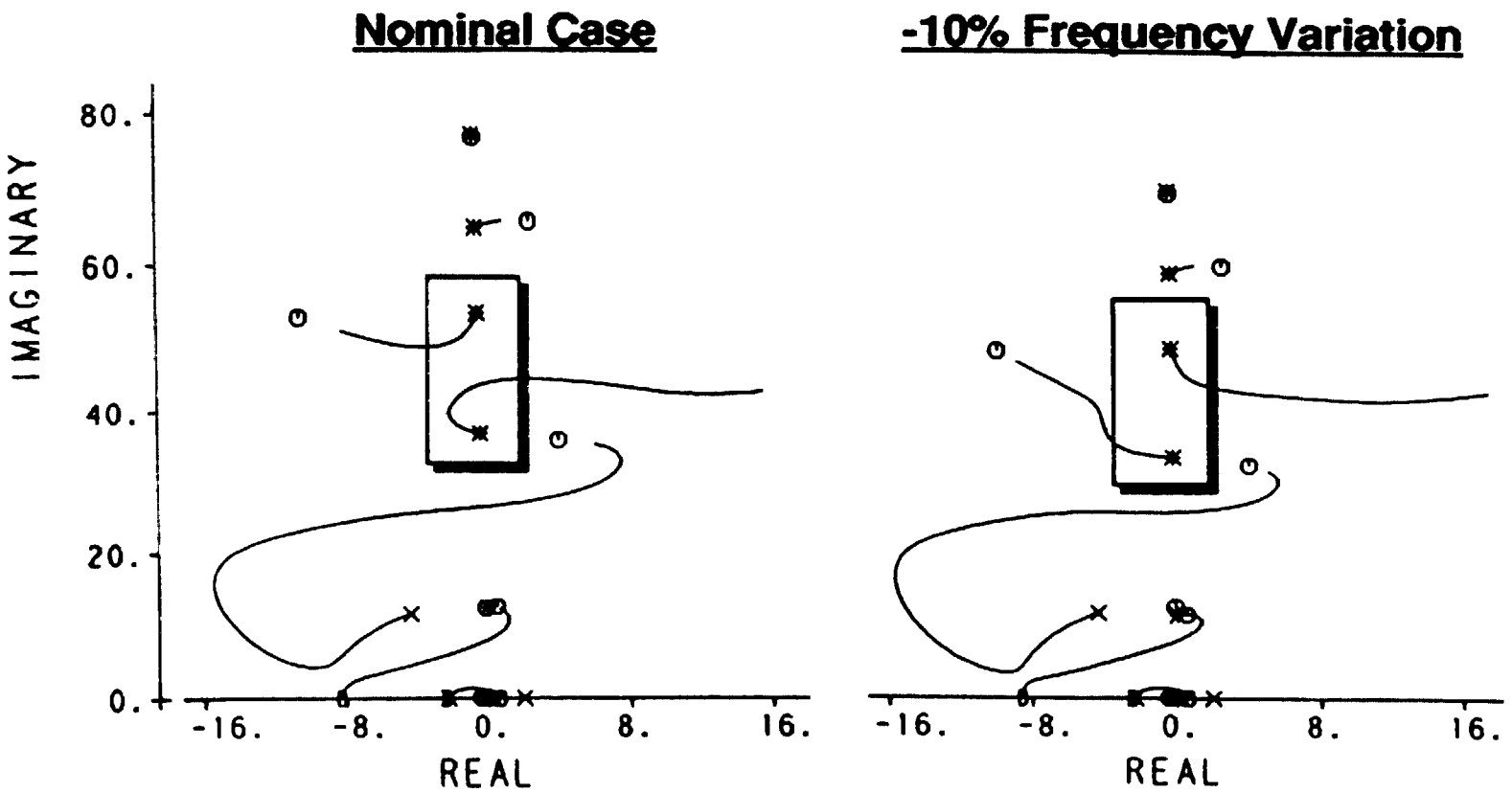

Figure 22. GS-I Root Locus Comparison

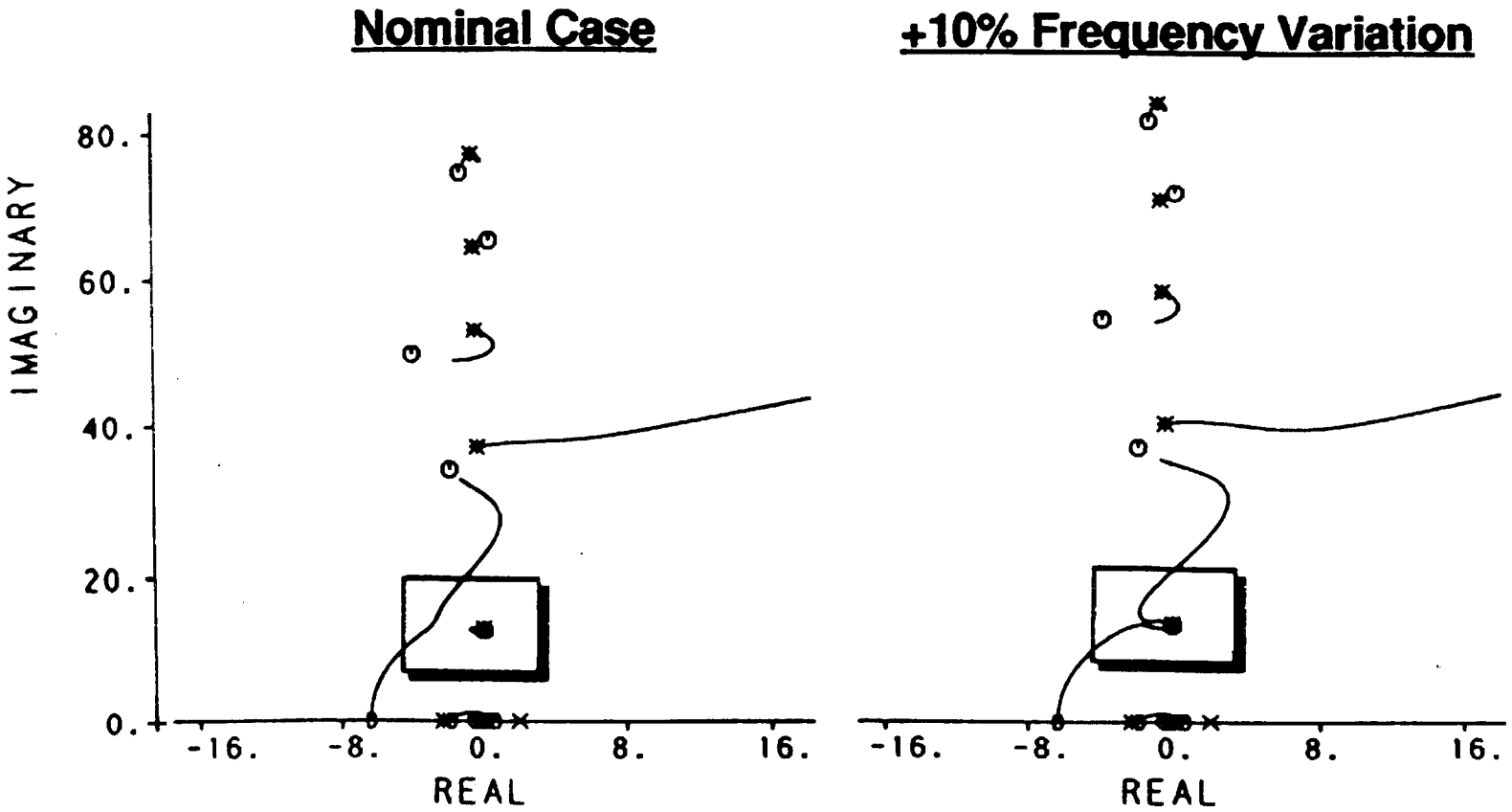

Figure 23. Phase I HPS Root Locus Comparison

This page is intentionally left blank.

Section IV

REQUIREMENTS DEVELOPMENT AND SYSTEM ASSESSMENT

A. Residual Response Metrics and Assessments

Based only on qualitative comparisons of pitch rate responses to step pitch rate commands (Section II), all of the HPS designs showed evidence of residual oscillations associated with the first structural mode which exceed those of the gain stabilized reference design. This is not surprising since the HPS designs do not have the notch filter at the first flexible mode used in the gain stabilized design. If this were the only issue, there would be no reason to consider the HPS designs further. There are of course other issues. Primary issue among these is the unacceptable effective time delay of the gain stabilized design, the problem which motivates HPS. As noted previously, designers will not have the luxury of overly conservative flight control design for HSV. Therefore, the tradeoffs between time delay, robustness and residual response will have to be made very carefully. All of the requirements that effect these tradeoffs will have to be well defined, traceable to physical principles and well validated for HSV. The greatest need is in the area of residual response requirements which are nearly nonexistent for HSV.

A residual response metric was developed in Phase I but it was recognized to be very questionable, in part because it was based on an inadequate estimate of the normal acceleration at the pilot's station. This problem has been remedied and an improved "Phase II" residual response metric will be reviewed later. However, even this Phase II metric is inadequate because it is still based on an ad hoc frequency dependent weighting. To address this limitation, studies of relevant aircraft-centered and human-centered phenomena were made to provide the foundation for more rational residual response metrics. These are presented in Sections IV-B and IV-C.

1. Normal Acceleration Frequency Response

As discussed previously in Section II-A, the structural dynamics model was extended in Phase II to properly compute the normal acceleration at the pilot's station. Figure 24 shows the magnitude plots of the pilot's station normal acceleration to pitch rate command for: (a) the baseline system (no structural mode treatment); (b) the gain stabilized

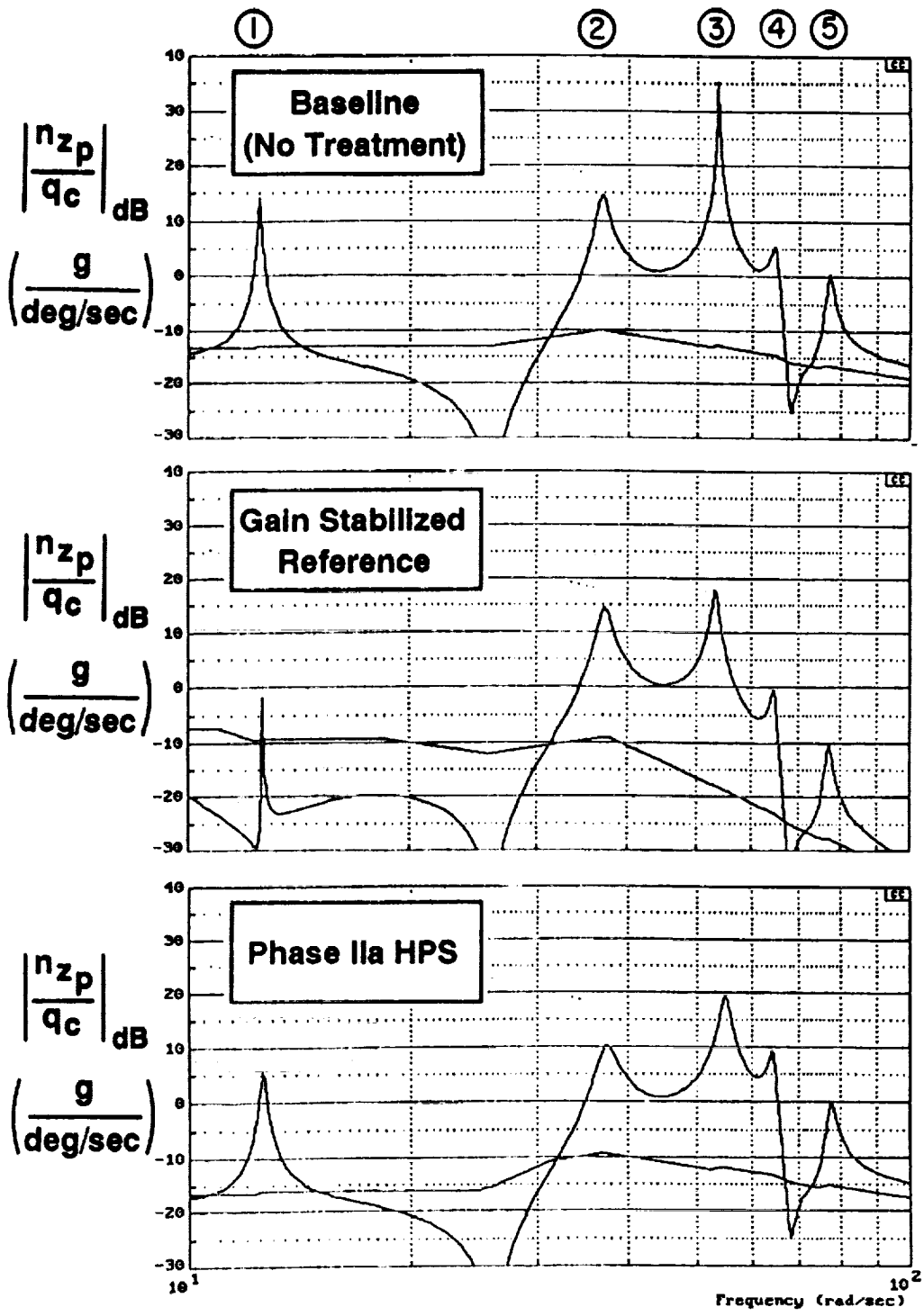

Figure 24. Normal Acceleration Magnitude Plots at the Pilot's Station

reference design; and (c) the final Phase IIa HPS design. The corresponding transfer functions are given in Table 9 in factored form. As expected, the two structural mode treatments each show clear reductions in normal acceleration at the structural modes when compared to the baseline case.

From Figure 24, the gain stabilized design shows somewhat lower acceleration peaks than the Phase IIa HPS design at the first, third and fifth structural modes but not at the second and fourth. Thus, a clear conclusion about structural response cannot be made from qualitative comparison of frequency response. The question ultimately requires that some frequency dependent weighting be applied to the response. Defining an appropriate weighting is, of course, the essence of the development of a residual response metric.

2. Normal Acceleration Step Response

Figure 25 shows the normal acceleration at the pilot's station (in g's) in response to a 1 °/sec pitch rate command step comparing the gain stabilized reference and the final Phase IIa HPS design. Figure 26 presents the same comparisons over a shorter time interval. The generally slow (rigid body) response of acceleration to pitch rate is a consequence of the pure pitch rate command stability and control augmentation system (SCAS) design coupled with the unconventionally low values of $1/T_{\theta 2}$ typical of hypersonic flight (Ref. 8 and 9). This characteristic is quite important in hypersonic flying qualities and has an impact here as will be discussed later.

The step response calculation has the benefit of applying an intrinsic weighting to the modal responses but only subjective assessments can be made by comparing the responses of the two designs. On this basis, however, no major differences are indicated between the Phase IIa HPS design and the gain stabilized reference design. The residual response of all designs appears dominated by the 53 rad/sec signature of the third structural mode which is consistent with the frequency responses shown in Figure 24. For the HPS designs (Figures 12, 13, and 17), the significance of the third structural mode in the n_{z_p} step responses contrasts with the 2 Hz residual oscillation from the first mode seen in the pitch rate responses. This arises because the higher frequency modes are accentuated by the inherent pitch rate to n_{z_p} due to gyro offset from the c.g. contribution.

Table 9. Normal Acceleration Transfer Functions at the Pilot's Station

Baseline

$$\frac{n_{z_p}}{q_c} = \frac{4.98E+07(-7.40E-04)(.44)(2.31)[-.04,\ 2.79][.12,\ 12.34]\ [-2.78E-03,\ 25.94][.38,\ 52.41][-8.69E-03,\ 67.99][.049,\ 74.66]}{(0)(.16)[.70,\ 1.46](2.31)[4.03E-03,\ 12.50](25.99)[.02,\ 36.68]\ [2.21E-03,\ 53.52][.012,\ 64.71][9.99E-03,\ 77.03][.51,\ 272.93]}$$

Gain Stabilized Reference Design

$$\frac{n_{z_p}}{q_c} = \frac{7.96E+10(-7.40E-04)(.44)(2.31)[-.042,\ 2.79][.12,\ 12.34][.01,\ 12.5]\ [-2.78E-03,\ 25.94][.38,\ 52.41][-8.69E-03,\ 67.99][.049,\ 74.66]}{(0)(.16)[.82,\ 2.05](2.31)[.66,\ 11.00][9.76E-04,\ 12.65](18.60)\ [.019,\ 37.13][.53,\ 37.77][.011,\ 53.13][9.42E-03,\ 64.71]\ [9.98E-03,\ 77.02][.51,\ 272.89]}$$

Final Phase IIa HPS

$$\frac{n_{z_p}}{q_c} = \frac{4.98E+07(-7.40E-04)(.44)(2.31)[-.042,\ 2.79][.12,\ 12.34](25)^3\ [-2.78E-03,\ 25.93][.38,\ 52.41][-8.69E-03,\ 67.99][.05,\ 74.66]}{(0)(.14)[.67,\ 1.20](2.31)[8.42E-03,\ 12.60](25)(25.30)[.96,\ 31.20]\ [2.87E-02,\ 37.25][.015,\ 54.79][.010,\ 64.32][.013,\ 77.55][.53,\ 253.23]}$$

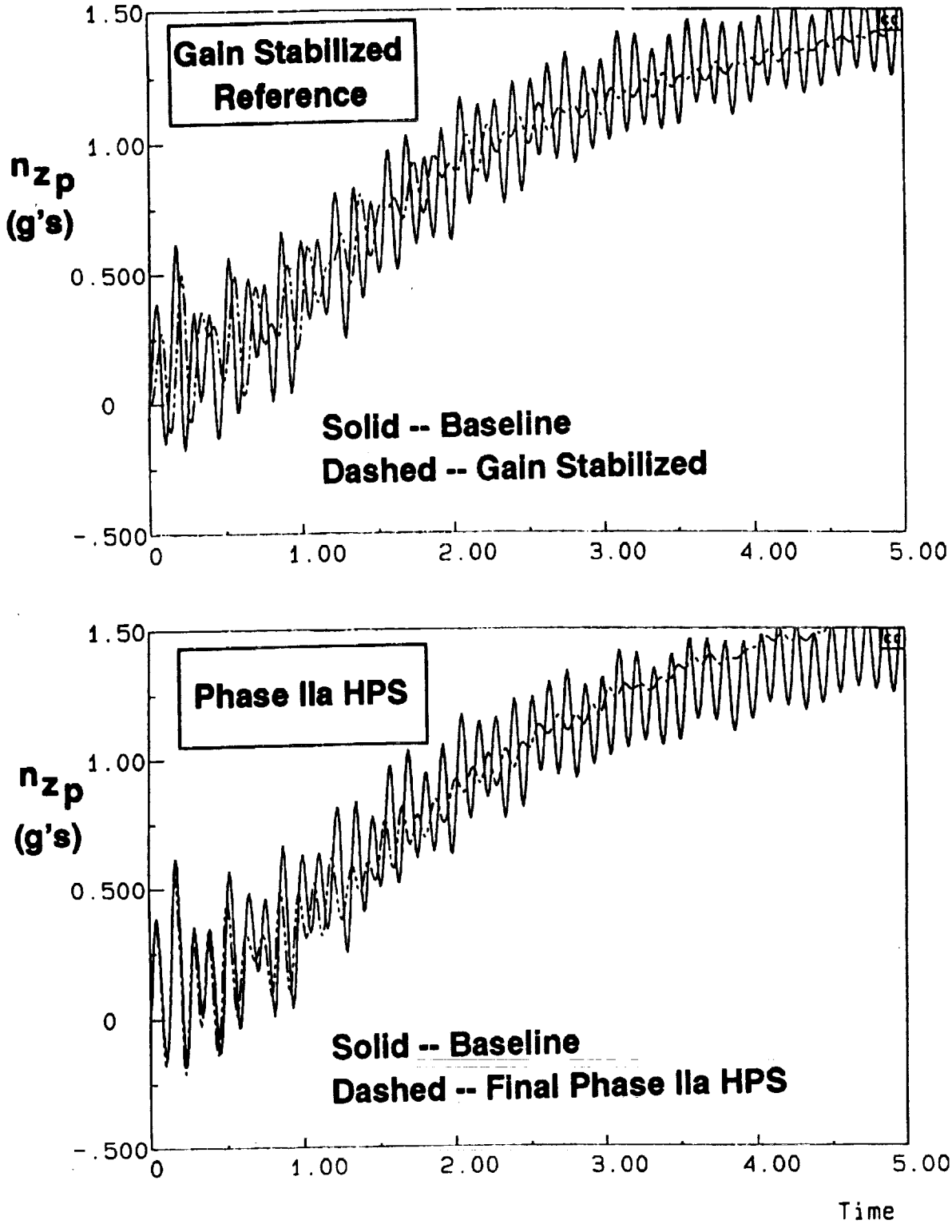

Figure 25. Responses of Normal Acceleration at the Pilot's Station to a Unit Pitch Rate Step Command - 5 Second Interval

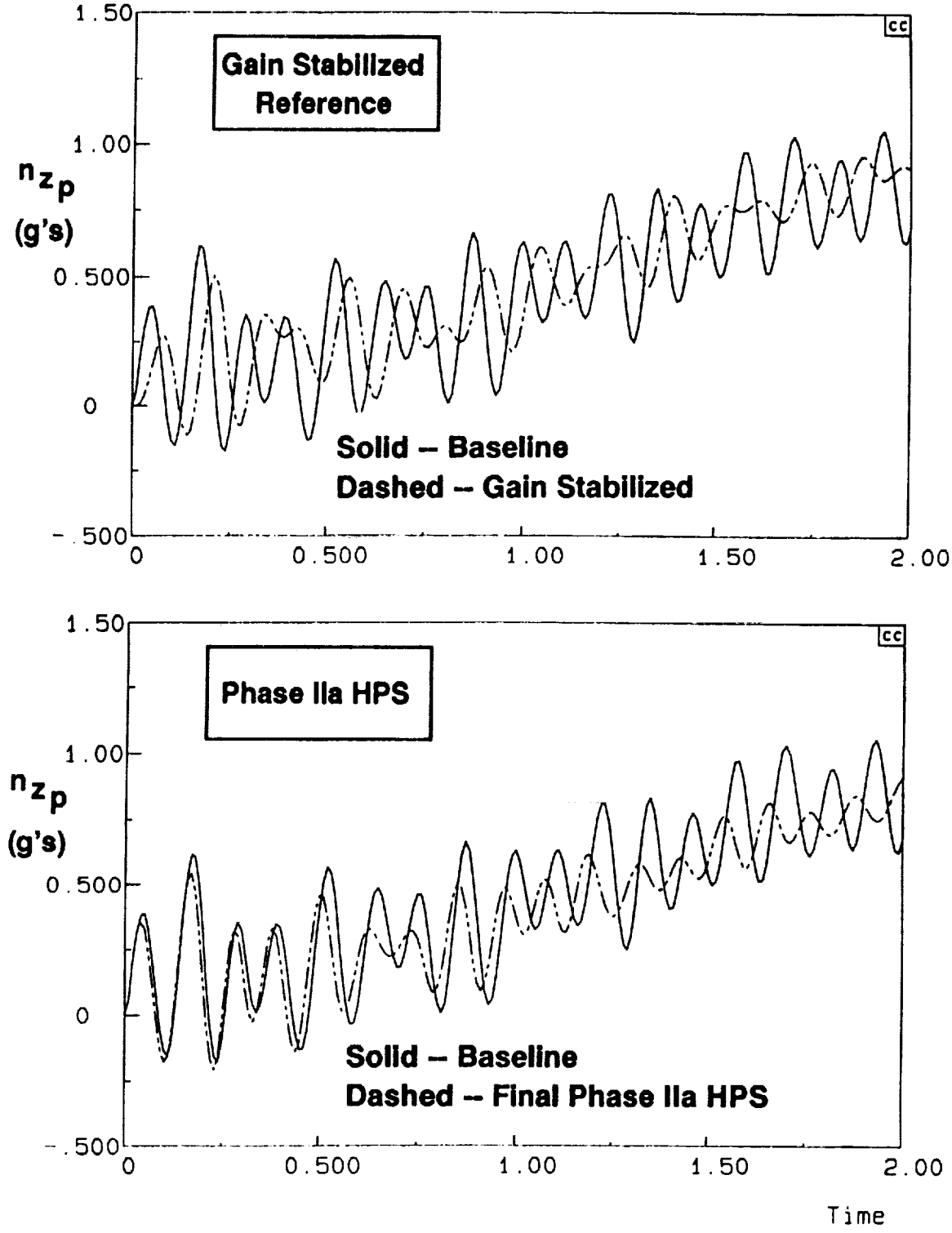

Figure 26. Responses of Normal Acceleration at the Pilot's Station to a Unit Pitch Rate Step Command - 2 Second Interval

3. Residual Response Metric Revisions

The acceleration residual response metric developed in Phase I (Ref. 1) is quantitative and based on a physically motivated, but ultimately arbitrary, frequency-dependent weighting. In Phase I, a crude estimate of normal acceleration at the pilot's station had to be used but this was replaced with the much better acceleration transfer function now available (Section IV-A-1) to form an improved "Phase-II" metric. The other elements such as the weighting function and the random disturbance injected at the elevator surface remains unchanged from the Phase I development. The Phase I and II residual response metrics are summarized in Figure 27.

The Phase I and Phase II residual (acceleration) response metrics are compared in Table 10. The values of the metric (rms acceleration) are generally an order of magnitude higher with the improved model which simply reflects the inadequacy of the Phase I normal acceleration model at high frequencies. See the frequency response comparison in Figure 27. However, the relative ranking of the designs does not change with the Phase II metric except that the Phase IIa HPS design appears equal to rather than superior to the gain stabilized design.

As noted above, even with an adequate normal acceleration model, the Phase II residual response metric must be questioned because it is based on a frequency domain weighting function which is ultimately arbitrary and is not based on relevant physical phenomena. Thus, two important areas were studied to develop deeper insight into the

Table 10. Comparison of Residual Response Metrics

System	Phase I Metric		Phase II Metric	
	σ_{n_z}(g/deg)	$(\sigma/\sigma_{Base})_{n_z}$	σ_{n_z}(g/deg)	$(\sigma/\sigma_{Base})_{n_z}$
"Baseline"	0.0872	1.000	0.750	1.000
Gain Stabilized Ref.	0.0587	0.673	0.350	0.476
Phase I HPS	0.0609	0.698	0.488	0.651
Final Phase IIa HPS	0.0441	0.506	0.350	0.467

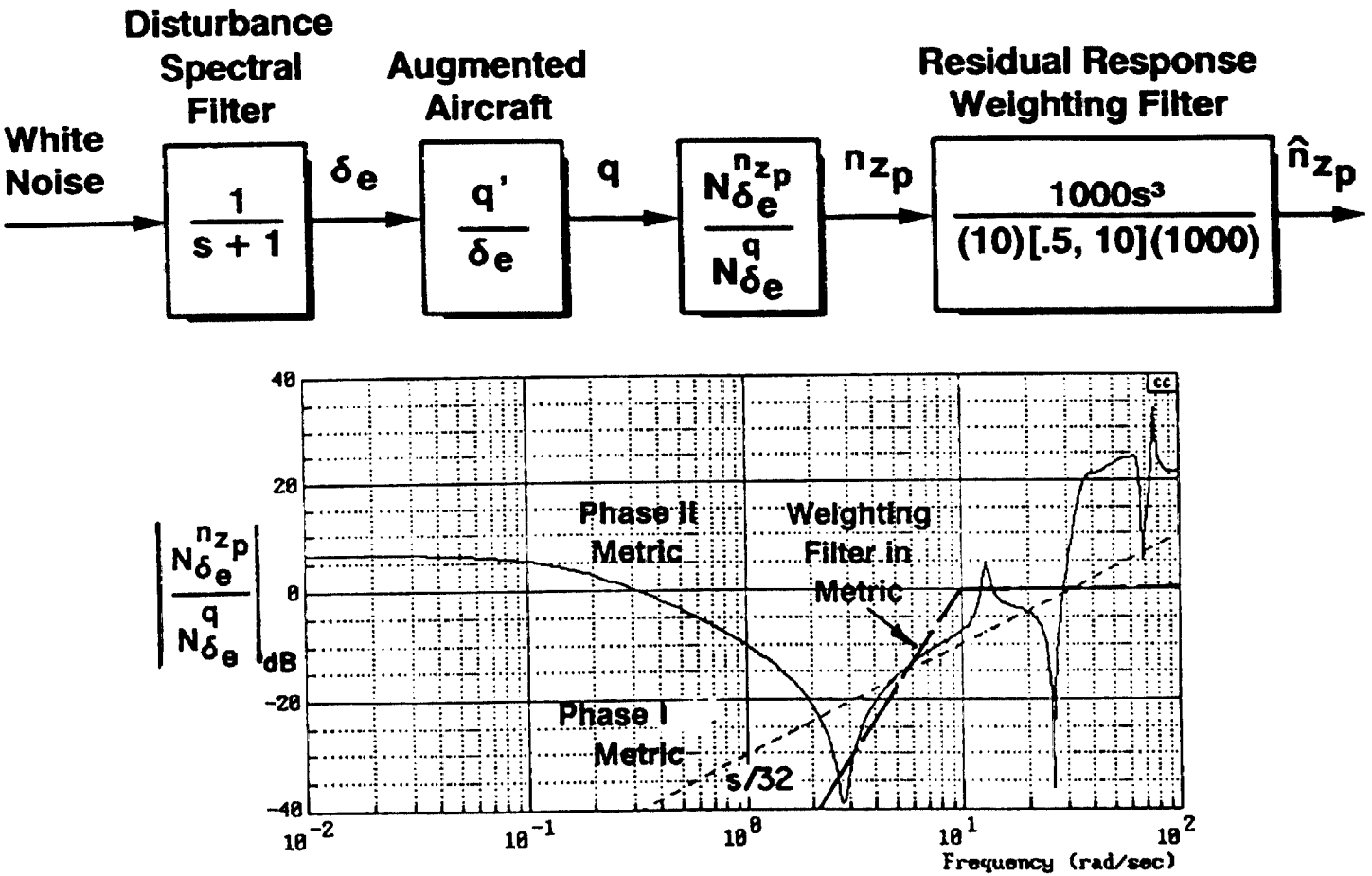

Figure 27. Residual Response Metric

significance of residual response and to search for more rational and physically traceable response metrics. These can be broadly partitioned into two groups: aircraft-centered issue which is independent of the human pilot or passengers, and human-centered issue which is dependent of the human pilot. The aircraft-centered issue of structural fatigue is discussed next in Section IV-B. The discussion of the human-centered problem of biodynamic vibration transmission to the stick follows in Section IV-C.

B. Aircraft-centered Requirements

Metal fatigue is a phenomenon experienced by structures when exposed to repetitive load cycles. These loads cause fatigue cracks which grow until fracture of the structural member occurs. The fatigue life of a structure is dictated by the number of cycles that cause fracture. Factors which affect fatigue include environmental conditions (that is, elevated temperature exposure) and stress concentrations (e.g., fastener holes, cutouts, etc.).

An assessment was performed to compare the fatigue life of a structure under loads caused by conventional gain stabilization and HPS. The time history of the normal acceleration at the pilot's station for a conventional gain stabilized design is shown in Figure 28. A similar time history plot for Phase IIa HPS is shown in Figure 29. These accelerations are assumed to be the loads that cause corresponding cyclic stress in the structure.

The material selected for the structural fatigue life analysis or assessment is titanium 6-4. This is a conventional titanium alloy used extensively for elevated temperature conditions. The titanium 6-4 fatigue properties required in the analysis were obtained from MCAIR's in-house material database and the military handbook (Ref. 10). Structural failure is defined by the predicted initiation of fatigue cracks. The tool used for the analysis is SPECCI, a MCAIR fatigue crack initiation prediction software (Ref. 11). Two (low and high) temperature settings were studied: room temperature and 600°F.

Results of the room temperature analysis for the gain stabilized design are shown in Figure 30. Stress on the vertical axis is in units of kilopounds per square inch (ksi) while the fatigue life on the horizontal axis is in number of maneuvers which cause structural failure. The maneuver for the gain stabilized design is the 15 second time history data as shown Figure 28. Similarly, the maneuver for the hybrid phase stabilized design is the 15 second time history data shown in Figure 29.

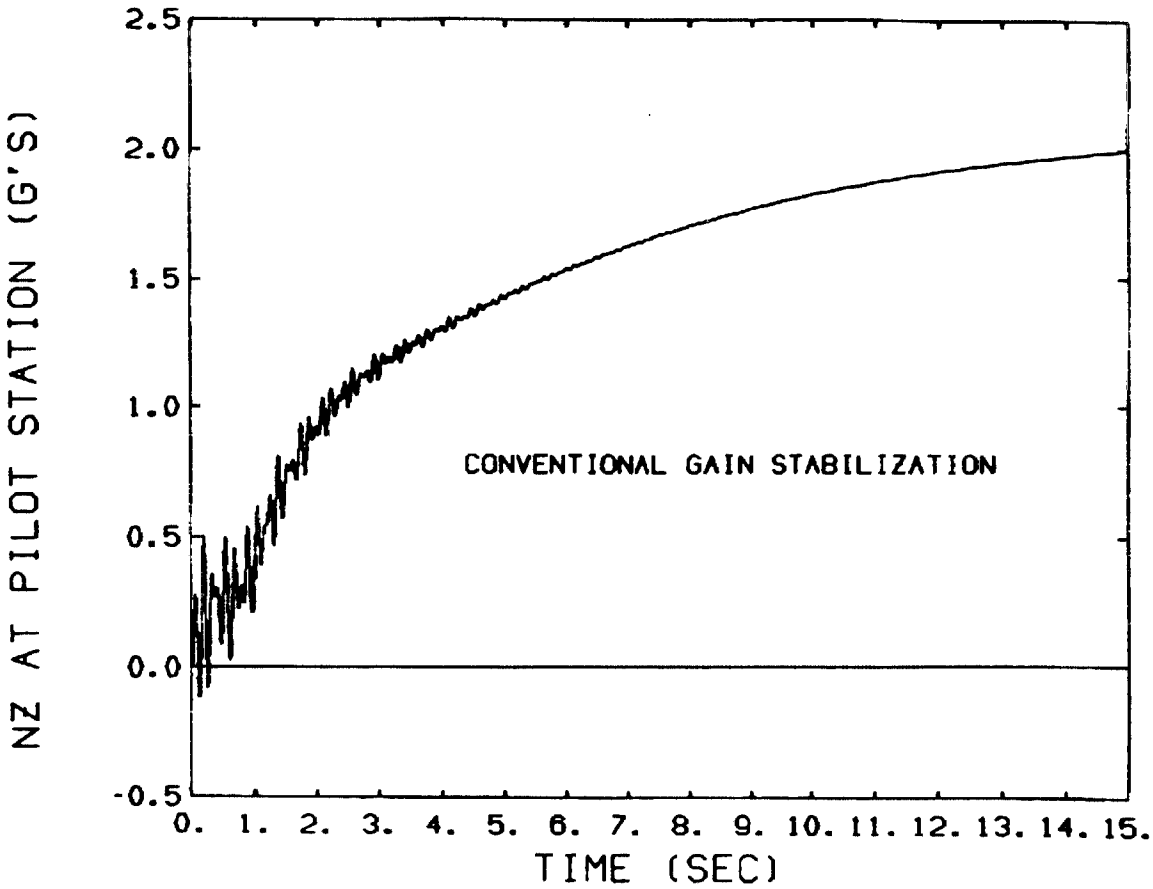

Figure 28. Time History of Normal Acceleration Response at the Pilot's Station to a Unit Pitch Rate Step Command for Gain Stabilized Reference Design

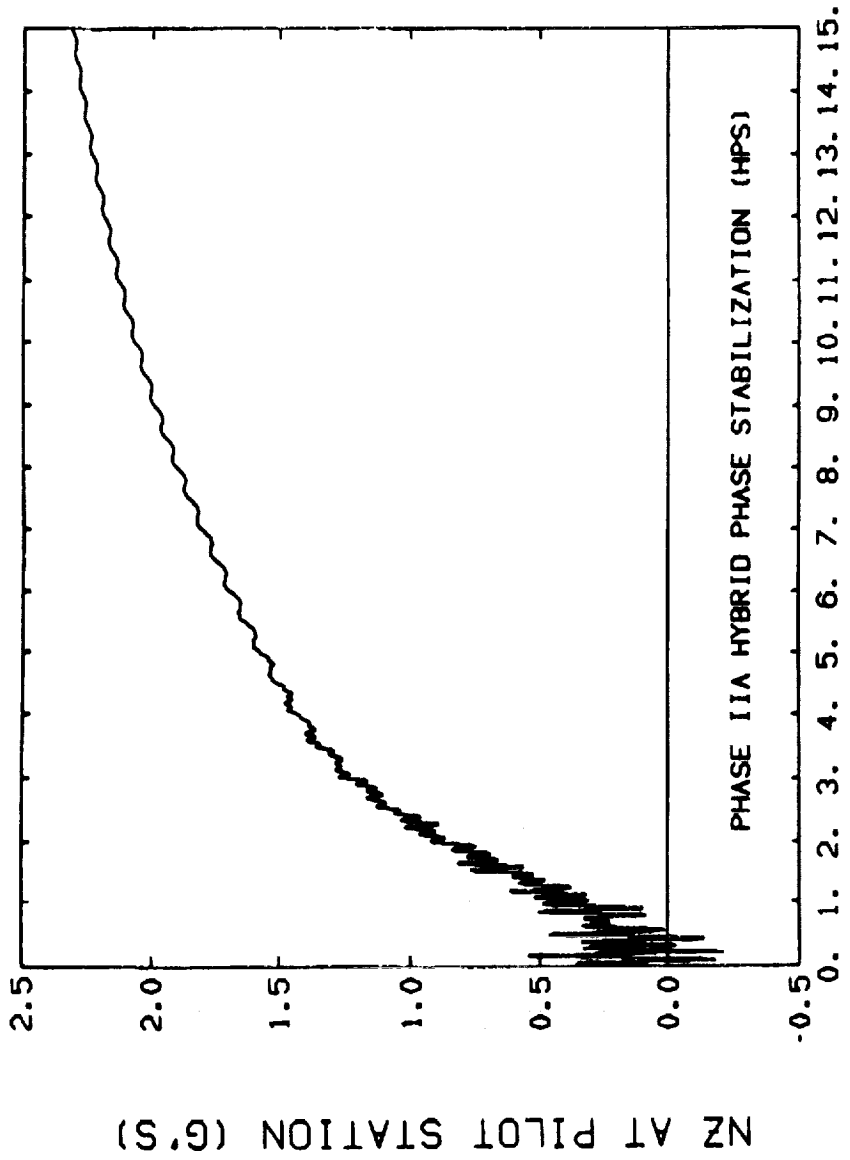

Figure 29. Time History of Normal Acceleration Response at the Pilot's Station to a Unit Pitch Rate Step Command for Final Phase IIa HPS Design

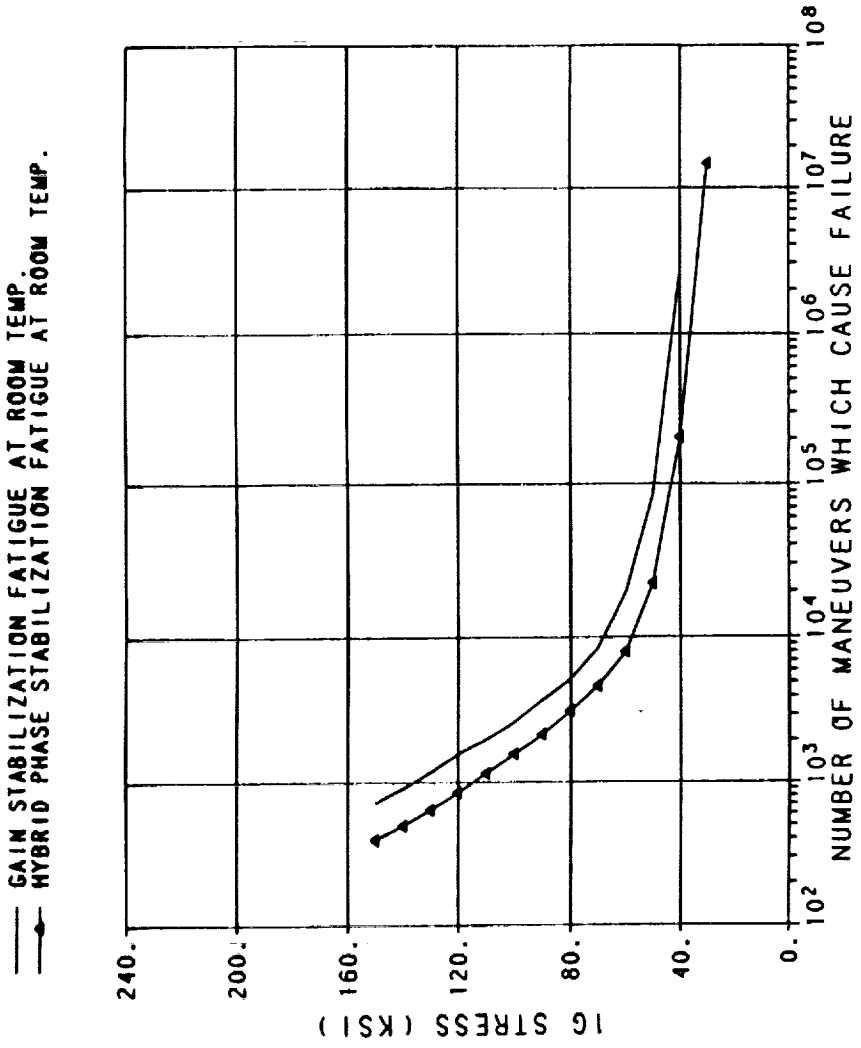

Figure 30. Comparison of Predicted Fatigue Life at Room Temperature

As illustrated in Figure 30, gain stabilization results in longer fatigue life than hybrid phase stabilization. This difference can translate into structural weight savings. For example, if a vehicle is required to sustain 8500 maneuvers, the allowable stress for HPS is 60 ksi. However, for gain stabilization, the stress can be increased to 70 ksi. This represents a 16% weight savings.

Results for the 600°F analysis is shown in Figure 31. Similar observation can be made as in the previous case. Results again indicate a longer fatigue life for the conventional gain stabilization. Figure 32 combines results of both temperature settings. Note that elevated temperature exposure reduces the fatigue lives for both stabilization techniques.

In connection with the reduced fatigue life for HPS, examination of the normal acceleration response can provide some insights. As shown in Figures 28 and 29, at the end of the maneuver, the normal acceleration for the HPS design displays a higher peak value at 15 seconds than that of the conventional gain stabilized design. This difference amounts to a 0.32g increase or a 16% change in peak value. In addition to the difference in peak acceleration value, the time history data for the Phase IIa HPS shows that a 2 Hz oscillation or residual response begins to develop at 3.5 seconds. Experience suggests that the peak normal acceleration value accounts for perhaps 75% of the contribution to the reduced fatigue life of a structure. The residual response accounts for roughly the remaining 25%.

In the original analysis, the 15 second duration of the maneuver was chosen somewhat arbitrary under the assumption that this would not be critical to the comparative assessment of the two designs. However because of the long path lag to attitude changes, coupled with small differences in the closed loop pitch responses at maneuvering frequencies, the differences in peak normal acceleration result. In a refined analysis, the differences in steady state normal acceleration would be removed to make the maneuver comparable for both designs. Thus, the primary remaining difference would be the 2 Hz oscillation associated with the first structural mode which is not filtered in the HPS design. This should considerably reduce the disadvantage of the HPS design.

Further, the fatigue analysis is an assessment procedure, i.e., it is an analysis done after a control design cycle. Further development (discussed in Section VI-B) could re-optimize the HPS design with explicit consideration of fatigue to further reduce or eliminate the disadvantage.

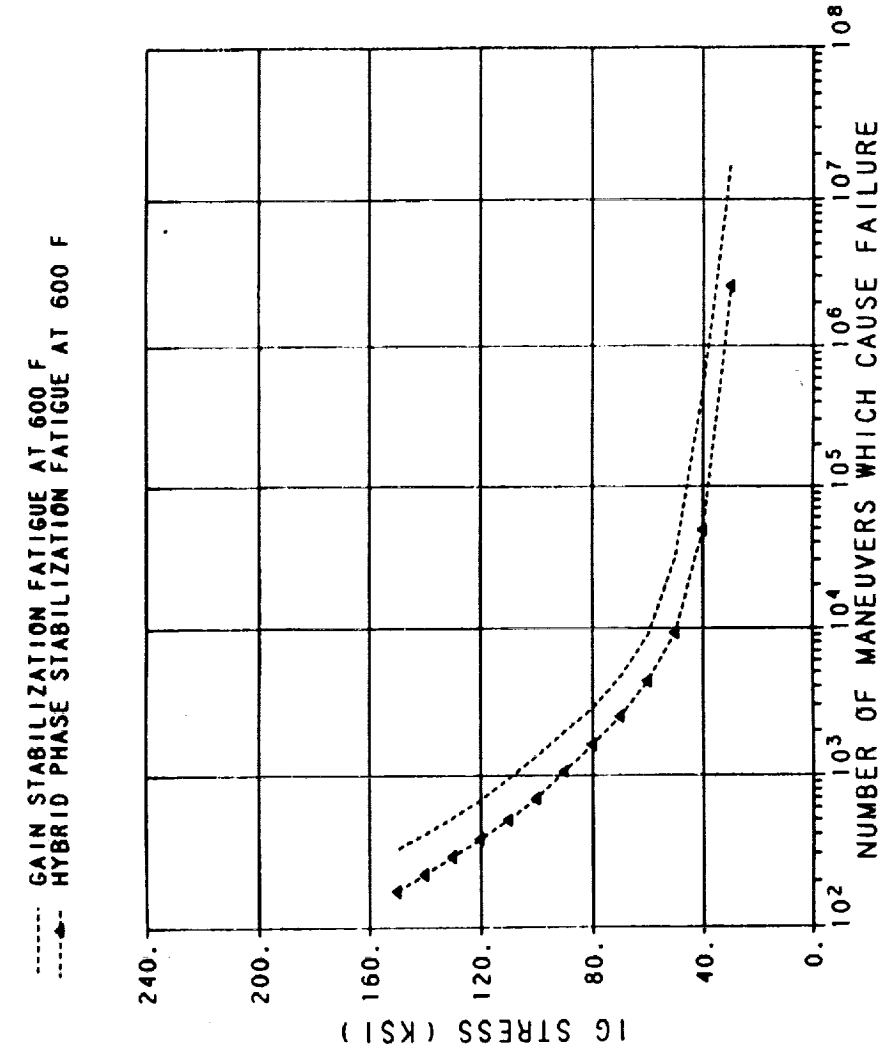

Figure 31. Comparison of Predicted Fatigue Life at 600 °F

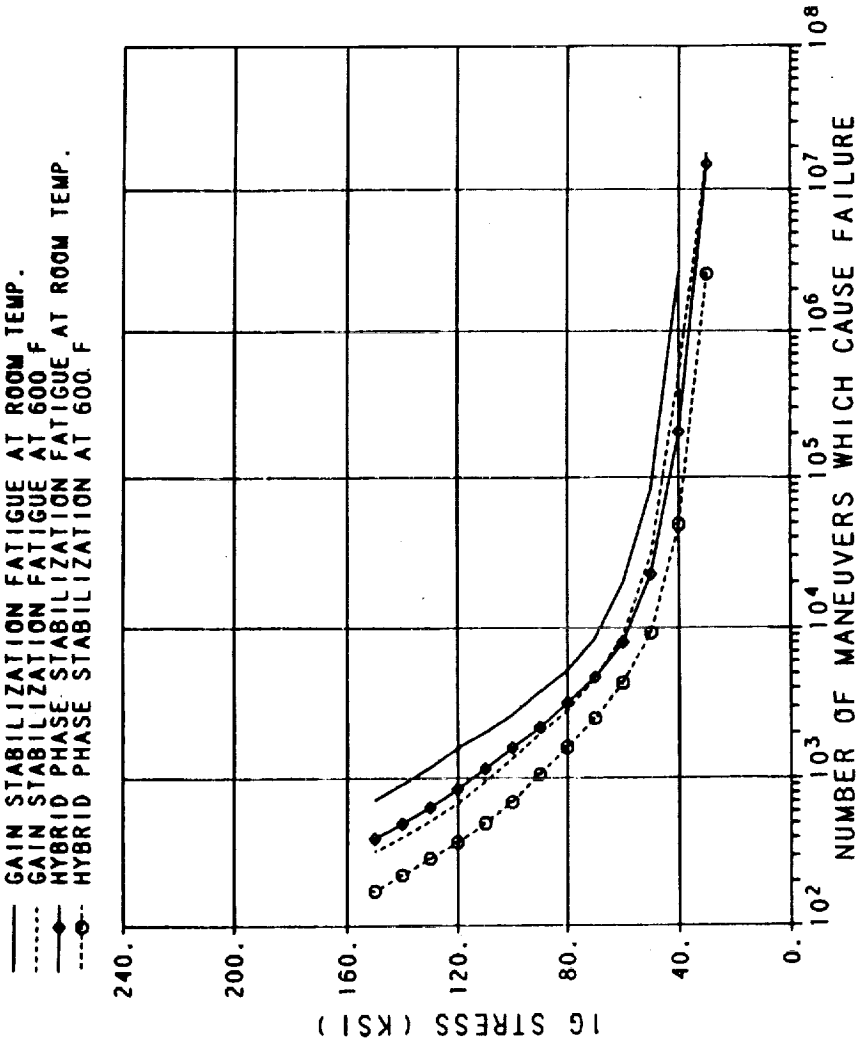

Figure 32. Comparison of Predicted Fatigue Life

C. Human-centered Requirements

Phenomena involving human pilots or passengers include "passive" considerations such as ride quality, but the focus here is on "active" considerations, i.e., manual control. Recent developments in hypersonic flying qualities (Ref. 8, 9, and 12) indicate that certain vehicle constraints unique to hypersonic aircraft (e.g., high minimum angle of attack limits) could necessitate complex and unconventional maneuvering. While such maneuvers might be routinely automated, provision for manual maneuvering at some level must be provided unless a radical departure from aircraft operational philosophy is accepted. That is, human pilots will be demanded by human passengers and adequate manual control provisions must be made for these human pilots. Manual control is, of course, a primary motivator for HPS in connection with effective time delay reduction, but any associated adverse effects on manual control must also be assessed.

The primary concerns are vibration feedthrough and interaction with the pilot's neuromuscular system. Vibration feedthrough occurs when normal acceleration (or acceleration in other axes) at the pilot's station is transmitted through the pilot's neuromuscular system to the stick. Preliminary assessments can be made using data available from biodynamic experiments (Ref. 13).

The phenomena can be treated with the model shown in Figure 33. The pilot/stick dynamics represent the composite of the seat, human pilot and stick mechanical characteristics that determine the transmission of structural vibration to the stick electrical transducer. A fly-by-wire system is, of course, assumed, but the stick may be either force-sensing or displacement sensing at this point. The command path gain/filter represents the dynamics between the stick electrical transducer and the pitch rate command signal. This includes stick filters generally used in fly-by-wire systems but not the mechanical stick feel elements which are included in the first block. The augmented vehicle dynamics are represented by the appropriate n_{z_p}/q_c transfer functions (Table 9).

Figure 34 presents human pilot transmissibility data in the form of the frequency response of the stick force/pilot normal acceleration transfer function (in Newtons/g). The discrete data points (squares) were obtained from human vibration experiments (Ref. 13). The solid lines are Bode plots generated from a model fitted to the discrete data using the STI BIODYN software (Ref. 14). The major elements of the BIODYN model are depicted in Figure 35. The stick used to generate the Figure 34 data was a center stick with a very stiff spring restraint similar to that of some fly-by-wire controllers. While this controller

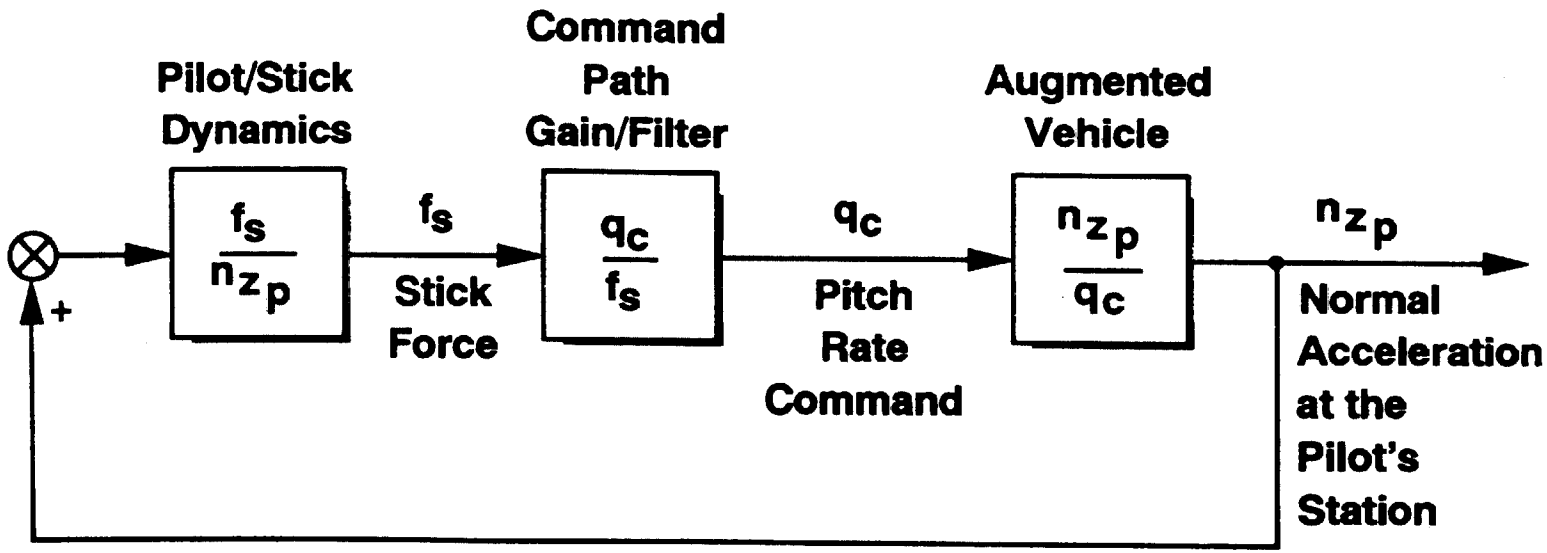

Figure 33. Biodynamic Analysis of Manual Control

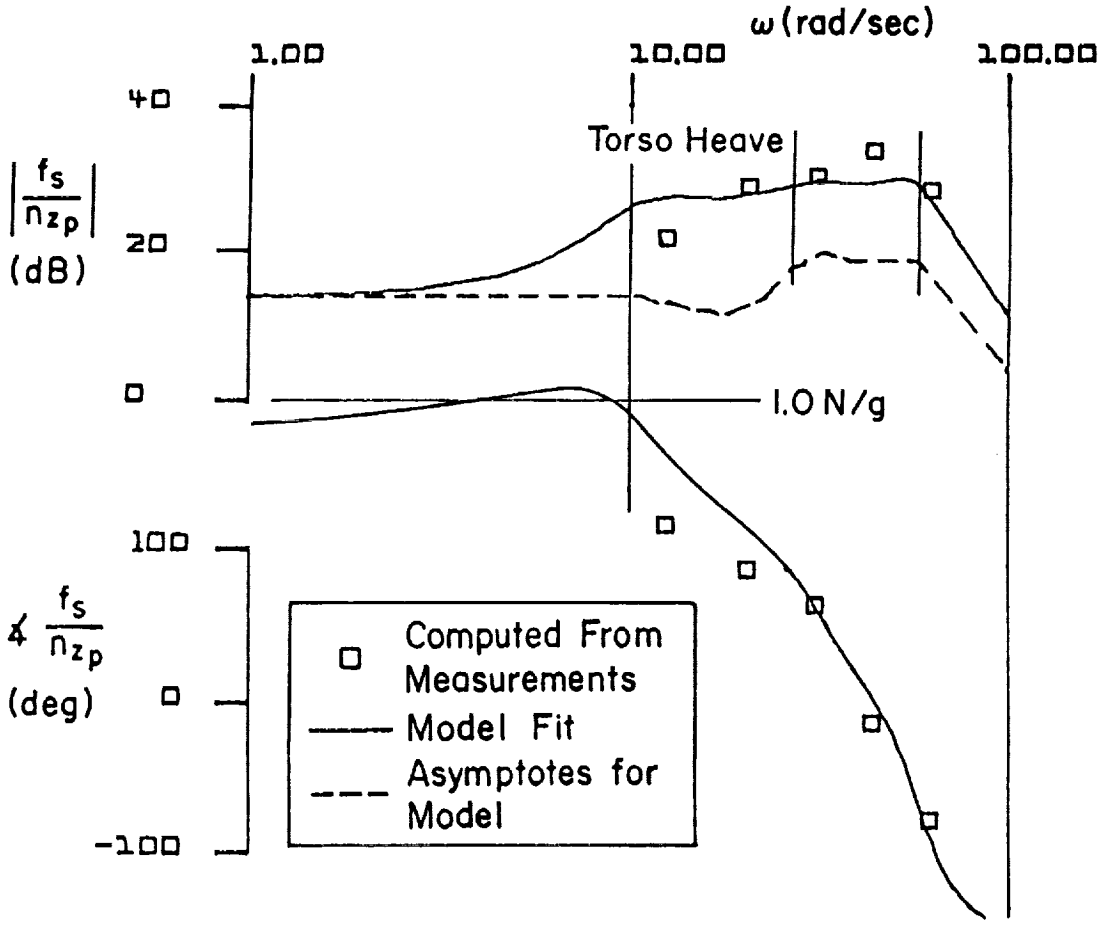

Figure 34. Frequency Response of Human Transmissibility

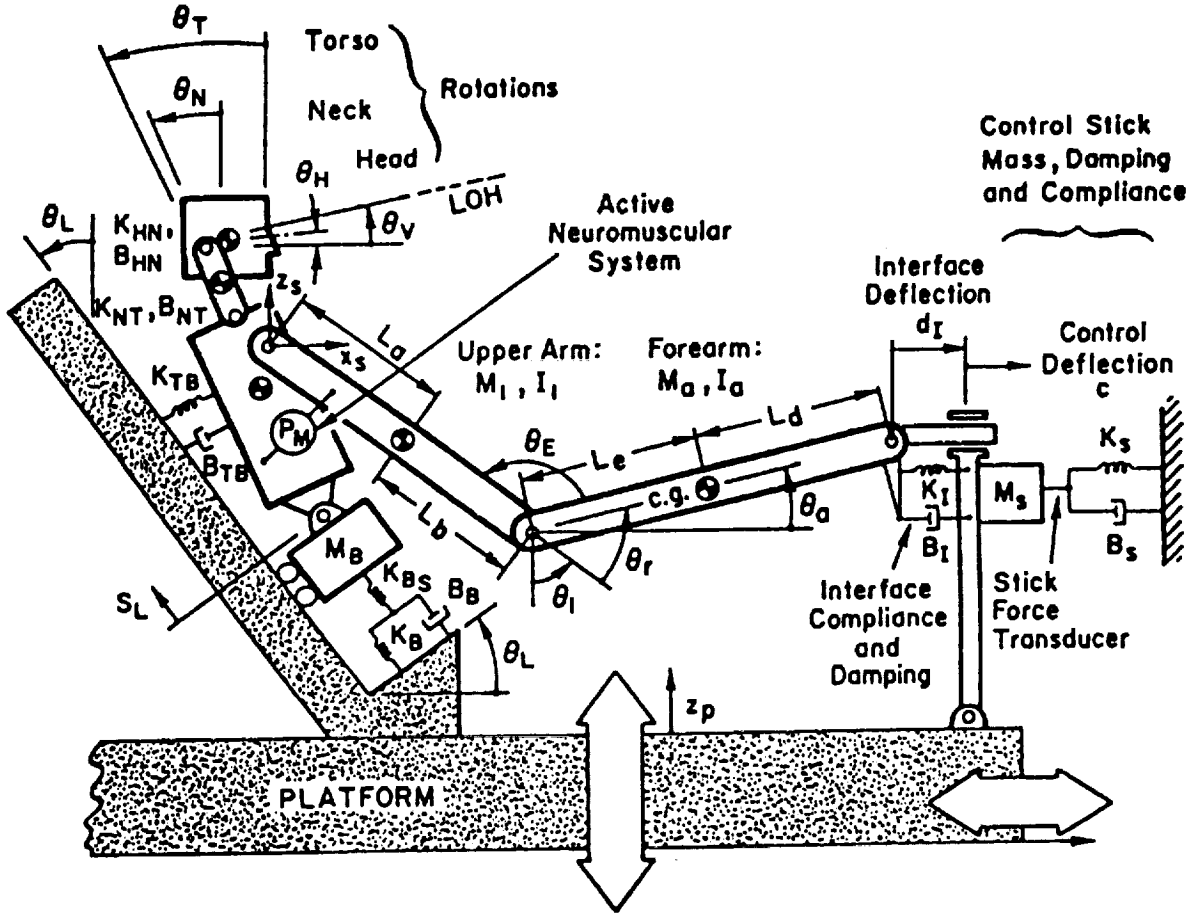

Figure 35. Elements of BIODYN Biodynamic Model

may differ somewhat from what would be expected for future HSV applications, the data is considered to be adequate for an initial comparative biodynamic assessment of HPS and conventional designs.

The presence of a detent/threshold around the zero position of a fly-by-wire stick will tend to reduce vibration transmission in cruise conditions. This factor will not be treated here, but the results obtained should be relevant to the maneuvering conditions of interest where the stick is generally out of the detent.

1. Pure Gain Approximation of n_{z_p}/q_c

The complete BIODYN model is relatively complex and high order and it is appropriate to make initial biodynamic assessments with much simplified models. As a first step, it can be noted from Figure 34 that the transmissibility magnitude is roughly constant over much of the frequency range of the aircraft structural modes. This would imply a pure gain first approximation except that there is a rapid phase angle decrease with frequency in this range. At this first level of approximation, some uncertainty must be accepted in phasing, i.e., in the sign of a pure gain approximation. Thus, both positive and negative gains were examined in the analyses.

If a pure gain command path characteristic (no bandlimiting stick filter) is also assumed, then the Figure 33 system becomes a pure gain feedback loop closure around the augmented airframe n_{z_p}/q_c transfer function. Figure 36 compares these pure gain closures as root locus surveys for the conventional gain stabilized design and the final Phase IIa HPS design. Loci are shown for both positive and negative gains to allow for phase uncertainty. Figure 37 shows the same closures (for positive gain only) in Bode root locus plots which give a clearer picture of gain sensitivity. It can be seen that for both designs there are several potential instabilities associated with several structural modes. The first instabilities (modes that go unstable at the lowest gain magnitude for both positive and negative gains) are indicated in each plot (hatched horizontal line segment). For either sign of the gain, a larger gain magnitude is required to destabilize the Phase IIa HPS design indicating an advantage over the conventional design. The minimum gains for instability are summarized in Table 11.

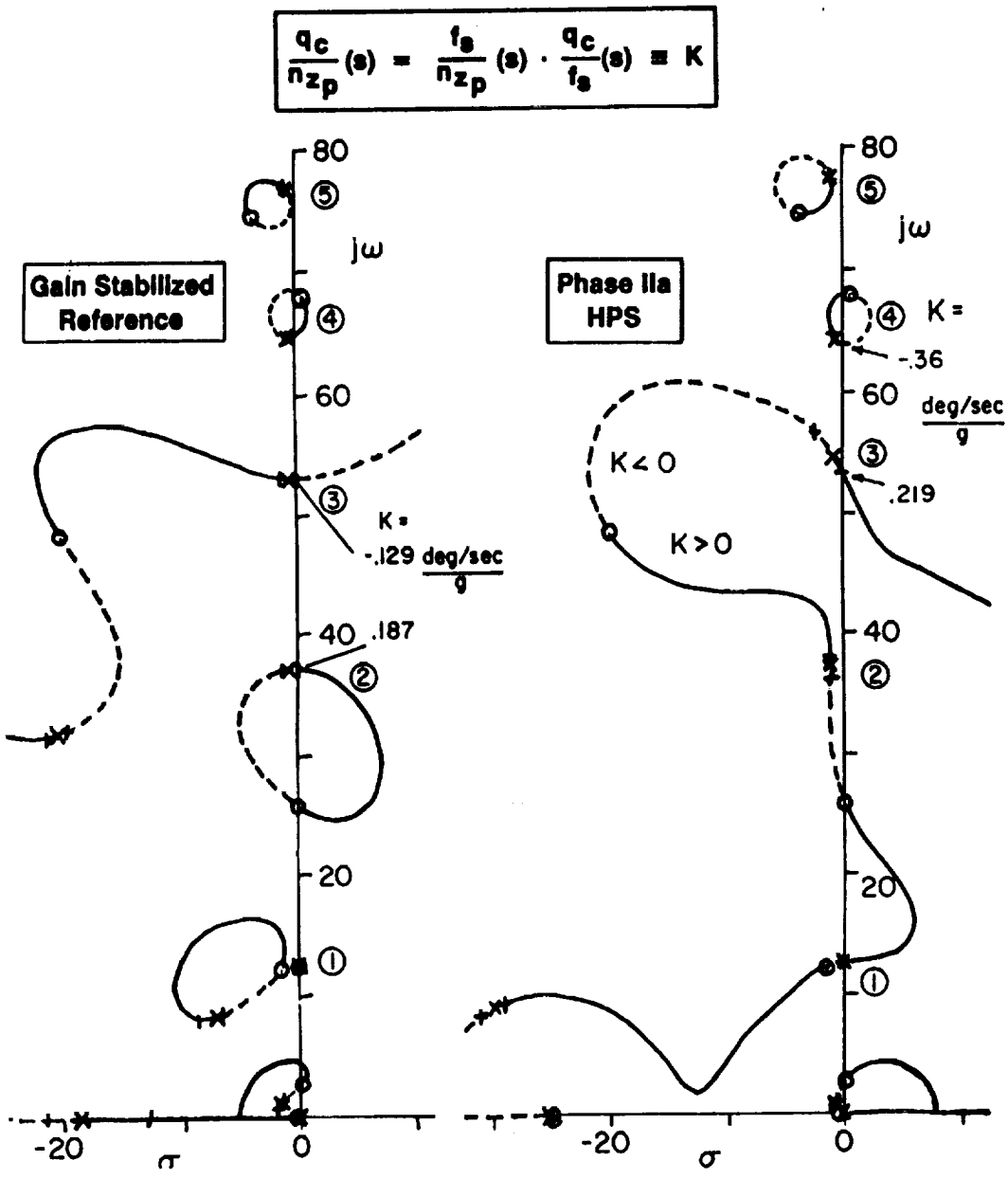

Figure 36. Root Locus Survey of Pure Gain Biodynamic Coupling

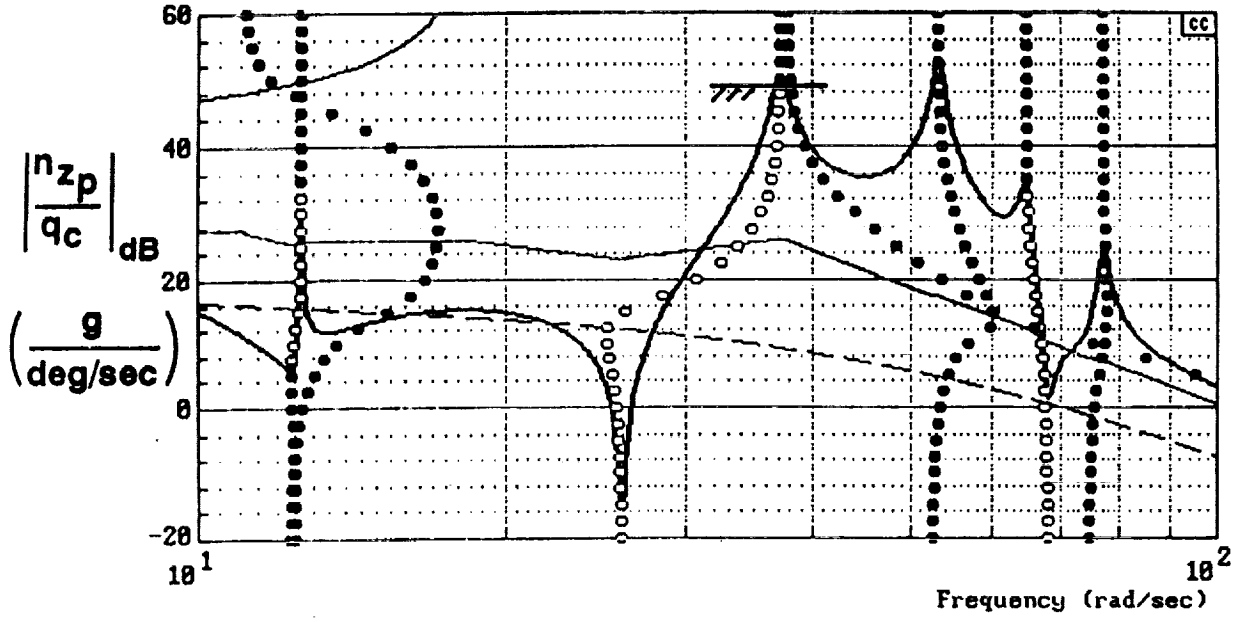

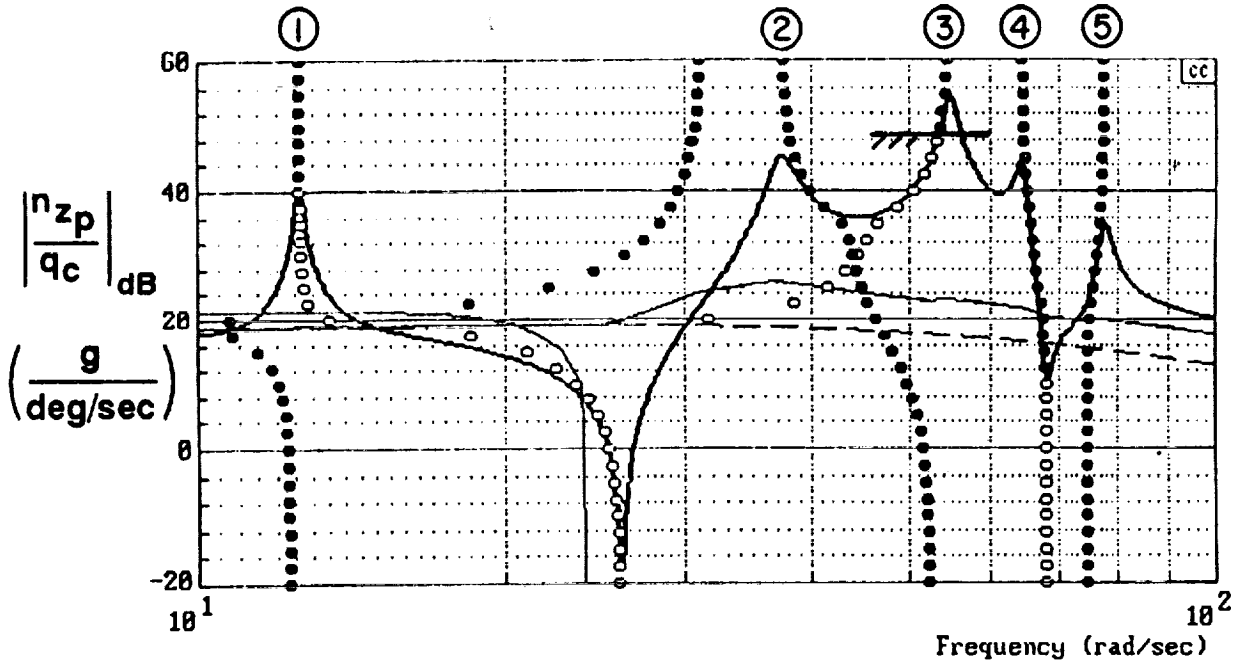

Figure 37. Bode Root Locus Survey of Pure Gain Biodynamic Coupling

Table 11. Summary of Biodynamic Coupling Comparison

Minimum Gain (deg/sec/g) in q_c/n_{z_p} Element for Instability

Integers in [] indicate structural mode driven unstable

Model	Gain Sign	Design	
		Conventional Reference	Ph IIa HPS
Pure Gain	+	0.19 [2]	0.22 [3]
	-	-0.13 [3]	-0.36 [4]
Mechanical Stick	+	0.25 [3]	0.46 [2]
	-	-0.13 [2]	-0.92 [2]
Stick Filter	+	2.29 [2]	1.19 [2]
	-	-3.43 [3]	-0.81 [3]

Estimated q_c/n_{z_p} Gain

$$\frac{q_c}{n_{z_p}} = \frac{f_s}{n_{z_p}} \cdot \frac{q_c}{f_s} = \begin{cases} 0.728\ °/sec/g \text{ for } f_s/n_z = 3lb/g \\ 0.078\ °/sec/g \text{ for } f_s/n_z = 28lb/g \end{cases}$$

2. Refined Transmissibility Model

Examination of Figure 34 shows a high frequency magnitude rolloff beginning around 50-60 rad/sec. This implies that a pure gain approximation is overly conservative with regard to pilot-transmitted excitation of the higher structural modes. To address this and to better model the phase characteristics, a third order transmissibility model was used in a refined analysis. This more detailed model (Ref. 13) was obtained from a second set of data as shown in Figure 38. This figure shows an even lower breakpoint (35 rad/sec) for the transmissibility rolloff, which should make it less conservative than the Figure 34 data. These dynamics are represented by the transfer function

$$\frac{f_s}{n_{zp}} = \frac{35^2(-s + 80)}{(s + 80)\left[s^2 + 0.03(35)s + 35^2\right]} \quad . \tag{5}$$

Note that this transfer function has unity low frequency gain and thus it simply models the spectral shape of the transmissibility.

Figure 39 shows the vibration feedthrough loop closures for this case. Again, the Phase IIa HPS design appears superior to the conventional design reflected in the higher stability margins. See Table 11.

3. Fly-by-Wire System with Stick Filter

As a final case, a controller configuration somewhat more representative of a modern fly-by-wire design was examined. This consisted of a relatively stiff stick (implying a high mechanical bandwidth) coupled with a stick filter (a command path electrical filter downstream of the stick transducer). This type of stick filter is largely intended to filter pilot remnant and thus tends to have a bandwidth well below the stick mechanical bandwidth. Therefore, the pilot/stick mechanical dynamics (transmissibility) was reasonably approximated by a (unity) pure gain. The command path dynamics created by the stick filter is modeled by

$$\frac{q_c}{f_s} = \frac{10}{(s + 10)} \quad . \tag{6}$$

Again, this transfer function has unity low frequency gain and represents the spectral shape of the command path.

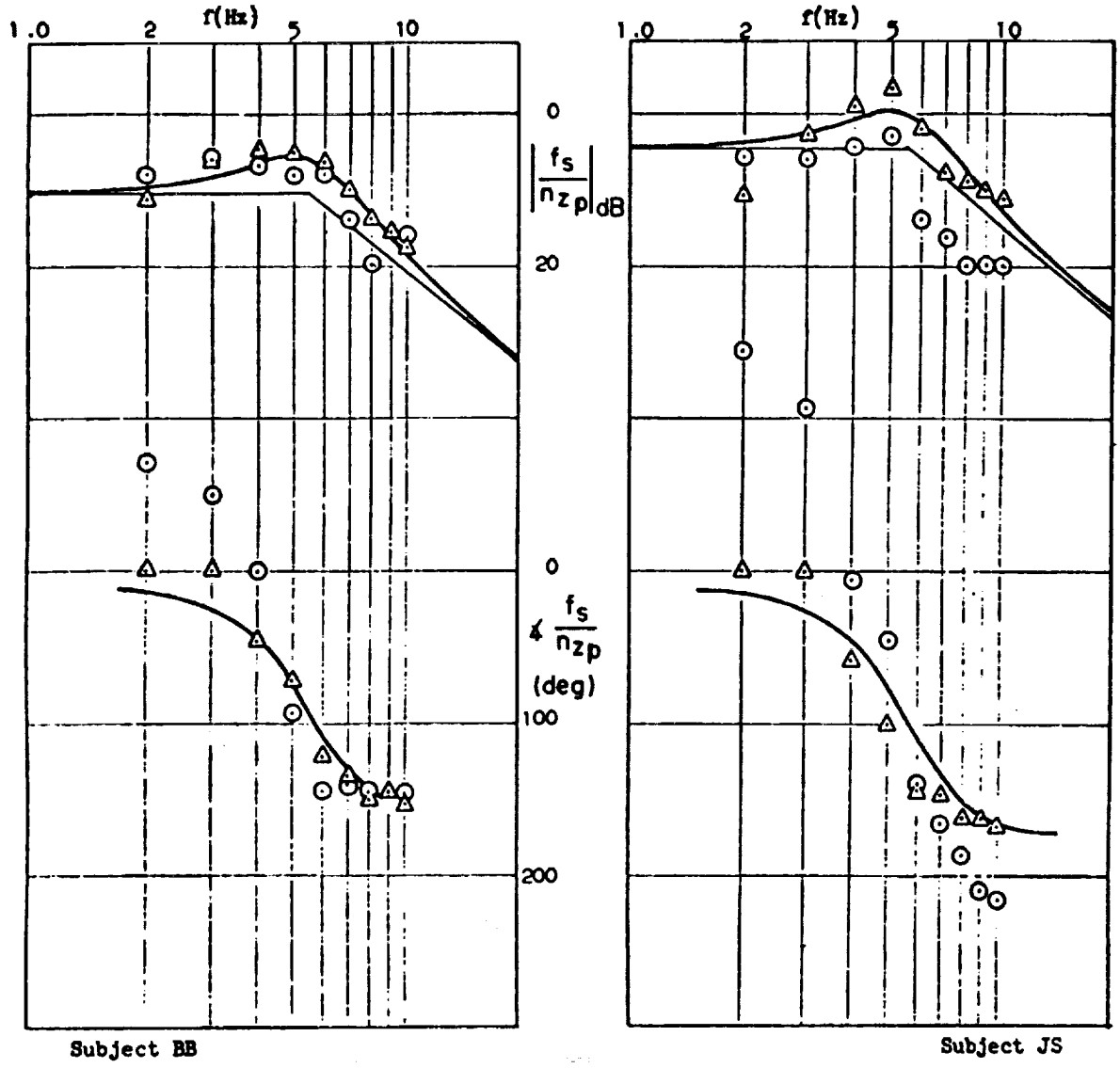

Figure 38. Vibration Feedthrough Frequency Response for a Spring Stick

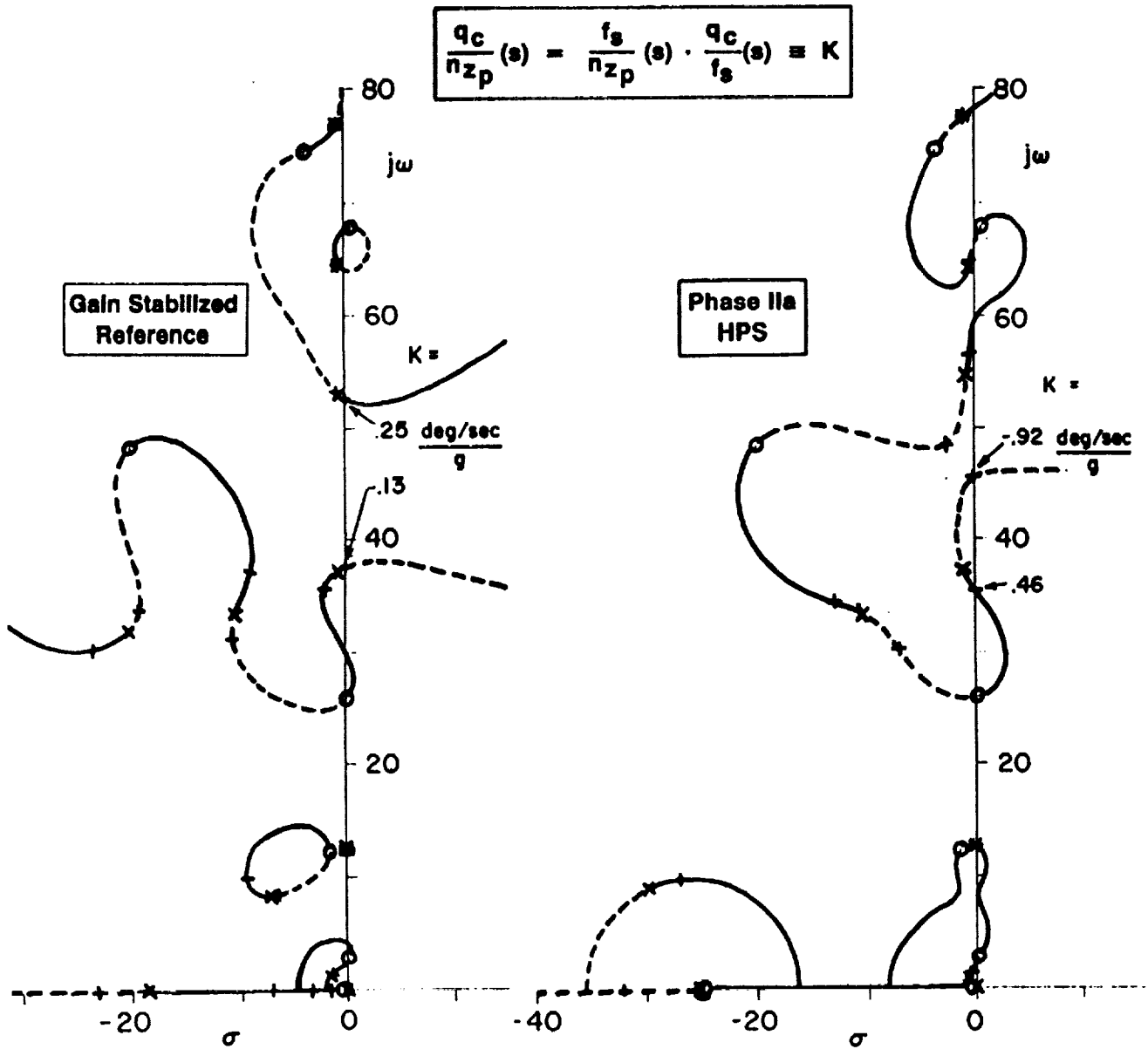

Figure 39. Root Locus Survey of Biodynamic Coupling with a Mechanical Stick

Figure 40 shows the normal acceleration feedback loop closures for this system as conventional root loci and Figure 41 shows the corresponding Bode root loci. Since the stick filter configuration has the lowest command path bandwidth of the three examined, the least excitation of structural modes would be expected and this is reflected in the Table 11 margins. Table 11 also shows that the gain stabilized reference design, with the stick filter, has higher margins than the Phase IIa design - a reversal from the situation in the two previous cases. With the stick filter, there is less uncertainty about phasing and the positive gain should be the physically meaningful case. On this basis, the conventional design has about twice the margin of the HPS design.

Some insight into this reversal of phenomenon can be gained from comparing the Bode root locus plots of Figures 37 and 41. With the introduction of the stick filter, the higher structural modes become less critical and the margin at the first structural mode becomes comparable to that at the (critical) higher modes. In this situation, the gain stabilized design has an inherent advantage due to the "notching" of the first mode. However, the ultimate significance of this depends on a more fundamental question, i.e., the significance of the margins on an absolute basis. This is addressed next.

4. Quantitative Assessment of Biodynamic Coupling

The question remains as to whether there is an actual potential for a closed loop biodynamic instability for any of the SCAS design/command path configurations considered above. To assess this, some absolute values for gains in the Figure 33 system must be determined. This is summarized in Figure 42 and explained further below.

The augmented vehicle dynamics have been given previously in Table 9. A representative magnitude for the pilot/stick dynamics in the structural mode frequency range can be obtained from Figure 34 as 30 dB in Newtons/g. This corresponds to 31.6 N/g or 7.1 lbs/g.

The final element, the command gain, requires some development. For a steady pullup,

$$\left[\frac{n_z}{q_c}\right]_{ss} \approx \left[\frac{n_z}{q}\right]_{ss} = \frac{V_{T_o}}{g} \quad . \tag{7}$$

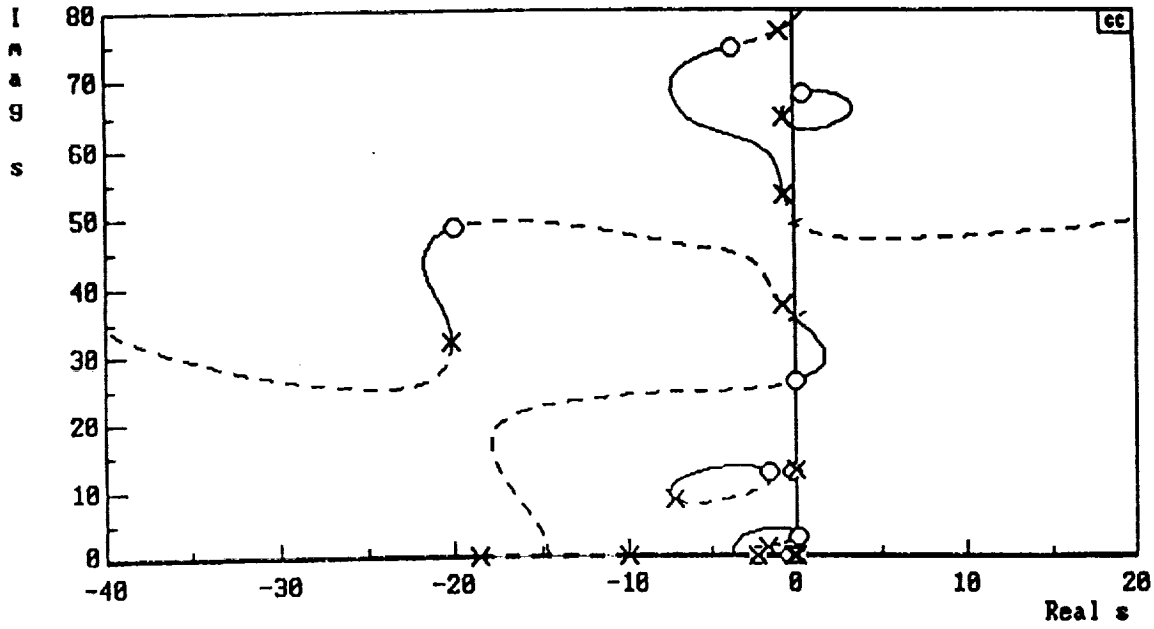

a) Gain Stabilized Reference Design

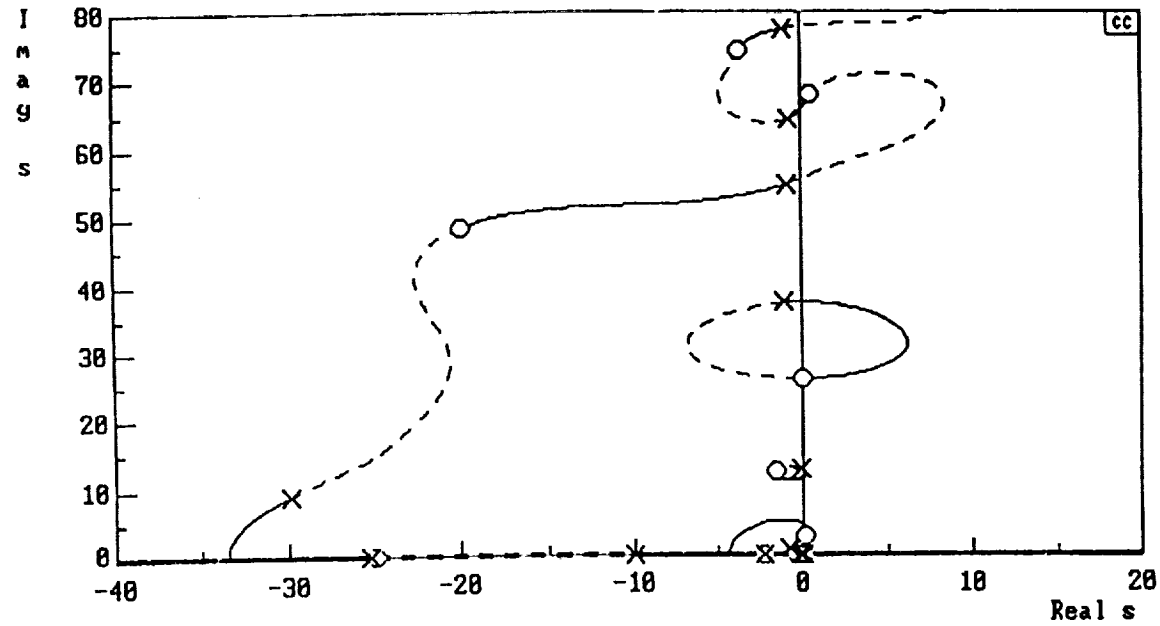

b) Phase IIa HPS Design

Figure 40. Root Locus Survey of Biodynamic Coupling with Fly-by-wire Stick and 10 rad/sec Stick Filter

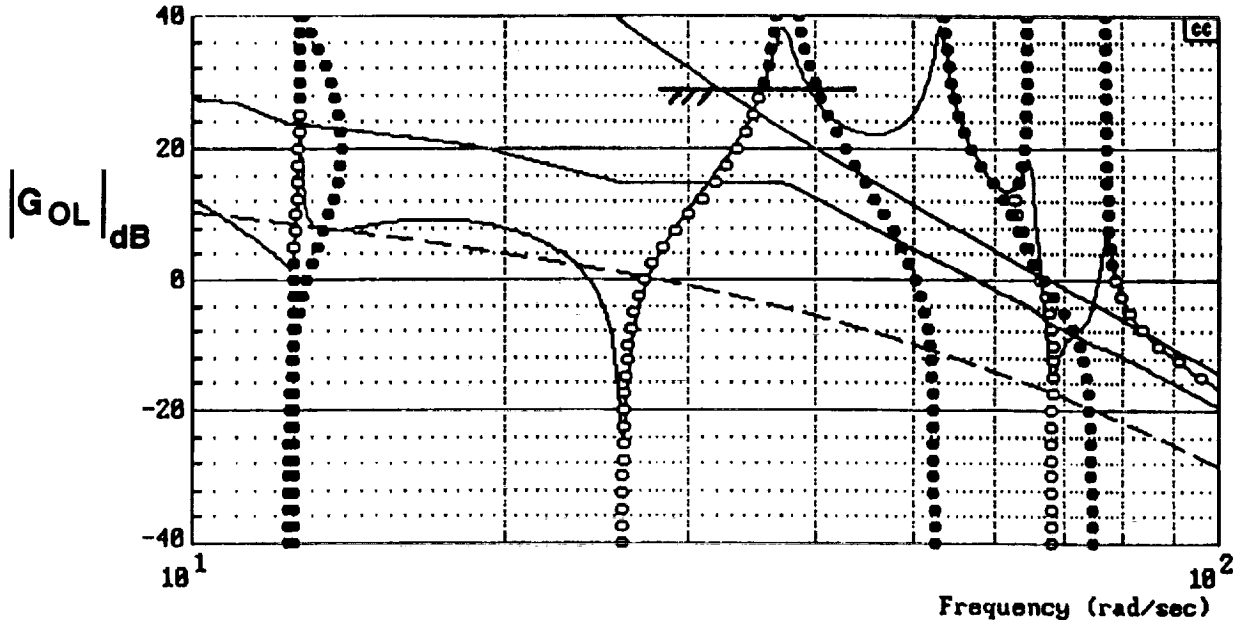

GAIN STABILIZED REFERENCE

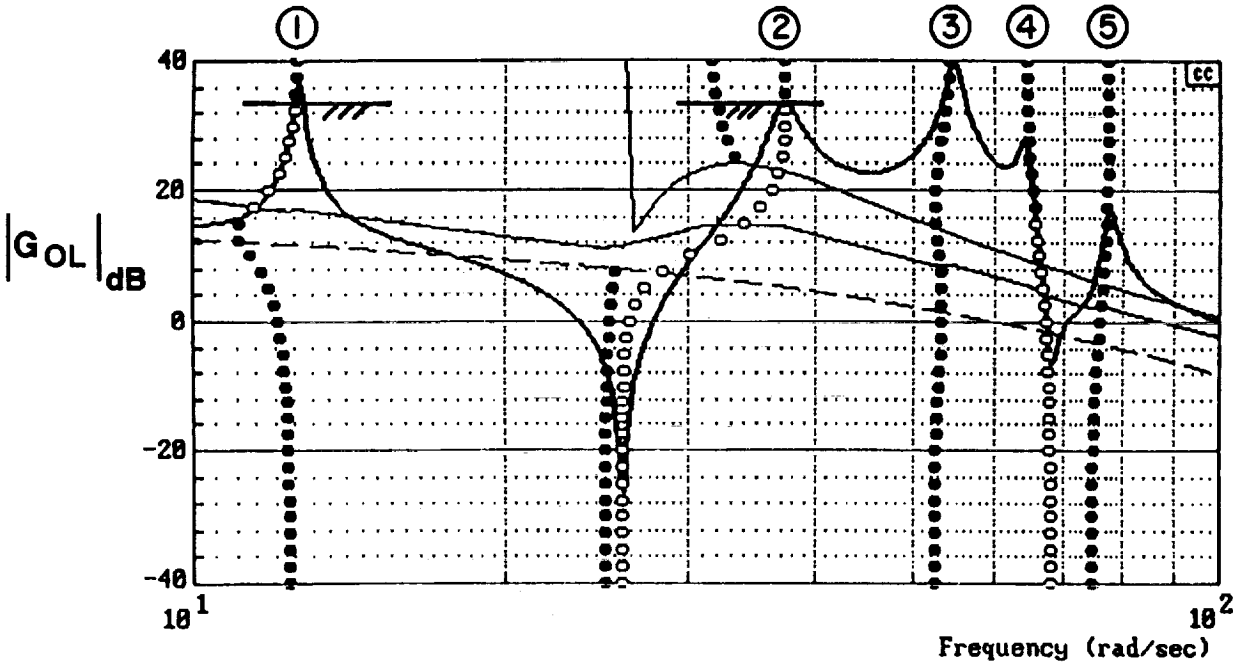

PHASE IIa HPS

Figure 41. Bode Root Locus Survey of Biodynamic Coupling with Fly-by-wire Stick and 10 rad/sec Stick Filter

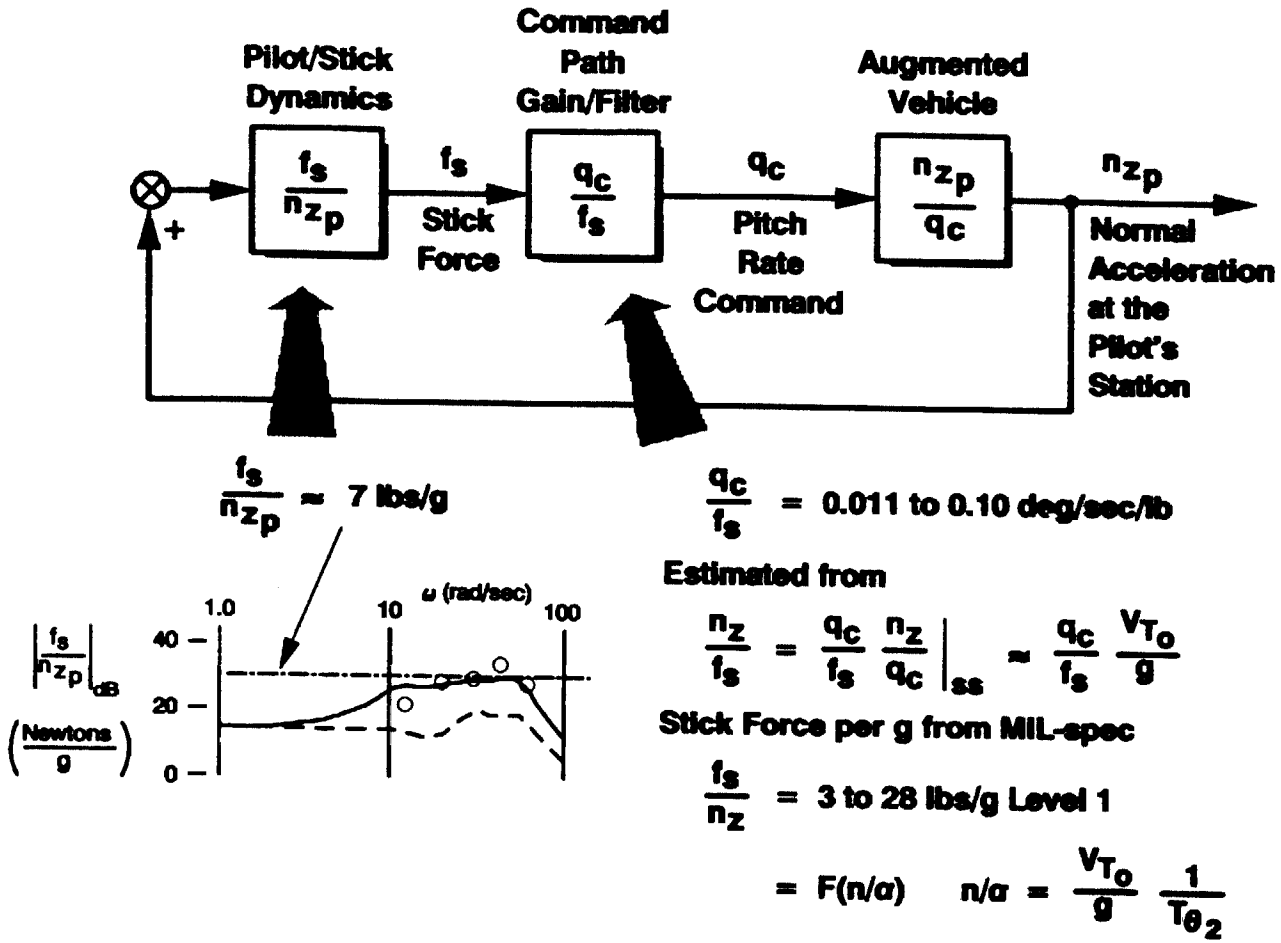

Figure 42. Quantification of Biodynamic Coupling

For the Mach 6 flight condition, $V_{T_o}/g = 186.3$ g/rad/sec or 3.25 g/deg/sec. Figure 43 compares this value with the low frequency asymptote of the n_{z_p}/q_c frequency response and shows the actual system response to be close, but a little low. This is due largely to imperfect command following of the pitch loop which was not optimized. The difference, however, is insignificant for the purposes of this study.

A point to be noted from the basic kinematics (Eqn. 7) is that hypersonic pitch rates must be much lower than for conventional aircraft to avoid exceeding structural load limits. However, it can be argued that the stick sensitivity, i.e. "stick force per g", will necessarily be much closer to conventional aircraft levels. For the purposes of this analysis, the MIL-STD-1797A Level 1 range of 3 to 28 lbs/g will be used. According to the MIL-spec, the actual values depend on the parameter

$$n_z/\alpha \approx \left(\frac{V_{T_o}}{g}\right)\left(\frac{1}{T_{\theta 2}}\right) \quad . \tag{8}$$

As is now well recognized, HSV will have unconventionally low values of $1/T_{\theta 2}$ (Ref. 8) which in turn implies that the existing database on stick sensitivity may be inadequate or inappropriate for HSV design. However, the above noted stick sensitivity range should serve for an initial analysis here.

Thus, given

$$\frac{n_z}{f_s} = \frac{q_c}{f_s}\frac{n_z}{q_c} \approx \frac{q_c}{f_s}\left(\frac{V_{T_o}}{g}\right) \tag{9}$$

the low frequency gain of the command path element can be estimated as

$$\left[\frac{q_c}{f_s}\right]_{ss} = 1.92\text{x}10^{-4} \text{ to } 1.79\text{x}10^{-3} \text{ rad/sec/lb}$$
$$= 0.0100 \text{ to } 0.103 \text{ °/sec/lb} \quad . \tag{10}$$

It should be noted that the stick force per g transfer function f_s/n_z is physically independent of the transmissibility transfer function f_s/n_{z_p}. Also, under the short period approximation used in this work, the steady state is the frequency range relevant to maneuvering and thus to the stick force per g specification.

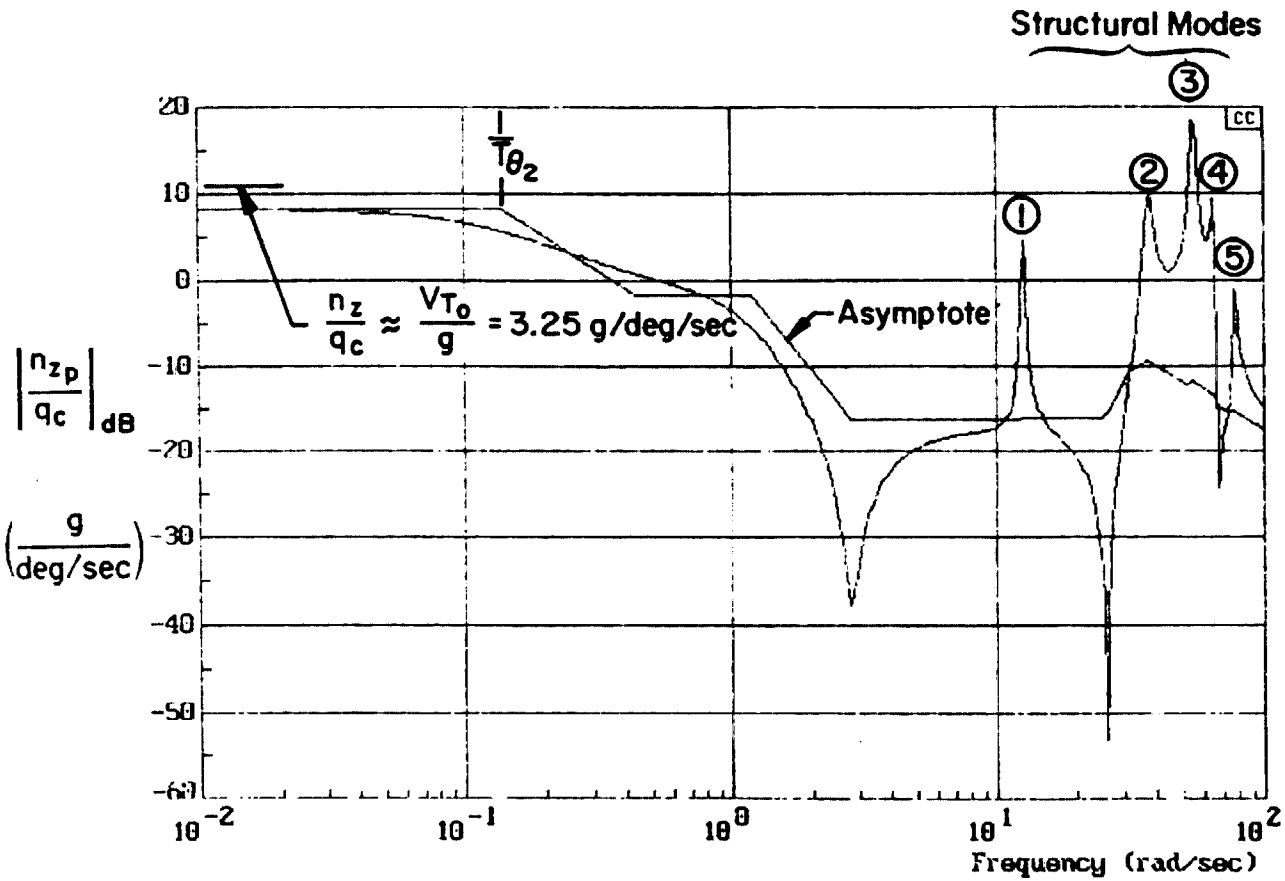

Figure 43. Closed Loop Normal Acceleration Magnitude Plot at the Pilot's Station for Phase IIa HPS Design

The low value in Eqn. 10 corresponds to the upper end (28 lbs/g) of the stick force per g range. Conventional practice would call for higher levels at high speeds, but the low hypersonic n_z/α clouds this issue.

To complete this analysis, the low frequency gain of q_c/n_{z_p} is calculated to compare with the values in Table 11.

$$\frac{q_c}{n_{z_p}} = \frac{f_s}{n_{z_p}} \frac{q_c}{f_s} = \begin{cases} 0.728\ ^\circ/\text{sec/g for } f_s/n_z = 3\ \text{lb/g} \\ 0.078\ ^\circ/\text{sec/g for } f_s/n_z = 28\ \text{lb/g} \end{cases} \quad . \qquad (11)$$

Comparison of Equation 11 with Table 11 (positive gains) indicates that only with the stick filter is there a stable margin, for either design, at low values of stick force per g. As noted above, the conventional design has about twice the margin of the HPS design, but whether either margin is adequate is somewhat uncertain. It should be noted that while positive margins imply stability, there is also an implication of some reduction in structural mode damping due to the pilot vibration transmission path, i.e., there is a potential for a special form of pilot induced oscillation. There is no existing specification for this biodynamic margin. No comparable analysis for a conventional aircraft is readily available.

As noted above, conventional practice would indicate higher stick force per g at higher speeds but this is associated with a corresponding increase in n_z/α. The unconventionally low values of hypersonic n_z/α create an uncertainty about the ideal HSV stick force per g and thus uncertainty about biodynamic coupling. There are other factors that may influence biodynamic coupling with structural dynamics. In particular, command path filters (beyond simple stick filters) may be needed to "quicken" HSV path response which may in turn affect biodynamic coupling. Recent work (Ref. 9) indicates that special roll maneuvering requirements may lead to requirements for response types other than pitch rate command which further complicates the analysis problem.

Given these uncertainties, it appears that these biodynamic issues should be considered in the stick path design for any HSV. Further investigation including specialized manned simulations are warranted particularly in connection with the development of HPS design criteria. The simulation problem for such an investigation has particular challenges which are addressed in the next section.

This page is intentionally left blank.

Section V

APPROACHES TO VALIDATION OF HPS DESIGN METHODS

A concept such as HPS flight control design must ultimately be validated. In general, this implies manned simulation studies and flight tests. For HSV, this process is particularly challenging but necessary in proportion to the challenge. Detailed consideration of flight validation is premature in the sense that initial HSV flight programs, e.g. the NASP, will be research programs in themselves. However, it was appropriate to begin consideration, in Phase II, of manned simulation studies, regardless of whether the final Phase IIa HPS design is sufficiently developed to validate. This reflects the complex problems to be solved to do meaningful simulation. To a large extent, these problems are related to the very wide frequency range that must be simulated. However, the need for such wide frequency range simulation arises not only for validation, but for further understanding of the impact of residual response and development of HPS design requirements. Even beyond these particular motivations, there appears to be an inherent need for wide frequency range simulation in HSV development. For example, investigating such complexities as propulsion system/structural dynamic coupling.

Of the issues addressed to date in this study, the questions of residual response are most appropriately addressed with manned simulation. The issues of effective time delay, system stability and robustness can all be examined with manned simulations. These areas can also be addressed analytically much more readily than can residual response questions. And even in the area of residual response, it should be noted that only the human-centered issues are really appropriate to address with manned simulation. Problems such as structural fatigue probably cannot be usefully studied directly with manned simulation.

In the dichotomy of passive and active human-centered problems noted above, the passive problems of ride quality are certainly important for HSV and similar aircraft such as the high speed civil transport (HSCT). However, the data from manned simulation studies related to ride quality (Ref. 15 and 16) are much richer than that for active issues such as biodynamic vibration transmission. Because this problem has intrinsic complexities for manned simulation beyond those of ride quality studies, it was the focus of consideration in Phase II for developing manned simulation approaches. At this point, there is no real need to distinguish between the simulation requirements for HPS validation and the requirements for supporting HPS concept development which precedes validation.

The primary HPS-related issues for biodynamic simulation studies of HSV manual control include:

- Overall assessment of the impact of residual response
- Development of biodynamic coupling data
  Controller (stick) design, stick filter design and seat design
- Impact of HSV maneuvers
- Impact of high altitude disturbances
- Impact of structural model uncertainty

As noted above, the primary driver for simulator capability is the wide frequency range required for this application. The unconventionally low value of hypersonic $1/T_{\theta 2}$ will tend to drive the minimum frequency range associated with maneuvering below 0.1 rad/sec. On the other end, simulation of the flexible modes could drive the simulator bandwidth above 10 Hz. Specialized simulators exist which can reach one end or the other of this frequency range, but generally not both ends.

A brief survey of existing simulators was made in Phase II to identify possibilities for hypersonic research. The capabilities of one such facility, a relatively small moving base simulator with a custom built hydraulic hexapod base, are summarized in Figure 44. This figure shows both simulator limits and human subject tolerance limits based on established standards. It can be seen that simulation in this facility is limited by human tolerance rather than simulator capability. It is interesting to note that this simulator, which in many respects is among the most well suited for hypersonic research, was built by an agricultural implement manufacturer for tractor development!

Existing moving base aircraft simulators designed for flying qualities and flight control research, such as the NASA LaRC VMS, can certainly accommodate the low frequency requirements. However, these simulators generally will not have the bandwidth desired for structural vibrations. This limitation is set primarily by high cab mass reflected in motion base lags and limiting although it might be possible to address the first structural mode (assumed around 2 Hz). Some sort of "shaker seat" might be obtainable to inject high frequency motion in series with the motion base to increase the effective bandwidth.

There are specialized vibration simulators, such as the Air Force AMRL "six-mode" (Ref. 14), which can meet the bandwidth requirements for this application. However,

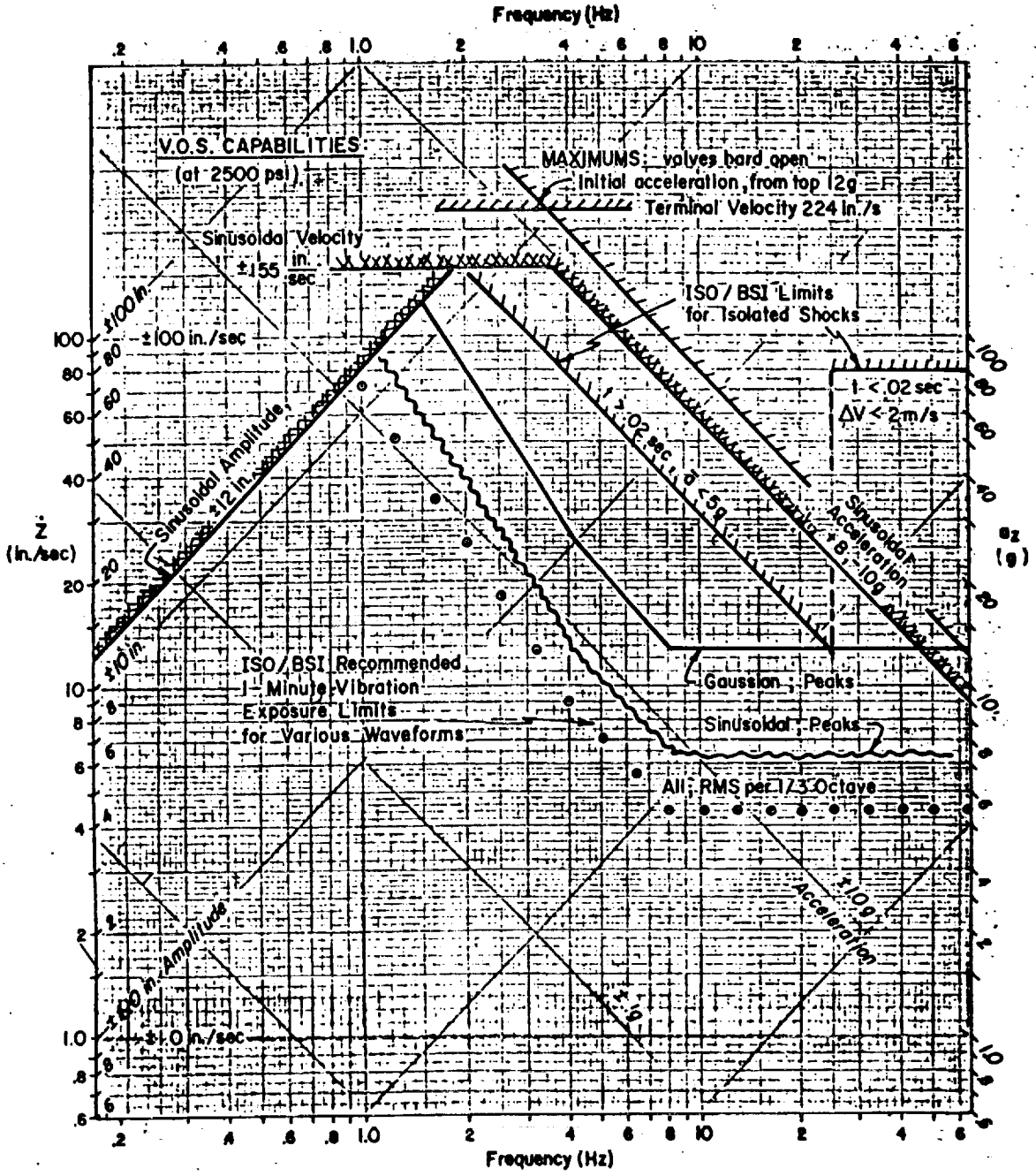

Figure 44. Vehicle Operations Simulator Performance Capabilities and Constraints

these facilities generally cannot achieve the low frequency requirements, i.e., they cannot simulate maneuvering. Further, there are typically limitations on mechanization of closed loop manual control experiments. For example, the AMRL six-mode could be run with the subject performing a tracking task, but for safety reasons the subject's input would not be fed back to the motion dynamics. During the Phase II work, discussions were held with AMRL personnel and the possibility of including the subject in the motion loop was discussed and it appears that there are possibilities for this.

One possibility, suggested by the above simulator limitations, is the use of both moving base flying qualities simulators and vibration simulators in coordinated experiments that would cover the wide frequency range of interest. The challenge, of course, is in integrating the results from several experiments in different simulator types. One possibility involves the use of a biomechanical model in the form of appropriate software, such as the STI BIODYN package (Ref. 17), to interface data from several simulators. Among the capabilities of the BIODYN package is the ability to identify the model parameters (see Figure 33) using frequency domain identification procedures applied to the measured simulator data.

To integrate data from several experiments in different simulator types, separate fits would be made with appropriate free parameters identified in BIODYN for each simulation. The aggregate of parameter values fitted would then constitute an overall model which in principle covers the frequency range of interest. This application of biodynamic modeling would require development and would be a significant effort in itself. However, it would provide a rational and systematic approach to the tricky problem of combining the results from distinctly different simulators. The end result would be a refined biodynamic model, tuned to the HSV situation, which could be used for development of physically-based design requirements or even used directly in the flight control design process.

Section VI

CONCLUSIONS AND RECOMMENDATIONS

A. Results and Conclusions

The hybrid phase stabilization design procedures were refined in this contract. The final Phase IIa HPS design is a significant improvement over the Phase I HPS design. It has achieved greater reduction in effective time delay as well as residual response. The final Phase IIa HPS design also meets the MIL-F-87242 gain and phase margin (8 dB and 60°, respectively) except for the third structural mode. This mode, however, is phase stable.

The final Phase IIa HPS design has a 36 msec effective time delay which is 41 msec less than Phase I HPS. This is also well below the 218 msec value for the gain stabilized reference design which greatly exceeds the MIL-STD-1797A Level 1 maximum of 100 msec.

The flexible HSV model was extended to provide normal acceleration at the pilot's station. Then, the Phase I residual response metric was revised by replacing the previous estimated model with the new model extension. Based on this revised metric, the residual response of the final Phase IIa HPS design was shown to be much improved over that of the Phase I HPS design and equivalent to that of the gain stabilized reference design.

The sensitivity of HPS designs to structural uncertainties were assessed by evaluating the stability metric with variations in structural damping ratio, mode shape and frequency. For the purpose of comparison, the sensitivity of gain stabilized designs were also evaluated. Both techniques appear to be somewhat sensitive to variation in structural frequency. While gain stabilization tends to be more sensitive to lower frequency variation, phase stabilization can be more sensitive to the higher frequency variation. One technique does not have distinct advantages over the other. Both HPS and gain stabilization techniques have their own potential problems and unique robustness characteristics.

The revised Phase II metric does not appear adequate for design based on the structural fatigue study and the analysis of biodynamic vibration feedthrough, but has potential for refinement based on such physical bases.

Assuming titanium 6-4 fatigue properties, the preliminary structural fatigue study predicts that while elevated temperature exposure reduces the fatigue lives for both the gain stabilized and HPS designs, gain stabilization exhibits a lower vehicle weight for a given number of maneuver cycles. However, re-optimization of the HPS design to explicitly accommodate fatigue could reduce or perhaps remove this shortcoming for HPS designs.

Biodynamic analysis of vibration feedthrough was performed for the gain stabilized reference design and the final Phase IIa HPS design. The two designs are roughly comparable, but the gain stabilized design may have an advantage due to the notch filtering of the first structural mode. However, there is a potential for destabilization of structural modes by the pilot with either system. It was found that biodynamic analysis of manual control is quite sensitive to the assumptions about the controller (stick) and command path dynamics and the stick force per g level appropriate for HSV.

Because its effective time delay is well below the MIL-spec requirement, the Phase IIa HPS design has apparent potential for further refinement to meet residual response requirements. The critical need to achieve this is refinement of the multiple aircraft and human-centered requirements in a form suitable for design.

B. Recommendations for Future Research

The final Phase IIa HPS design is a clear improvement over the earlier HPS designs, but still has some apparent shortcomings with respect to the conventional gain stabilized reference design. This is based primarily on the structural fatigue and biodynamic coupling assessments made after the last design iteration. However, this is not conclusive because these assessments are not validated design requirements. Furthermore, the conventional reference design fails to meet established design requirements (in particular, MIL-spec phase margin and time delay) so it cannot actually be considered superior to the HPS designs.

The final Phase IIa HPS design satisfies the time delay requirement by a wide margin (36 msec which is much less than the 100 msec required) which suggests that this margin could be traded for improvements in other areas. This in turn suggests that the problem is reaching the stage where more formal design optimization methods may be appropriate to efficiently address increasing subtle tradeoffs among multiple requirements. To this point in the project, problem definition, basic control system architecture, and

physical interpretation have been emphasized to understand design requirements and their implications. Standard classical control system synthesis methods have been adequate and appropriate for this activity, and thus, synthesis methodology has not been emphasized. With considerable basic development work done, it now appears appropriate to begin considering how optimal synthesis methods could be exploited to carry the HPS developments forward.

However, to lead to useful design procedures for hypersonic flight control, a "problem-driven", as opposed to "methods-driven", approach to optimal synthesis methods must be adopted. That is, the procedure must begin with the best possible development of the design requirements for the HSV control problem. A search of existing optimization methods can then be made for those with the best potential for this application. Next, refinement of selected synthesis methods to meet the specific requirements of this application and the HPS concept would be made. The design requirements of this particular application can be translated to meet the format of specific optimization algorithms as long as the intent of the original requirement is not compromised. The basic principal is that the method must accommodate the application and not the reverse.

The basic elements of recommended future work include development of the following: requirements, basic architecture, design strategies, and synthesis methods.

In terms of requirements, the premise is that formulation of a complete and appropriate set of requirements is the key step in the design problem. Without these, no optimal synthesis method can produce a good HSV design. The practical problem is that there are multiple requirements which may even conflict. Major requirements include: effective rigid body dynamics, effective time delay, control power, MIL-spec gain and phase margins, specialized robustness specification, human-centered residual response requirements, and aircraft-centered residual response requirements.

Regardless of the requirements and synthesis procedures used, the basic system architecture must be maintained under the direct control of the designer; the methodology must react accordingly. This includes the imposition, by the designer, of the standard filter forms such as notches and lags with constraints on order and location. For HPS design, this must also allow the blending of specified multiple sensor signals with constraints on location. Ultimately, the inclusion of estimators should be provided for.

For a given architecture, there are still degrees of design freedom that the designer must be able to constrain as part of a design strategy. For HPS designs, the major issue is deciding which modes will be primarily gain stabilized and which will be phase stabilized. A directly related strategy issue is the tradeoff between damping a structural mode and filtering it out. Part of the overall strategy used to date is to treat the structural modes in a way which does not significantly affect the effective rigid body mode. This has the significant advantage of allowing the rigid body compensation to be designed independently, but it also constrains the positioning of the first flexible mode zero in HPS designs. Furthermore, integration of the rigid and flexible control design might allow further improvement in the HPS model damping. The real issue here is to improve the designer's productivity by reducing his computational load without eliminating the added value of his design guidance.

Efforts are being made to investigate applications of new methods such as H-infinity control to the control of flexible vehicles in ways which address the above issues. Progress has been made in guiding H-infinity designs procedures to produce standard lag and notch filters. More importantly, procedures for damping modes in H-infinity designs have been developed which are relevant to HPS applications. In addition to these H-infinity approaches, validated software, having the capability for fixed form optimization, exists which could be used to optimize HPS architectures.

REFERENCES

1. Chan, S. Y., P. Y. Cheng, D. M. Pitt, T. T. Myers, D. H. Klyde, R. E. Magdaleno, and D. T. McRuer, " Aeroservoelastic Stabilization Techniques for Hypersonic Flight Vehicles", NASA CR-187614, September 1991.

2. Military Specification, "General Specification for Flight Control System", MIL-F-87242, 31 March 1986.

3. Military Standard, "Flying Qualities of Piloted Vehicles", MIL-STD-1797, 31 March 1987.

4. Klyde, D. H. and T. T. Myers, "Initial Refinements of the Phase I Hybrid Phase Stabilization (HPS Design)", Systems Technology, Inc., WP-2399-5, October 1991.

5. Pitt, D. M. and C. E. Goodman, "FAMUSS: A New Aeroservoelastic Modeling Tool", AIAA-92-2395, 33rd AIAA/ASME/ASCE/AHS/ASC Structures, Structural Dynamics and Materials Conference, Dallas, TX, 13-15 April 1992.

6. Hamilton, P. N., "Flexible Body Stabilization for Space Shuttle Aerosurface Control Loops", AIAA-82-1532, AIAA Guidance, Navigation, and Control Conference, San Diego, CA, August 1982.

7. Haiges, K. R., K. P. Madden, B. G. Eller, A. Emami-Naeini, M. R. Anderson, and T. L. Tranke, "Robust Control Law Development for Modern Aerospace Vehicles, Task 2: Control System Criteria and Specifications", WRDC-TR-90-3005, January 1990.

8. Myers, T. T., D. H. Klyde and G. Larson, "Hypersonic Flying Qualities", Systems Technology Inc., ITR-1277-1, June 1991.

9. McRuer, D. T. and T. T. Myers, Considerations for the Development of NASP Flying Qualities Specifications, WL-TR-92-3042, June 1992.

10. "Metallic Materials and Elements for Aerospace Vehicle Structures, Military Handbook", MIL-HDBK-5F, 1 November 1990.

11. "SPECCI, Fatigue Crack Initiation Life Prediction Software", MDC FFM-92001, 31 January 1992.

12. Raney, D. L. and F. J. Lallman, "Control Integration Concept for Hypersonic Cruise-Turn Maneuvers", NASA TP-3136, February 1992.

13. Allen, R. W., H. R. Jex and R. E. Magdaleno, "Manual Control Performance and Dynamic Response During Sinusoidal Vibration", AMRL TR-73-78, October 1973.

14. Jex, H. R. and R. E. Magdaleno, "Biomechanical Models for Vibration Feedthrough to Hands and Head for a Semisupine Pilot, Presented at Symposium on Biodynamic Models and their Applications", AFOSR TR-79-1065, 15-17 February 1977.

REFERENCES (Continued)

15. Jex, H. R., R. J. DiMarco and S. H. Schwartz, "A Review and Updating of Surface Effects Ships Seakeeping and Handling Qualities Specification HQ-1, PARA. 3.6 - Habitability", Systems Technology, Inc., TR-1031-1A, February 1975.

16. Stone, R.W., Jr., "Ride-Quality Overview", Symposium on Vehicle Ride Quality, NASA TM-2620, October 1972.

17. Jex, H. R., R. E. Magdaleno and B. L. Aponso, "User's Guide for Biodyn-86/HMD: (An Interactive Program Ensemble for Modeling Biodynamic Feedthrough to Helmet-Mounted Displays Including Image Motion Compensation)", Systems Technology, Inc., TR-2308-1, June 1988.

18. Myers, T. T., D. T. McRuer, and D. E. Johnston, "Flying Qualities and Control System Characteristics for Superaugmented Aircraft", NASA CR-170419, December 1984.

Appendix A

LOW FREQUENCY GAIN MARGIN

The main focus of HPS design, once the superaugmented pitch loop is established at the rigid body level, is on the high frequency (structural mode) region. However, as can be seen in Table 1, the low frequency gain margins of all four designs (at the phase angle crossover around 1 rad/sec) are below the MIL-F-87242 minimum. The low frequency phase crossover arises from the inherent conditional stability of the superaugmented pitch loop design applied to a statically unstable airframe (Ref. 18). The final Phase IIa HPS design comes closest to meeting the requirement and the gain stabilized reference design is the most deficient. These deficiencies were considered minor with reasonably straightforward solutions, but no attempt was made to rectify the designs because this deficiency has very little significance with respect to the critical questions of HPS design.

However, the possibilities for improving the low frequency gain margin were examined briefly at the outset of Phase II, based on the Phase I HPS design, to verify the above assumptions. Lag-lead filters were inserted in the pitch loop to boost the low frequency gain margin by extending the k/s asymptote below 2 rad/sec. This can be accomplished by placing the compensator lag at 1.5 rad/sec and the lead at 2 rad/sec. The effects of this compensator are shown in Figures A-1 through A-4 which should be compared to Figure 7. As can be seen in Figures A-1 (Bode root locus plot) and A-2 (Bode magnitude and phase plots), the k/s asymptote has been extended below 2 rad/sec, thus increasing the low frequency gain margin above the required 6 dB. Figure A-3 displays the root locus for this system. Notice that the compensation creates a potential for increasing the damping of the first flexible mode. Because of the gain limitation implied by the desired rigid body bandwidth, this potential is not exploited in this design.

The closed loop pitch rate response to a step pitch rate command is shown in Figure A-3. Comparison with the original Phase I HPS design (Figure 13) shows that the modified system approaches the steady state value considerably faster. This difference results from increased closed loop frequency of the effective short period mode. That is, the presence of the lag-lead compensator has changed the bandwidth of the design. This is not surprising, but does imply that further design iteration would be required if the original dominant mode target was to be achieved. However, as noted above, the only purpose of this exercise was to demonstrate that the low frequency gain margin problem would

respond to standard treatment. This treatment was not applied to later designs since the issue is not considered significant with respect to the objectives of the project.

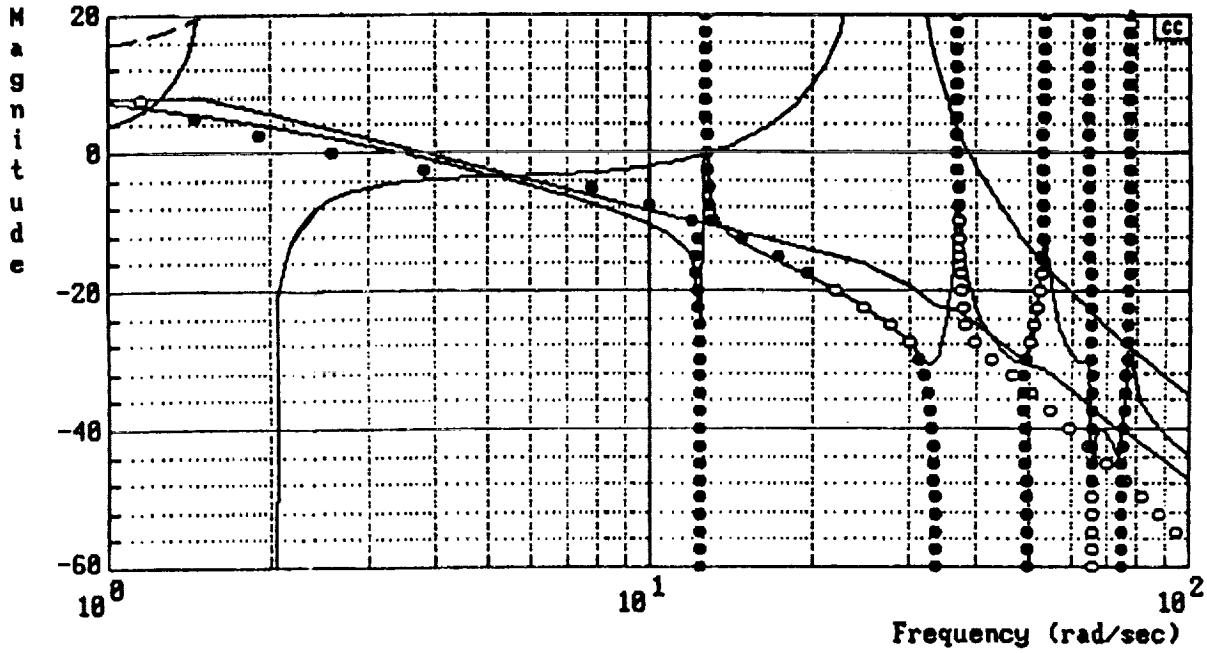

Figure A-1. Bode Root Locus Plot of Phase I HPS Design with Low Frequency Lag-lead Compensator

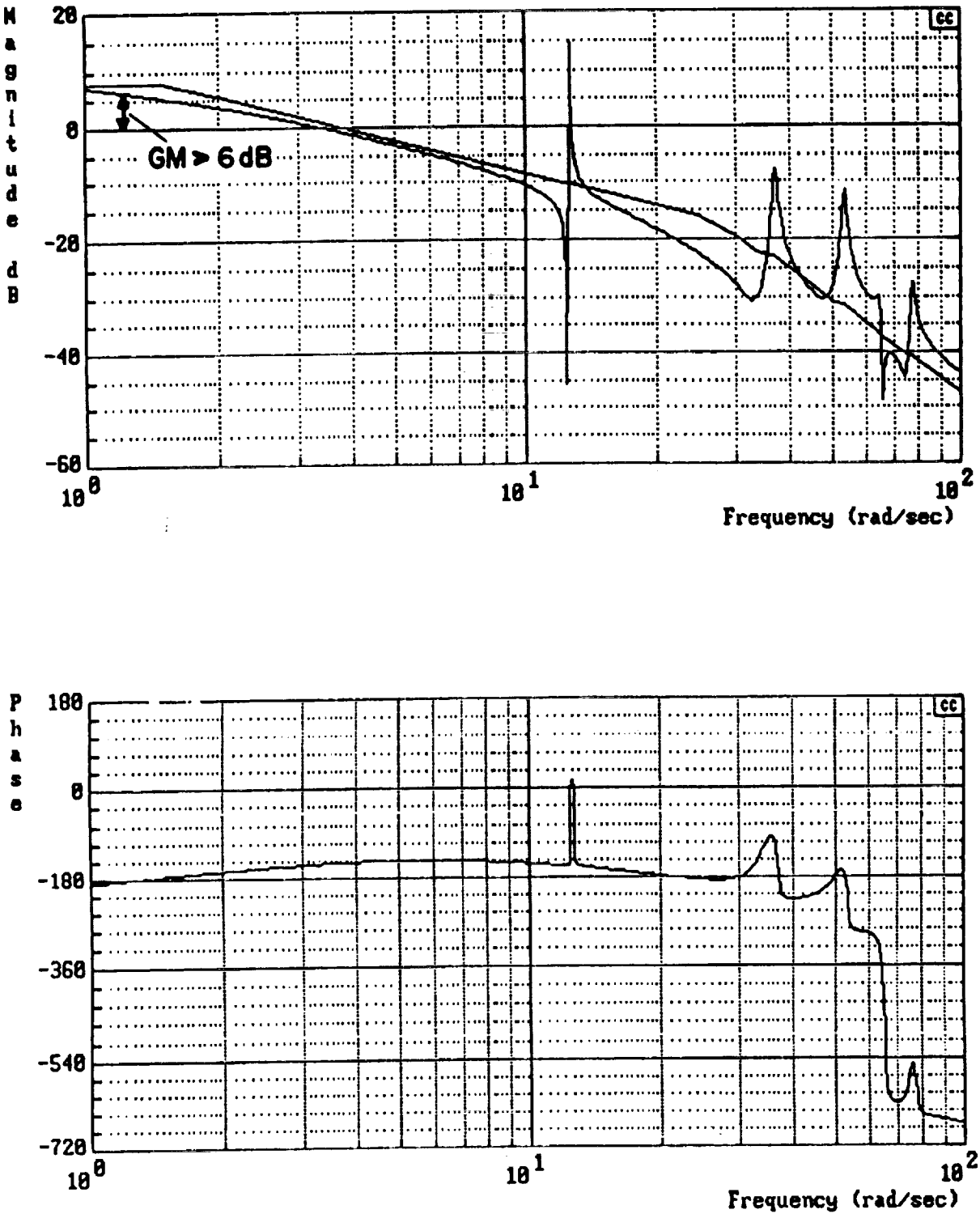

Figure A-2. Bode Plot of Phase I HPS Design with Low Frequency Lag-lead Compensator

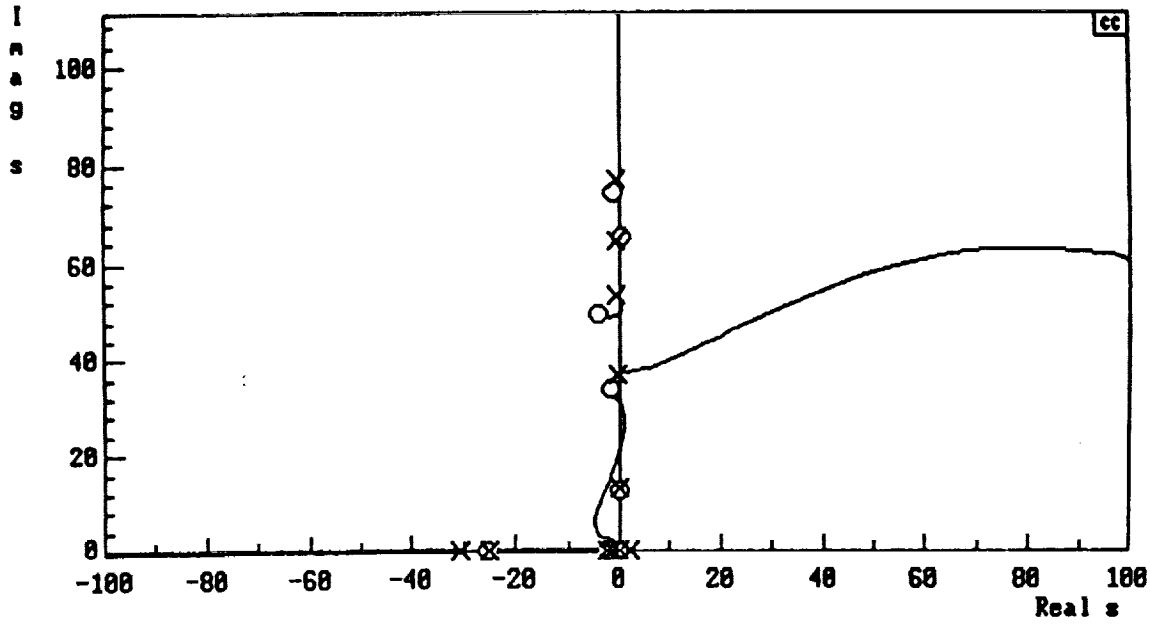

a) Complete System

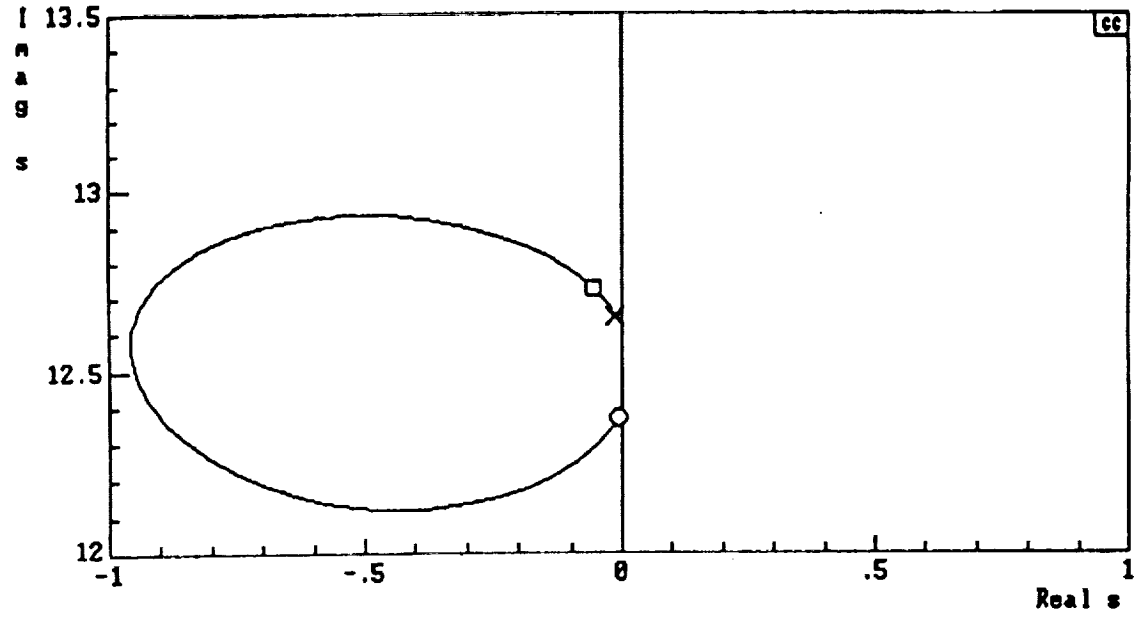

b) 1st Flexible Mode Dipole

Figure A-3. Root Locus of Phase I HPS Design with Low Frequency Lag-lead Compensator

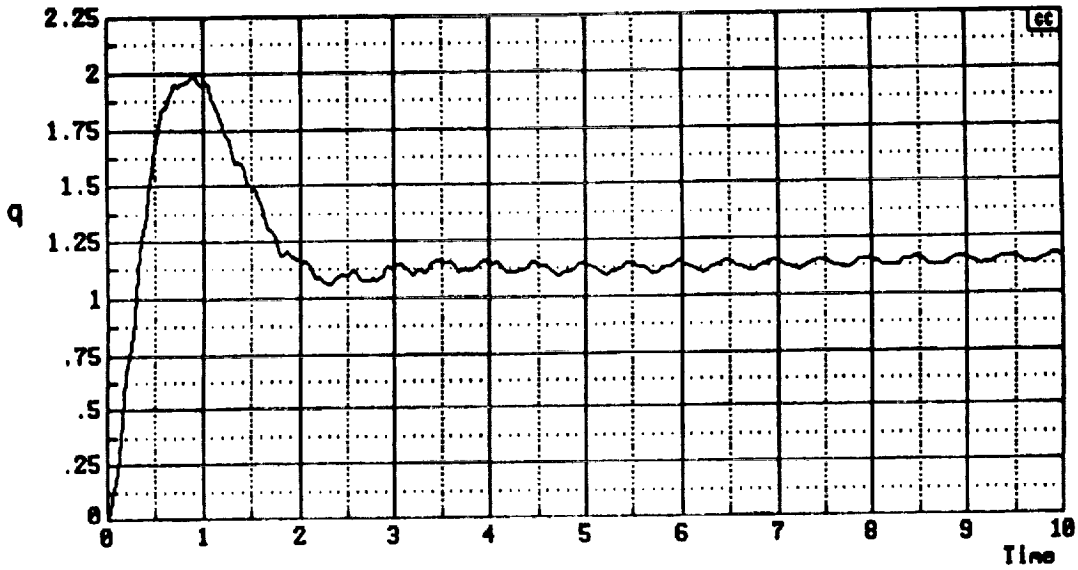

$$\left.\frac{q}{q_c}\right|_{C.L.} = \frac{-6860(.169)(.44)(2)(2.31)[-.0375, 12.7](25)^2 [-.111, 36.3][.196, 53.9][-.0366, 65.5][.00961, 76.6](-1260)}{(.14)(.75)(2.31)[.54, 2.58][.00447, 12.7](13.1)(25.3)[.00626, 37](38.8)[.00817, 53.3][.0102, 64.7][.00971, 77][.507, 273]}$$

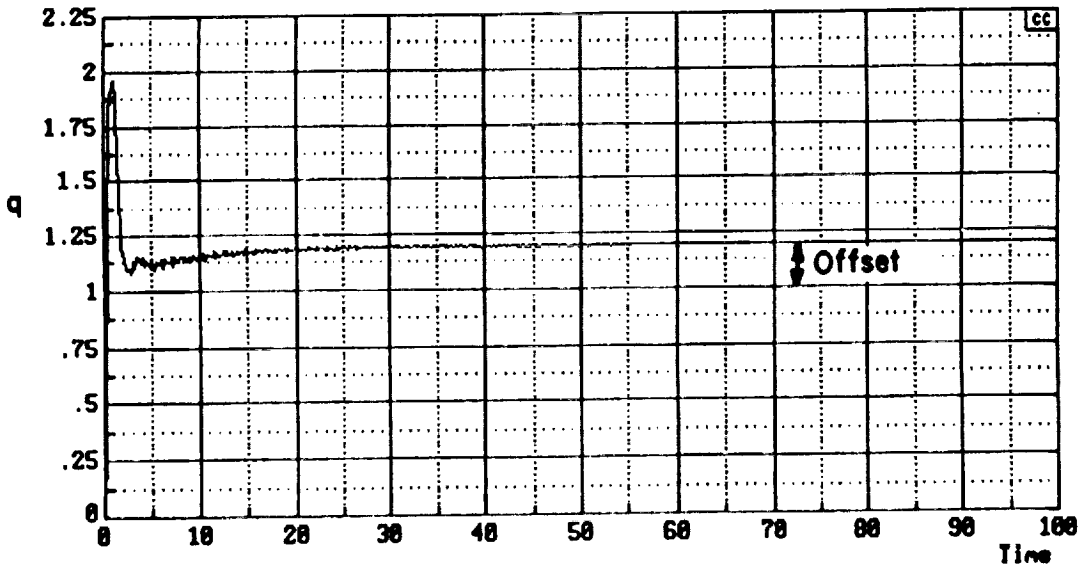

Figure A-4. Closed Loop Pitch Rate Response at the Pilot's Station to a Unit Step Command for the Phase I HPS Design with Low Frequency Lag-lead Compensator

This page is intentionally left blank.

Appendix B

SIGNIFICANCE OF NEGATIVE PHASE MARGINS FOR HPS DESIGNS

Phase stabilized control system designs (or the phase stable regions of HPS designs) have an identifying characteristic in the phase curve of their frequency responses. This is the "sawtooth Bode" characteristic seen in the Figure 16 phase curve. One important consequence of this is that the open loop transfer function phase angle generally remains between -180° and +180° in the phase stable region. This is distinct from the phase characteristic of gain stabilized designs (cf. Figure 5, noting that the phase curve is "folded" whenever it crosses the edge of the plot). In these designs, the phase angle typically crosses -180° just before the first structural mode and decreases continuously through the structural mode region.

These differences in phase characteristics imply a need for some care in interpreting phase margin between conventional and HPS designs. Specifically, while a negative phase margin for a gain stabilized design generally implies an instability, this is not the case for an HPS design. For example, the complete tabulation of phase margins for the Phase IIa HPS design (Table B-1) shows two negative phase margins associated with the first 0 dB gain crossings at the first two structural modes. HPS designs will tend to have more 0 dB crossings than gain stabilized designs, thus creating more phase margins. In particular, HPS designs create two phase margins for every sawtooth that peaks above 0 dB. This is illustrated in Figure 16.

Table B-1. Phase Margin Tabulation for Phase IIa HPS Design

Structural Mode No.	--	1	1	2	2	3	3
Zero dB Gain Crossing (r/s)	3.46	12.6	12.9	36.3	37.8	52.3	54.8
Phase Margin (deg)	60.63	-96.7	96.9	-166.7	79.7	142.6	27.1

Figure B-1 shows a sketch of the Bode plot around a phase stable dipole. Note that phase angle peak implies net phase lead from higher frequency dynamics not shown. The sketch of the phase curve around the dipole shows that when the phase angle of G_{OL} is, say, +90°, then the phase margin is 270° which is the same as -90° and phase stable. The important question is what does this really indicates about robustness? The phase margin should indicate if the system is robust with respect to phase uncertainties. For flight control design, particularly with the rigid body models ordinarily used, the concern is with unmodeled high frequency lags due to actuators, sensors and (gain stabilizing) structural filters (often not well defined in preliminary FCS design). The simplest approximation for these is a pure time delay.

For the case of pure time delay, a -90° phase margin implies a much more robust design than one with a +90° phase margin. The question that remains is that of robustness with respect to unmodeled phase lead. For the conventional case of flight control design using rigid body models noted above, unmodeled dynamics would be very unlikely to produce phase lead. However, when working with more complete models including structural modes, and detailed sensor and actuator models, this assumption may not be so reliable; conceivably the unmodeled dynamics in more sophisticated models could result in net lead.

Thus, the possibility that unmodeled lead could drive a positive phase "blip" unstable should be at least considered in an HPS design. Subtleties occur, e.g. a -90° phase margin is more robust to unmodeled lead than a -45° margin, but its the other way around for unmodeled lag. This raises new questions of what phase margins should be with possible unmodeled lead. As a minimum, the existing MIL-specs should be applied thoughtfully (as they always should be in any case!).

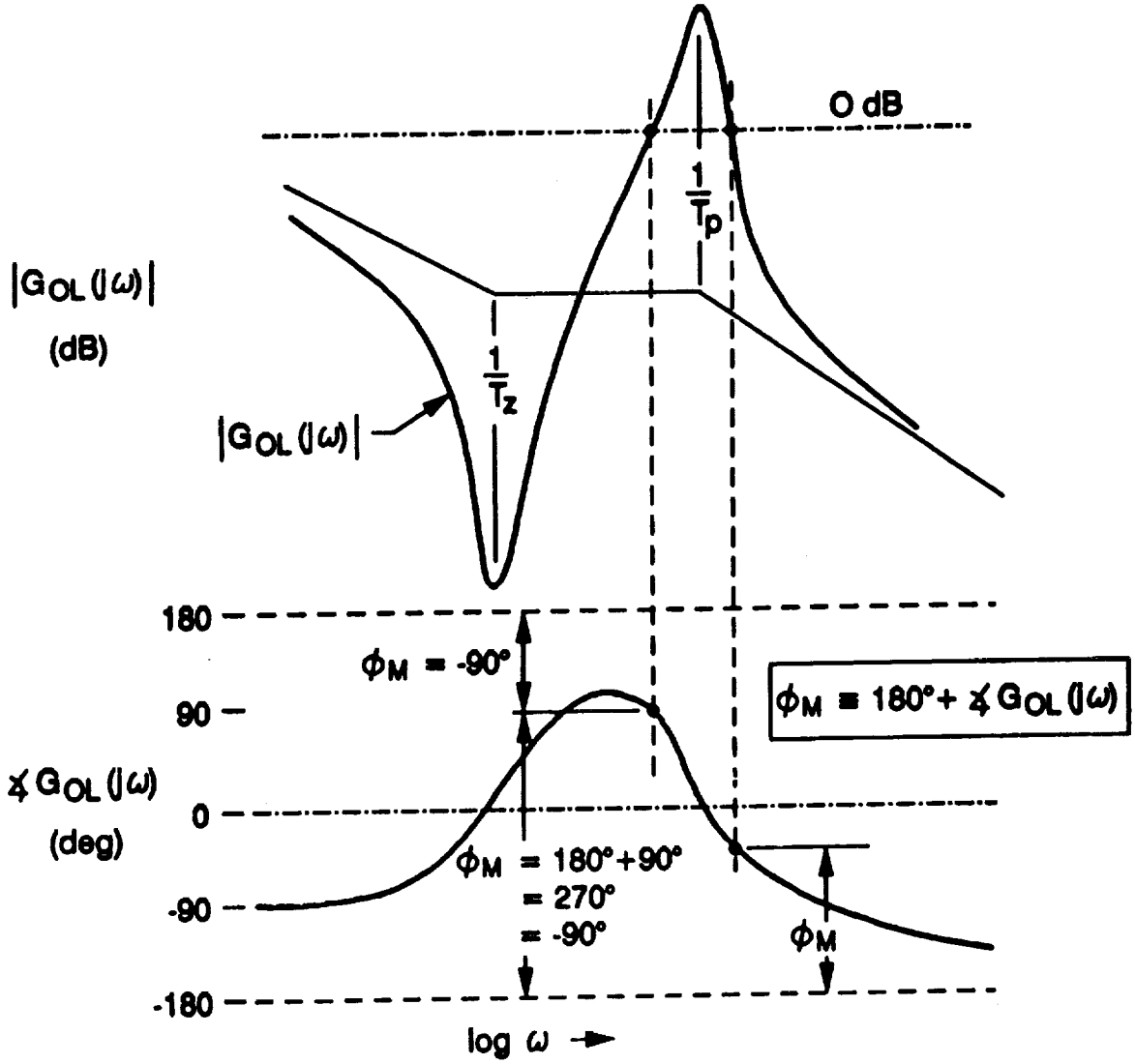

Figure B-1. Illustration of Negative Phase Margin for a Phase Stabilized Design

This page is intentionally left blank.

Appendix C

ACCELEROMETER DYNAMICS IN HYPERSONIC FLIGHT OVER A SPHERICAL EARTH

As noted in Ref. 8, "rotation of vertical" (R.O.V.) due to hypersonic flight over a curved earth (for nominally level flight) does not effect the force equations. Rather, the effects of "centrifugal relief" enter the dynamics through the kinematic relations between angular velocity (with components P, Q and R referenced to inertial space) and the Euler angles (Ψ, Θ and Φ referenced to local vertical). The dynamics of an accelerometer (on a rigid HSV) will be formally developed here to exhibit the R.O.V. effects. It will be shown that R.O.V. effects are of such low frequency that they do not affect HPS design.

A. ACCELERATION EQUATIONS

From Figure C-1,

$$m\,(A_a \cdot e_a + \ddot{x}) = -c\dot{x} - kx + mg \cdot e_a \qquad \text{(C-1)}$$

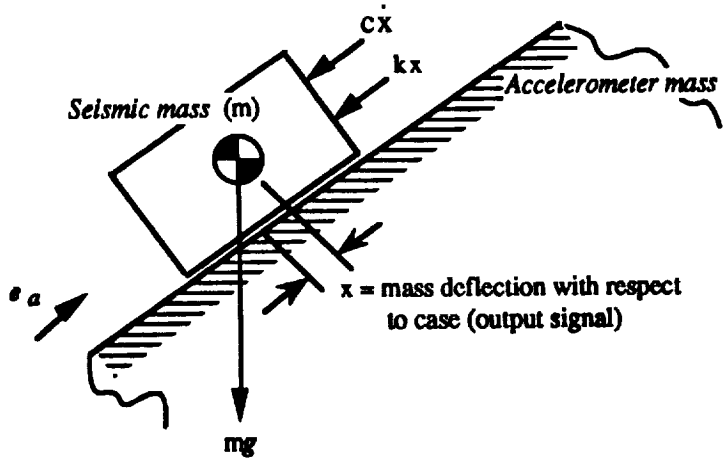

Figure C-1. Freebody Diagram of Accelerometer Seismic Mass

where

A_a = acceleration of case with respect to inertial space
e_a = unit vector in direction of accelerometer sensitive axis
m = mass
c = damping coefficient (c > o)
k = spring constant (k > o)
g = gravitational acceleration vector
x = displacement of seismic mass

Rearranging,

$$-m\left(\ddot{x} + \frac{c}{m}\dot{x} + \frac{k}{m}x\right) = m\,(A_a - g)\cdot e_a \qquad \text{(C-2)}$$

At frequencies well below the accelerometer natural frequency $\sqrt{k/m}$,

$$-\frac{k}{m}x \approx (A_a - g)\cdot e_a \qquad \text{(C-3)}$$

The accelerometer signal S_a is

$$S_a \equiv -\frac{k}{m}x = (A_a - g)\cdot e_a \qquad \text{(C-4)}$$

This formulation is conventional and applies whether or not the earth is assumed flat. Further, g does not (and should not) contain any centrifugal relief corrections; these effects enter through the kinematics. Inverse square correction for altitude would be made directly to g, but this is small (a few percent) for flight within the atmosphere.

If $\frac{d\xi}{dt}$ and $\dot{\xi}$ are defined as the derivatives of ξ with respect to inertial frame and body frame, respectively, then from Figure C-3, the velocity equation of the accelerometer in body axis can be written as

$$V_a = \frac{dR}{dt} = \frac{d}{dt}(r + \rho)$$

$$= V_{cg} + \dot{\rho} + \Omega \times \rho \qquad \text{(C-5)}$$

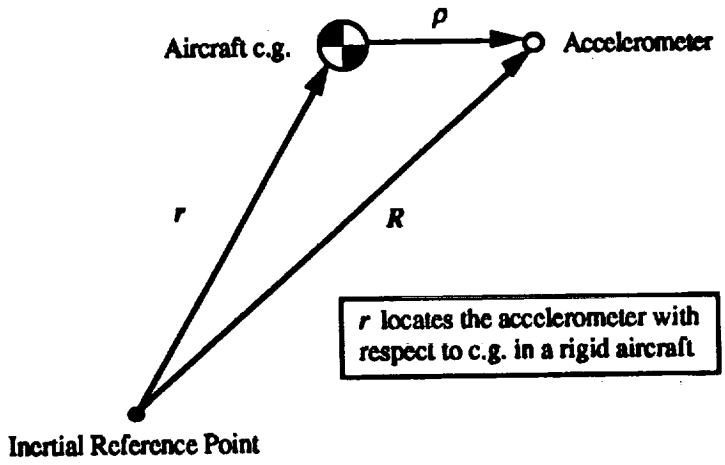

Figure C-2. Accelerometer Location

where $\dot{\rho} = 0$.

$$A_a = \dot{V}_{cg} + \Omega \times V_{cg} + \frac{d\Omega}{dt} \times \rho + \Omega \times \frac{d\rho}{dt}$$

$$= \dot{V}_{cg} + \Omega \times V_{cg} + (\dot{\Omega} + \Omega \times \Omega) \times \rho + \Omega \times (\Omega \times \rho)$$

$$= \dot{V}_{cg} + \Omega \times V_{cg} + \dot{\Omega} \times \rho + \Omega \times (\Omega \times \rho) \qquad \text{(C-6)}$$

Since

$$\Omega = \begin{bmatrix} P \\ Q \\ R \end{bmatrix}, \quad \rho = \begin{bmatrix} x \\ y \\ z \end{bmatrix} \text{ and } V_{cg} = \begin{bmatrix} U \\ V \\ W \end{bmatrix},$$

expressing A_a in the aircraft body frame yields

$$A_a = \begin{bmatrix} \dot{U} \\ \dot{V} \\ \dot{W} \end{bmatrix} + \begin{bmatrix} 0 & -R & Q \\ R & 0 & -P \\ -Q & P & 0 \end{bmatrix} \begin{bmatrix} U \\ V \\ W \end{bmatrix}$$

$$+ \begin{bmatrix} 0 & -\dot{R} & \dot{Q} \\ \dot{R} & 0 & -\dot{P} \\ -\dot{Q} & \dot{P} & 0 \end{bmatrix} \begin{bmatrix} x \\ y \\ z \end{bmatrix}$$

$$+ \begin{bmatrix} 0 & -R & Q \\ R & 0 & -P \\ -Q & P & 0 \end{bmatrix} \left\{ \begin{bmatrix} 0 & -R & Q \\ R & 0 & -P \\ -Q & P & 0 \end{bmatrix} \begin{bmatrix} x \\ y \\ z \end{bmatrix} \right\} \qquad \text{(C-7)}$$

Neglecting vertical and lateral offsets in the accelerometer, y = z = o.

$$A_a = \begin{bmatrix} A_{a_x} \\ A_{a_y} \\ A_{a_z} \end{bmatrix}$$

$$= \begin{bmatrix} \dot{U} - RV + QW - (R^2 + Q^2)x \\ \dot{V} - RU - PW - \dot{R}x + QPx \\ \dot{W} - QU + PV - \dot{Q}x + PRx \end{bmatrix} \qquad \text{(C-8)}$$

Expression of the gravity vector in the body axes introduces the Euler angles referenced to the local vertical (not inertial space).

$$g = g \begin{bmatrix} -\sin\Theta \\ \sin\Phi \cos\Theta \\ \cos\Phi \cos\Theta \end{bmatrix} \qquad \text{(C-9)}$$

Assuming the vertical accelerometer sensitive axis is aligned with the z body axis, i.e., $\boldsymbol{e_a} = -\boldsymbol{k_b}$,

$$A_z = (\boldsymbol{A_a} - \boldsymbol{g}) \cdot - \boldsymbol{k_b}$$

$$= \dot{W} - QU + PV - \dot{Q}x + PRx - g\cos\Phi\cos\Theta \qquad \text{(C-10)}$$

B. PERTURBATION EQUATIONS

The reference condition is constant altitude flight in the vertical plane over a spherical earth (great circle orbit) in a wings level attitude. Thus, $\dot{W}_o$, P_o, R_o, $\dot{Q}_o$, and Φ_o are all zero. The perturbation normal accelerometer output, a_z is

$$a_z = \dot{w} - Q_o u - qU_o - \dot{q}x + (g\sin\Theta_o)\theta \qquad \text{(C-11)}$$

where lateral-directional perturbations are assumed zero ($p = r = 0$). The steady orbital pitch rate is (Ref. 8)

$$Q_o = -\frac{V_{T_o}}{R_g} \qquad \text{(C-12)}$$

where

$$R_g = R_e + H \qquad \text{(C-13)}$$

is the orbital radius and

$$U_o = V_{T_o}\cos\Theta_o \qquad \text{(C-14)}$$

Further (Ref. 8),

$$q = \dot{\theta} - \Delta V_T / R_g \qquad \text{(C-15)}$$

But $V_T = \sqrt{U^2 + W^2}$, thus

$$\Delta V_T = \frac{1}{2}(2u + 2w) / \sqrt{U_o^2 + W_o^2} = (u + w) / V_{T_o} \qquad \text{(C-16)}$$

Eliminating ΔV_T,

$$q = \dot{\theta} - \frac{1}{V_{T_o} R_g}(u + w) \qquad \text{(C-17)}$$

Thus,

$$a_z = \dot{w} + \frac{V_{T_o}}{R_g} u - \dot{\theta} U_o - \frac{U_o}{V_{T_o} R_g}(u + w) - \dot{q}x + (g \sin\Theta_o)\theta$$

$$= \dot{w} - \dot{\theta} U_o - \ddot{\theta} x + (g \sin\Theta_o)\theta$$

$$\underline{+ \frac{V_{T_o}}{R_g} u - \frac{\cos\Theta_o}{R_g}(u + w) - \frac{1}{V_{T_o} R_g}(\dot{u} + \dot{w}) x} \qquad \text{(C-17)}$$

↑ R.O.V. terms

And for constant speed ($u = 0$, short period) approximation,

$$a_z = \dot{w} - \dot{\theta} U_o - \ddot{\theta} x + (g \sin\Theta_o)\theta$$

$$\underline{- \frac{\cos\Theta_o}{R_g} w + \frac{x}{V_{T_o} R_g} \dot{w}} \qquad \text{(C-18)}$$

↑ R.O.V. terms

$x / V_{T_o} R_g$ is much less than 1 and , and thus, the last R.O.V. term can be thrown out. Taking the LaPlace Transform gives the following expression.

$$a_z = \left(s - \frac{\cos\Theta_o}{R_g} \right) w - \dot{\theta} U_o - \ddot{\theta} x + (g \sin\Theta_o)\theta$$

There is only one R.O.V. term ($\cos\Theta_o/R_g$) with an effective frequency of 10^{-7} rad/sec associated with it. This term should have negligible effect at the structural frequencies and can be neglected. Thus, approximating in the frequency range of interest for HPS design, the accelerometer output is conventional which is consistent with the "flat earth" approximation.

$$a_z = \dot{w} - \dot{\theta}U_o - \ddot{\theta}x + (g \sin\Theta_o)\theta$$

and

$$q \approx \dot{\theta}$$

REPORT DOCUMENTATION PAGE

Form Approved
OMB No. 0704-0188

1. AGENCY USE ONLY *(Leave blank)*	2. REPORT DATE	3. REPORT TYPE AND DATES COVERED
	November 1992	Contractor Report

4. TITLE AND SUBTITLE
Advanced Aeroservoelastic Stabilization Techniques for Hypersonic Flight Vehicles

5. FUNDING NUMBERS
C NAS1-18763
WU 505-70-64-01

6. AUTHOR(S)
Samuel Y. Chan, Peter Y. Cheng, Thomas T. Meyers, David H. Klyde, Raymond E. Magdaleno, and Duane T. McRuer

7. PERFORMING ORGANIZATION NAME(S) AND ADDRESS(ES)
McDonnell Aircraft Company
McDonnell Douglas Corporation
P. O. Box 516
St. Louis, MO 63166-0516

8. PERFORMING ORGANIZATION REPORT NUMBER

9. SPONSORING / MONITORING AGENCY NAME(S) AND ADDRESS(ES)
National Aeronautics and Space Administration
Langley Research Center
Hampton, VA 23681-0001

10. SPONSORING / MONITORING AGENCY REPORT NUMBER
NASA CR-189702

11. SUPPLEMENTARY NOTES
Langley Technical Monitor: E. Bruce Jackson
Chan and Cheng: McDonnell Aircraft Company, St. Louis, MO
Myers, Klyde, Magdaleno, and McRuer: Systems Technology, Inc., Hawthorne, CA

12a. DISTRIBUTION / AVAILABILITY STATEMENT
Unclassified-Unlimited

Subject Category 08

12b. DISTRIBUTION CODE

13. ABSTRACT *(Maximum 200 words)*

Advanced high performance vehicles, including Single-Stage-To-Orbit (SSTO) hypersonic flight vehicles, that are statically unstable, require higher bandwidth flight control systems to compensate for the instability resulting in interactions between the flight control system, the engine/propulsion dynamics, and the low frequency structural modes. Military specifications, such as MIL-F-9490D and MIL-F-87242, tend to limit treatment of structural modes to conventional gain stabilization techniques. The conventional gain stabilization techniques; however, introduce low frequency effective time delays which can be troublesome from a flying qualities standpoint. These time delays can be alleviated by appropriate blending of gain and phase stabilization techniques (referred to as Hybrid Phase Stabilization or HPS) for the low frequency structural modes. The potential of using HPS for compensating structural mode interaction was previously explored. It was shown that effective time delay was significantly reduced with the use of HPS; however, the HPS design was seen to have greater residual response than a conventional gain stabilized design.

This report presents additional work performed to advance and refine the HPS design procedure, to further develop residual response metrics as a basis for alternative structural stability specifications, and to develop strategies for validating HPS design and specification concepts in manned simulation. In this report, stabilization design sensitivity to structural uncertainties and aircraft-centered requirements are also assessed.

14. SUBJECT TERMS
HPS, SSTO, HSCT, Hypersonic, Aeroservoelasticity, time delays, hybrid stabilization, phase stabilization, structural modes, structural dynamics, and flying qualities.

15. NUMBER OF PAGES
116

16. PRICE CODE
A06

17. SECURITY CLASSIFICATION OF REPORT	18. SECURITY CLASSIFICATION OF THIS PAGE	19. SECURITY CLASSIFICATION OF ABSTRACT	20. LIMITATION OF ABSTRACT
Unclassified	Unclassified	Unclassified	